Paper A

MENA compared to Europe: The influence of land use, nuclear power, and transmission expansion on renewable electricity system costs

Energy Strategy Reviews 33 (2021) 100590

Contents lists available at ScienceDirect

Energy Strategy Reviews

journal homepage: http://www.elsevier.com/locate/esr

MENA compared to Europe: The influence of land use, nuclear power, and transmission expansion on renewable electricity system costs

H. Ek Fälth [a,*], D. Atsmon [a], L. Reichenberg [a,b], V. Verendel [c]

[a] Department of Space Earth and Environment, Chalmers University of Technology, 412 96, Göteborg, Sweden
[b] Department of Mathematics and Systems Analysis, Aalto University, Otakaari 1 F, Espoo, Finland
[c] Department of Computer Science and Engineering, Chalmers University of Technology, 412 96, Göteborg, Sweden

ARTICLE INFO

Keywords:
Weather conditions
Public concern
Nuclear power
Transmission
Variable renewable energy
Electricity system modeling

ABSTRACT

Most studies that examine CO_2-neutral, or near CO_2-neutral, power systems by using energy system models investigate Europe or the United States, while similar studies for other regions are rare. In this paper, we focus on the Middle East and North Africa (MENA), where weather conditions, especially for solar, differ substantially from those in Europe. We use a green-field linear capacity expansion model with over-night investment to assess the effect on the system cost of (i) limiting/expanding the amount of land available for wind and solar farms, (ii) allowing for nuclear power and (iii) disallowing for international transmission. The assessment is done under three different cost regimes for solar PV and battery storage.

First, we find that the amount of available land for wind and solar farms can have a significant impact on the system cost, with a cost increase of 0–50% as a result of reduced available land. In MENA, the impact on system cost from land availability is contingent on the PV and battery cost regime, while in Europe it is not. Second, allowing for nuclear power has a minor effect in MENA, while it may decrease the system cost in Europe by up to 20%. In Europe, the effect on system cost from allowing for nuclear power is highly dependent on the PV and battery cost regime. Third, disallowing for international transmission increases the system cost by up to 25% in both Europe and MENA, and the cost increase depends on the cost regime for PV and batteries.

The impacts on system cost from these three controversial and policy-relevant factors in a decarbonized power system thus play out differently, depending on (i) the region and (ii) uncertain future investment costs for solar PV and storage. We conclude that a renewable power system in MENA is likely to be less costly than one in Europe, irrespective of future uncertainties regarding investment cost for PV and batteries, and policies surrounding nuclear power, transmission, and land available for wind- and solar farms. In MENA, the system cost varies between 42 and 96 $/MWh. In Europe, the system cost varies between 51 and 102 $/MWh.

1. Introduction

The 2015 UN climate summit in Paris (COP21) demonstrated a broad consensus on the need for comprehensive action to reduce greenhouse gas emissions and keep global warming in check. The electricity sector is a major contributor to CO_2 emissions, accounting for around one-quarter of total emissions [1]. Global electricity consumption is projected to grow due to improved living standards in developing economies [2] and electrification of other sectors, such as transportation [3]. Meanwhile, mitigating CO_2 emissions in the power sector is less expensive than in other sectors [3]. For these reasons, the literature on CO_2-neutral,[1] or near-CO_2-neutral, power systems is expanding. A subset of the literature on CO_2-neutral power systems uses investment models to investigate economic feasibility for different conceivable future power systems. Many of these studies span entire continents and employ a large share of variable renewable energy (VRE), i.e. they are systems that mainly rely on solar irradiation and wind [4–29]. The majority model Europe, the United States, or other temperate regions, while continents with warmer climates have received less attention. There are, however, a few such studies: Aghahosseini et al. studied the Middle East and North Africa region (MENA) [15], Barbosa et al. studied South and Central America [10] and, Blakers et al. studied Australia

* Corresponding author.
E-mail address: hannafa@chalmers.se (H.E. Fälth).

[1] By the term CO_2-neutral power systems, this study refers to a system consisting of generation technologies that do not emit CO_2 during power generation, such as solar-, wind-, and nuclear power. Biogas is also considered CO2-neutral, despite its controversies.

https://doi.org/10.1016/j.esr.2020.100590
Received 18 October 2019; Received in revised form 1 September 2020; Accepted 24 November 2020
Available online 13 December 2020

[30]. With the exception of [15], MENA has been modeled mainly as a potential provider of solar power for Europe [13,31,32]. However, the MENA region merits investigation in its own right, not least because of its current reliance on fossil fuels, with a power plant mix comprising 68% natural gas and 23% oil [33]. The high carbon intensity of the MENA electricity generation, improving living standards in the region, concerns about pollution, and the possibility of electrification of, for instance, transportation, entail large potential benefits of decarbonizing the MENA power sector. Aghahosseini et al. show that a 100% renewable energy system in MENA in 2030 can be less costly than the system corresponding to a BAU trajectory. Thus, both the weather conditions, which are different relative to those of more commonly studied power systems, particularly in terms of more abundant solar resources, and the urgent need to replace carbon-intensive power generation, motivate giving MENA more attention from energy-system studies.

The prospect of CO_2-neutral power systems raises different public concerns, and the literature on social acceptance of renewable energy technologies and associated infrastructures has expanded [34]. Large-scale wind and solar farms, nuclear power, and transmission expansion are three issues commonly addressed in this literature [35–49]. Bolwig et al. [43] argue that social acceptance is important to consider in energy system modeling, policy and planning due to its impact on consumer costs, energy mix, and revenue distribution.

Regarding wind- and solar power deployment, large-scale farms have sparked local resistance and are of public concern [37] [–] [39,50,51]. With increased competition of land and environmental concerns for wind and solar power, suitable sites for wind and solar farms could be a constraint necessary to consider in energy system planning. A limited access to suitable sites for wind- and solar power could have an effect on system cost for large scale CO_2-neutral power system. However, potential constraints due to public concern regarding large-scale wind- and solar farms have received little attention in the energy system modeling community. Schlachtberger et al. [4] found an increase in system cost in Europe by about 10% when the land available for onshore wind was reduced to zero. Bolwig et al. [43] modeled the Nordic-Baltic region and found that the consumer costs for electricity could increase with 12% as a result of low social acceptance for wind power. Both of these studies were done on temperate regions, and the investigation regarding the availability of land focused on wind-, rather than both wind- and solar-, power.

The role of nuclear power has been investigated in several energy system studies [17,52–57], although only in temperate regions and with a large spread regarding its resulting potential to reduce system cost. Nuclear power is a contentious issue, both in society at large [45–49] and in the modeling community [52,53]. Some authors have argued that nuclear power (or other carbon-neutral baseload technologies) is a crucial technology for keeping costs down in a future low carbon emissions power system [17,54,55], while others find only moderate cost benefits of including nuclear power [56,57]. Yet other studies exclude nuclear power by design and find that a future power system based on VRE may be achieved at low to moderate cost [15,16,18]. Sepulveda et al. [17] model systems with and without what they term "firm low-carbon technologies" (essentially CCS technologies and nuclear), and find that excluding such technologies increases the system cost by 10–100%. Jägemann et al. [56] found a cost difference of between 11 and 44% between a system with or without nuclear in Europe, depending on the investment costs mainly for wind and solar. Pattupara et al. [57] modeled Switzerland and neighboring countries and found a 15% decrease in system cost when nuclear power was allowed, while Hong et al. [55] found that replacing current nuclear power in Sweden with wind- and solar power would yield a system cost around five times higher than the current cost for electricity. However, these previous studies all apply different system boundaries and differ both with regards to trading of variations through transmission, as well as the inclusion of long-term storage options.

Transmission expansion has shown to be essential to keep costs down in electricity systems dominated by VRE [4,6–15,58,59], with previous studies showing a cost decrease of about 10–30% if continental grid connections is allowed [6,7,10,11,13,14,58,59]. However, massive transmission expansion may not be politically feasible or publicly acceptable [35,40–44]. The transmission expansion in the EU is slow, despite promotion from the EU commission, with the critical reasons being regulatory issues and permitting issues including bureaucracy and public opposition [60,61].

This paper investigates the importance of these three controversial issues associated with CO_2-neutral power systems for two regions with different weather conditions, Europe and MENA. We test the effects on system cost of (i) different levels of restriction on land use for wind- and solar deployment, (ii) allowing/not allowing nuclear power, (iii) allowing/not allowing international transmission. In addition, we examine how conditions that may be known from readily available data, such as population density, land area, and climate, may be used to predict the cost of a renewable power system. We use MENA and Europe as test cases since they differ in terms of resources. Applying the model to Europe allows us to benchmark our results against those in the literature, e.g., Ref. [4,11,24]. The overarching research questions in this paper are:

1. What is the cost of a CO_2-neutral future power system in MENA/Europe?
2. What is the impact of weather conditions and demand density on the cost of CO_2-neutral power systems?
3. What is the impact of (i)-(iii) on system cost?

Hence, this study contributes to the literature gap in two main areas regarding CO_2-neutral power systems. Firstly, by investigating how different climates can affect system costs. Secondly, by examining how the three aforementioned socio-political factors can influence economic feasibility. The paper is organized as follows: Section 2 describes the scenarios, model, and data input, and provides resource availability in the two regions in the form of supply curves for wind and solar. In Section 3, the results for the four scenarios (base, land availability, nuclear, and transmission expansion) are presented, and we discuss the results relative to the literature as well as policy. Section 4 provides concluding remarks and indicates a direction for future research.

2. Method

We develop a green-field linear capacity expansion model with overnight investment to model a future power system in MENA and Europe. The model minimizes the total cost for a CO_2-neutral power system that meets the electricity demand in each region at each hour in 2040. The model is described in detail in Section 2.1. By evaluating both regions, MENA and Europe, using the same model, the difference in results between the two regions may be attributed to differences in demand and weather, rather than different model formulations and cost assumptions. Hence, we can examine the first and the second research question: the comparison between MENA and Europe regarding the system cost of a CO_2-neutral power system in MENA and Europe and the impact of weather conditions and demand density on these costs.

In order to examine the third research question, the effects on system cost of (i) different levels of restriction on land that may be used for wind-and solar deployment, (ii) allowing/not allowing nuclear power, (iii) allowing/not allowing international transmission, four different scenarios are evaluated: One base scenario as a reference, and three scenarios where the conditions regarding transmission expansion, nuclear power, and land availability for wind- and solar farms are varied, see Table 1. Nuclear power and international/inter-subregional transmission are either available as investment options without any upper limit on capacity, or they are excluded by removing that technology as an investment option. As an upper limit on possible investments for solar and wind power capacity, all scenarios restrict land available for wind-

Table 1
Modeled scenarios.

Scenario	Nuclear Power	Transmission	Available land [%of remaining land]
Base	No	Yes	10
Varying land restriction	No	Yes	2–20
Nuclear	Yes	Yes	10
No Transmission	No	No	10

and solar exploitation by excluding unsuitable locations for wind- and solar farms (see section 2.2.3 for more details). We then assume that a percentage of the remaining land is available for onshore wind- and utility solar PV. This percentage is varied between 2 and 20%, in order to examine the effect on system cost from different levels of restriction on land use for wind- and solar deployment. The percentages are indicated in Table 1 and apply to each technology, e.g. 10% means that 10% of the remaining land is available for wind power and 10% of the remaining land is available for solar power, which makes 20% of the remaining land available for onshore wind- and utility solar PV in total.

All scenarios are evaluated for high-, mid- and low PV- and battery costs, see Table 2. The PV costs are retrieved as the low, mid, and high cost-scenario projections by NREL [62]. In addition to the technologies listed in Table 2, there is the option of residential PV, PV rooftop. The cost for PV rooftop is assumed to be 50% higher than the cost for PV Utility, see Section 2.2.2 below. The evaluated costs for batteries are retrieved from utility-scale lithium-ion storage projections made by Cole [63], as the highest, midrange, and lowest projected costs.

2.1. Model

We develop a linear capacity expansion model with hourly resolution for a full chronological year, to minimize total system cost for a power system that meets the demand at all times. Since the focus is to evaluate the cost-efficiency of a future system with inter-continental grid connections, rather than the pathway to reach such a system, we employ over-night investment in a green-field optimization approach. The exception is hydropower, which is assumed to be installed at its present capacity, as reported by the World Energy Council [64]. Technology costs and electricity demand are projections for 2040. Demand- and weather data, as well as costs and technology performances, are exogenous to the model. The model is implemented in Julia using JuMP, a domain-specific modeling language for mathematical optimization embedded in Julia. Subregion data, capacity factors, capacity limits for solar- and wind power, and electricity demand profiles are generated by the GlobalEnergyGIS package described in Refs. [65] and publicly available at GitHub [66].

Variables subject to optimization are capacity investments, electricity generation, storage, and transmission. These variables are functions of the subregions $R = \{r_1, ..r_n\}$, the technologies possible to invest in $K = \{k_1, ..k_n\}$, different classes of solar- and wind power $C = \{c_1, ..c_n\}$ (depending on capacity factor) and the hours over one year $H = \{h_1, ..h_n\}$. Parameters given to the model include technology costs, technology efficiencies, demand, the distance between subregions, and capacity factors. The model represents wind and solar power using five resource classes for each region, see details in the supplementary material. We use the GlobalEnergyGIS package [65,66] to generate the maximum potential capacity (in *GW*) and hourly capacity factors for each technology, resource class, and region.

Table 2
PV- and battery costs.

	High-Costs	Mid-Costs	Low-Costs
PV Utility [$/kW]	1200	800	400
Battery [$/kWh]	375	230	87.5

The objective function to be minimized is the total system cost. The total system cost ($SC, [M€/year]$) is a function of electricity generation ($G_{r,k,c(k),h}, [GWh/h]$), operation and management cost ($omc_k, [€/GWh]$), fuel cost ($fuc_k, [€/GWh]$), technology efficiency ($\eta_k, [\ -\ ]$), installed capacity ($C_{r,k,c(k)}, [GW]$), investment cost ($ic_k, [€/GW]$), annualisation factor (af_k), fixed cost ($fc_k, [€/GW/year]$), transmission capacity ($TC_{r_1,r_2}, [GW]$) and transmission cost ($tc_{r_1,r_2}, [€/GW]$).

$$SC = \sum_{r,k,c(k),h} G_{r,k,c(k),h}(omc_k + fuc_k / \eta_k) + \sum_{r,k,c(k)} C_{r,k,c(k)}(ic_k \cdot af_k + fc_k) + 0.5\sum_{r_1,r_2} TC_{r_1,r_2} \cdot tc_{r_1,r_2} \quad (1)$$

By convention we use uppercase for variables and lowercase for parameters.

The transmission cost is divided by two since the model is investing in transmission lines between subregions r_1 and r_2 and between r_2 and r_1, even though only one line is needed. The transmission cost (tc, [€/GW]) is a function of transmission line cost ($tlc, [€/GW/km]$), distance between subregions ($di_{r_1,r_2}, [km]$), transmission substation cost (tsc, $[€/GW]$) and a fixed transmission cost ($tfc, [\%ofic]$). Two substations are assumed to be needed for each transmission line.

$$tc_{r_1,r_2} = (tlc \cdot di_{r_1,r_2} + 2 \cdot tsc) \cdot (af + tfc) \quad (2)$$

The implemented constraints follow. First, we need to ensure load balance, i.e., make sure that demand is met at all times. The total generated electricity ($G, [GWh/h]$) less the electricity used for storage charging ($CH, [GWh/h]$) plus the imported electricity ($TG_{r_2,r,h}, [GWh/h]$) and less the exported electricity ($TG_{r,r_2,h}, [GWh/h]$) must be greater than or equal to the demand ($d, [GWh/h]$), for each hour in every subregion. The transmission losses ($tl, [\%/1000km]$) depends on the distance between subregions ($di_{r_1,r_2}, [km]$) and are assumed to occur only for imports, to avoid double-counting.

$$\sum_{k,c} G_{r,k,c(k),h} - \sum_{k=storage} CH_{r,k,h} + \sum_{r_2}(1 - tl_{r_2,r}) \cdot TG_{r_2,r,h} - TG_{r,r_2,h} \geq d_{r,h} \quad (3)$$

The electricity generation per hour ($G, [GWh/h]$) must be less then or equal to the installed capacity ($C, [GW]$) multiplied by the capacity factor (cf) for each technology, hour and subregion.

$$G_{r,k,c(k),h} \leq C_{r,k,c(k)} \cdot cf_{r,k,c(k),h} \quad (4)$$

The storage level ($SL_{r,k,h}, [GWh/h]$) cannot be negative:

$$SL_{r,k,h} \geq 0 \quad (5)$$

The maximum storage level depends on the installed capacity ($C_{r,k,c}$, $[GW]$) and the discharge time ($dt_{r,k}, [h]$) for the storage technology. For batteries, the discharge time is set to 8 h; for hydro dams, it depends on the dam size.

$$SL_{r,k,h} \leq C_{r,k,c(k)} \cdot dt_{r,k} \quad (6)$$

The present storage level ($SL_{r,k,h}$, $[GWh/h]$) depends on battery charging ($CH_{r,k,h}, [GWh/h]$), the water flow in-to the dams, i.e. a capacity factor for hydro inflow ($cfh_{r,h}, [\ -\ ]$), the installed capacity of hydro dams ($C_{r,dam}, [GW]$), the electricity going from the storage to the grid ($G_{r,k,c,h}$, $[GW]$) and the electricity losses. These losses depend on the efficiency for each storage technology ($\eta_k, [\ -\ ]$). The storage balance is written as, for h¿1:

$$SL_{r,k,h} \leq SL_{r,k,h-1} + CH_{r,k,h} + cfh_{r,h} \cdot C_{r,dam} - \frac{G_{r,k,c(k),h}}{\eta_k} \quad (7)$$

If h = 1, the first term after the inequality sign is instead the storage level in the last hour of the previous year. Note that the first term is less than or equal to and not simply equal to. This is due to spillage when the water inflow is greater than the amount of water that the dam can handle.

Charging batteries requires batteries:

$$CH_{r,battery,h} \leq C_{r,battery} \tag{8}$$

Transmission constraints assure that the transmitted electricity (TG_{r_1,r_2}, $[GWh/h]$) does not exceed the installed transmission capacity ($[TC_{r_1,r_1}, GW]$) and that the installed transmission between subregion r_1 and r_2 is the same as between r_2 and r_1.

$$\begin{aligned} TG_{r_1,r_2,h} &\leq TC_{r_1,r_2} \\ TC_{r_1,r_2} &= TC_{r_2,r_1} \end{aligned} \tag{9}$$

In order to partially mimic realistic constraints on nuclear power plants, ramping constraints and a minimum generation level in percentage of installed capacity are imposed.

$$\begin{aligned} G_{r,nuclear,h} &\leq G_{r,nuclear,h-1} + 0.2 \cdot C_{r,nuclear} \\ G_{r,nuclear,h} &\geq G_{r,nuclear,h-1} - 0.2 \cdot C_{r,nuclear} \\ G_{r,nuclear,h} &\geq 0.6 \cdot C_{r,nuclear} \end{aligned} \tag{10}$$

We assume a limited stock of biogas. No more than 5% of the total annual electricity generation can be produced by biogas turbines. This assumption is based on estimates on waste, agricultural residues, and manure [67–70]. There are indeed other feed-stocks for biogas such as forest residues, but there is also a demand for bio energy from sectors not included in this study (heat and transport).

$$\sum_{r,h} G_{r,biogas,h} \leq \sum_{r,k,c(k),h} G_{r,k,c(k),h} \cdot 0.05 \tag{11}$$

2.2. Data

Input data include: definition of subregions; estimates of transmission distances between subregions; cost- and performance data for technologies and fuels; hourly subregional demand for a full chronological year; capacity factors; and capacity limits for solar power, wind power, and hydropower. This section contains information on how these input data were retrieved and implemented in the model.

2.2.1. Regions and transmission

MENA is modeled with 13 subregions and Europe with 10. All subregions are treated as "copper plates" internally, i.e., transmission within each subregion is assumed to be unconstrained. HVDC transmission lines are assumed to be available for investment between neighboring subregions. Data on the countries aggregated to each subregion, maps, possible interconnections, and interconnection distances may be found in the supplementary material.

The assumed transmission costs are presented in Table 3 and are retrieved from ETSAP [71], except for the fixed cost which is taken from NREL [72]. The lifetime of HVDC lines is assumed to be 35 years [73].

2.2.2. Technology- and fuel costs

The power generating technology options are wind power (on- and offshore), PV (utility and rooftop), concentrated solar power (CSP) and biogas turbines (GT). The assumed costs and efficiencies for each technology are shown in Table 4. The costs are retrieved from the National Renewable Energy Laboratory's (NREL) Annual Technology Baseline (ATB) Database 2018 [62]. This database contains technology cost projections for 2040 for a low-, mid-, and high-cost scenario; the assumed costs used in this study are the mid-cost scenario projections in the NREL database [62]. For PV rooftop, the cost is assumed to be 50% higher than PV utility due to higher installation costs for smaller systems, which is in line with the cost projections in NREL database 2018 [62]. The investment cost for batteries is retrieved from utility-scale lithium-ion storage projections by Cole [63]. Lifetime and round-trip efficiency for the batteries are also retrieved from Cole [63]. The modeled batteries are assumed to be lithium-ion battery packs with a discharge time of 8 h, as in Ref. [63], and the cost can be converted from $/kW to $/kWh with a factor 8. All investment costs are annualized using a social discount rate of 5%. Our assumption lies within the 2–7% range used in previous studies [4–6,11,12,14–27,29] and is in line with the recommendation of a discount rate of maximum 5% for energy systems optimization models, proposed by Garcia-Gusano et al. [74].

We assume the cost of biogas to be the average biogas cost in Ref. [17], USD 60 per MWh.

Table 3
Transmission costs.

Trans. Line [$/MW/km]	Substations [$/MW]	Losses [%/1000 km]	Lifetime [yr]	Fixed O&M Cost [% of Inv. Cost]
2030	17,350	3	35	0.8

2.2.3. Wind- and solar data

The wind- and solar input data were constructed using the GlobalEnegyGIS package [65,66]. In this package, installation limits for wind and solar power capacity are based on assumptions on typical wind and PV farm densities (W/m^2) and available land (m^2). Several auxiliary datasets are used to exclude areas less suitable for solar- and wind power which, together with the meteorological data, leads to an estimate of solar- and wind potentials for each region. The datasets include population (GPWv4 [75]), land cover (MODIS [76]), protected areas (WDPA [77]), and topography and bathymetry (ETOPO1 [78]) [66]. After masking out unsuitable locations, a certain fraction of the remaining area is considered available for solar and wind farms, see available land in Table 5. Assumptions on typical wind and PV farm densities (W/m^2) are used to convert the resulting available area to potential capacity (GW).

Hourly time series with capacity factors for PV and wind power are constructed using the ECMWF ERA5 [79] database and data from the Global Wind Atlas [80]. The procedure for this is described in detail in Refs. [65,66]. The modeled subregions are divided into pixels ($0.01°x0.01°$), capturing the different solar and wind conditions with an hourly time resolution. Solar irradiation is used to calculate the annual PV capacity factor profiles assuming fixed-latitude-tilt; wind speed is translated into capacity factors based on a power curve for a typical wind park with Vestas 112 3.075 MW wind turbines [65,66]. The pixels in each subregion are aggregated into five classes, depending on yearly average capacity factors for solar- and wind power, to reduce the computational demand. The pixels within a resource class, in each subregion, are assumed to have the same capacity factor time series (the average of all capacity factor time series in those pixels), see Supplementary Material and [65,66].

Supply curves for PV and wind power, based on the input data retrieved with the GlobalEnergyGIS package [65,66], are shown in Fig. 1. The supply curves display the wind- and solar power potential in relation to electricity demand and reveal the resource prerequisites for a VRE based power system for the two different regions. The numbers are percentages of net demand that can be supplied at different Technology levelized cost of electricity (Technology LCOE) for each technology (wind- and solar power). Technology LCOE ($/MWh) is defined as the net present value of all costs related to producing electricity with that technology per electricity output. Net demand is defined as the total electricity demand minus hydropower generation. The supply curves in Fig. 1 are the results of an assumption of 10% available land for wind and solar deployment (see section 2 for the definition of available land) and midrange costs for PV (see Table 2). It can be seen in Fig. 1 that MENA can produce more of its electricity demand with either wind- or solar power to a lower cost than can Europe. Supply curves for other costs and assumptions on available land are presented in the Supplementary Material.

Table 4
Technology costs and efficiencies.

	Investment Cost [$/kW]	O&M Cost [$/MWh]	Fixed Cost [$/kW/yr]	Lifetime [yr]	Efficiency [−]
Nuclear	5570	2	99	60	0.32
Wind Onshore	1227	0	42	25	–
Wind Offshore	2317	0	130	25	–
PV Utility	800	0	6	25	–
PV Rooftop	1200	0	6	25	–
CSP	5225	3.5	50	30	–
GT	830	4	11	30	0.38
Hydro Power	0	0	0	–	–
Battery	1850 (230 $/kWh)	1.32	6	15	0.9

Table 5
Capacity limit assumptions.

	PV Utility	PV Rooftop	CSP	Wind Onshore	Wind Offshore
Density [W/m^2]	45	45	35	5	8
Available land [% of remaining land area]	10	10	10	10	33

2.2.4. Hydropower

Installed hydropower capacities and annual generation in each subregion are assumed to be as in 2016 according to the World Energy Council [64] and can be found in the Supplementary Material. Monthly hydro inflow profiles for each region were retrieved from the Global-EnergyGIS package [65,66] which uses the GRanD database [81,82]. The inflow profiles are converted to hourly inflow assuming an even flow within each month and the dam size is assumed to be equal to the annual generation divided by 12, i.e., the dam can roughly hold a months's worth of energy before spillage occurs, depending on the inflow profile.

2.2.5. Hourly demand profiles

Due to a lack of comprehensive real-world demand data for each of our 23 subregions, we generate synthetic hourly electricity demand using machine learning to algorithmically generate a model directly from available data, and then extrapolate the resulting series to 2050. More specifically, we fit a gradient boosting regression model with decision trees as base learners [83] and evaluate it using cross-validation on data for currently available countries, and then scale the generated time series to fit a projected yearly total in 2050. We model the profile of how the current hourly electricity demand per capita varies over the year as a function of three types of data. First, to describe a country/region, we include purchase-power adjusted regional GDP [84] and gridded global population of the world (GPW-4) [85]. Second, we include information about temperature time series for 2015 from NASA MERRA-2 [86] with country-level temperature averages and extremes, as well as variables for the hour of the day, weekday, and month of the year. Finally, we have country-level annual electricity generation for 2017 from Ref. [87] scaled to match regional final electricity demand in the SSP2-34 scenario for 2050 [84]. After fitting the model based on electricity demand for 44 countries to the normalized demand time series, the resulting predictions for our regions are extrapolated to 2050 by scaling the total to the level corresponding to SSP2-34 scenarios. For more details and evaluation of the approach with gradient boosting regression, see Ref. [65]. The resulting synthetic demand series are treated as inelastic in the optimization model.

3. Results and discussion

The results are structured as a comparison between MENA and Europe regarding system cost in general (Section 3.1); when varying

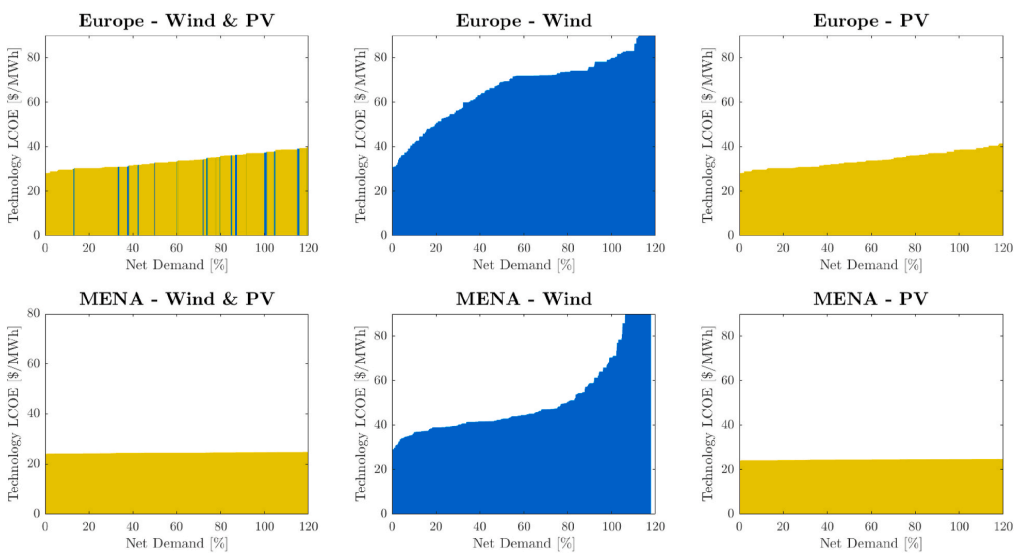

Fig. 1. Supply curves for PV and wind power assuming 10% available land and midrange costs for PV.

land availability (Section 3.2); with the investment option of nuclear power (Section 3.3); and excluding the option of inter-subregional transmission (Section 3.4), see Table 1 for the specifics of each scenario. Each scenario was investigated with a range of cost projections for solar PV and battery storage (see Table 2). The obtained system costs are presented as System levelized cost of electricity (System LCOE), in $/MWh, defined as total electricity system cost per total demand subtracting the annual hydropower generation. Hydropower generation is subtracted since hydropower is modeled as no-cost in this study.

3.1. Comparison between europe and MENA: system cost and technology mix

We begin by presenting a summary of the cost range obtained by modeling the different scenarios as well as PV and battery costs. We find that System LCOE varies substantially, between 51 and 102 $/MWh (Europe) and 42–96 $/MWh (MENA), depending on scenario and PV and battery costs (see Fig. 2). Previous cost estimates in MENA [15] and Europe [4,11,24] lie in this interval. The System LCOE corresponding to midrange costs for PV and batteries for the base scenario, a system with inter-subregional transmission and without nuclear power, is 72 $/MWh for Europe and 61 $/MWh for MENA (denoted with a black line in Fig. 2).

Depending on the scenario, and the cost level for PV and battery investments, the System LCOE is 6–35% lower for MENA compared to Europe. Thus, for any given assumption on land availability, PV and battery costs, transmission expansion, and nuclear power option, the System LCOE is lower in MENA than in Europe.

Fig. 3 shows the optimal generation mixes as a share of total electricity generation in the base scenario for low-, mid- and high-cost PV and batteries for MENA and Europe. All demanded electricity is generated by either hydropower, wind power, PV, or biogas turbines, and together adds up to 100% in Fig. 3. Transmission and batteries are displayed as the shares of total power generation that pass through transmission lines and battery storage, respectively, which is why the total generation exceeds 100% in Fig. 3. The generation mix is dominated by wind power for high- and mid-cost PV and batteries. In these cases, more electricity is traded through transmission lines than is stored and delivered through battery storage. For low-cost PV and batteries, the generation mix is instead dominated by solar power. In this case, more electricity is stored and delivered through battery storage than is traded through transmission lines, especially so in MENA, see Fig. 3. For the optimal generation mix for the other scenarios, see the Supplementary Material.

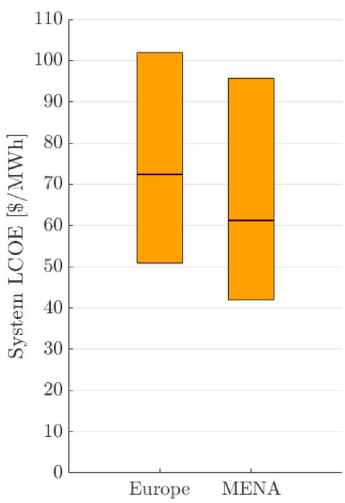

Fig. 2. Range of System LCOE in Europe and MENA, obtained by modeling the different scenarios as well as PV and battery costs. The black line corresponds to the System LCOE assuming midrange costs for PV and batteries for the base scenario.

Our resource quality assessment (Fig. 1) shows that MENA can satisfy its demand with either solar or wind power at a lower Technology LCOE than Europe. We also find that for all investigated scenarios, MENA has a lower System LCOE than Europe. Our results thus show a correlation between resource quality and system cost. However, many additional factors determine the cost and capacity mix of optimal renewable power systems, including the available variation management strategies, e.g. the abundance of reservoir hydropower, as well as the nature of spatial and temporal variations in VRE resources. Solar and wind power display different spatial and temporal variations, with solar power having a diurnal pattern, while wind power generation displays variations on both shorter and longer time scales [88,89]. Complexities associated with how technologies complement each other in time and space influence cost and other features of a renewable power system, including the technology mix. Without prior knowledge of the system properties of wind and solar, respectively, it would, for instance, be difficult to infer that the system mix in the base scenario for midrange costs on PV and batteries is dominated by wind (Fig. 3, middle bar), since solar sites with lower Technology LCOE than wind are abundant in both Europe and MENA (Fig. 1, left column). However, our results still indicate that some factual information on System LCOE may be inferred simply from considering the supply curves. In order to understand that connection better, more research is needed, both on other regions and with other technology scenarios.

3.2. Amount of land available for wind and solar farms

By decreasing the land available for wind and solar farms, the supply curves (Fig. 1) become steeper. It is then necessary to exploit sites with a lower output to cover the demand, thus increasing System LCOE. Assuming less land is available for wind and solar farms (2% instead of 10% as in the base scenario) increases the System LCOE by up to 47% in MENA and 25% in Europe, see Fig. 4. In Europe, the increase in System LCOE due to less land being available is up to 23–25%, regardless of PV and battery costs. See Section 2 for the definition of available land applied in this study.

In MENA, the increase of System LCOE due to less available land for VRE exploitation is dependent on investment costs for PV and storage, see Fig. 4, with land availability having almost no effect for low investment costs and a significant effect for high investment costs. This has to do with the technological LCOE for wind power being significantly more affected by available land compared to PV (as may be seen from Fig. 1). This shows also in the resulting generation mix: When there is less available land, deployment of wind decreases, while solar generation increases, an example of which may be seen in Fig. 5.

The reason the System LCOE does not increase in MENA as land becomes more scarce in the low cost case may be explained by the generation mix already being dominated by solar in that case, and thus the impact of the land constraint on wind power is less relevant, see Fig. 6. Solar figures prominently in the mix for Europe too, in the low cost case, but wind is still important, see Fig. 3.

Both wind and solar power face social opposition in some regions in the world [37–39,50,51]. We show that the assumptions on available land are indeed an important determinant for the System LCOE of a CO_2-neutral system. In fact, if the available land for VRE exploitation is reduced from 10% to 2%, the System LCOE may increase by up to 25% in Europe and 47% in MENA, depending on the cost for solar PV and battery storage, see Fig. 4. Schlachtberger et al. [4] found an increase in system cost by 10% when the land available for onshore wind was reduced to zero. Unlike in the present study, the set-up used in

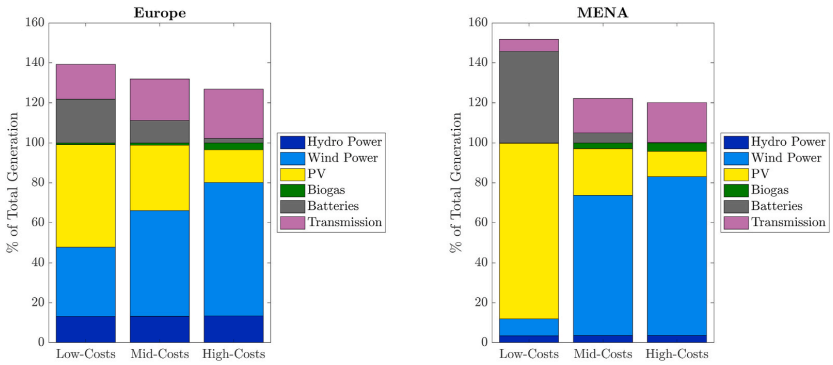

Fig. 3. Optimal generation mix in MENA and Europe.

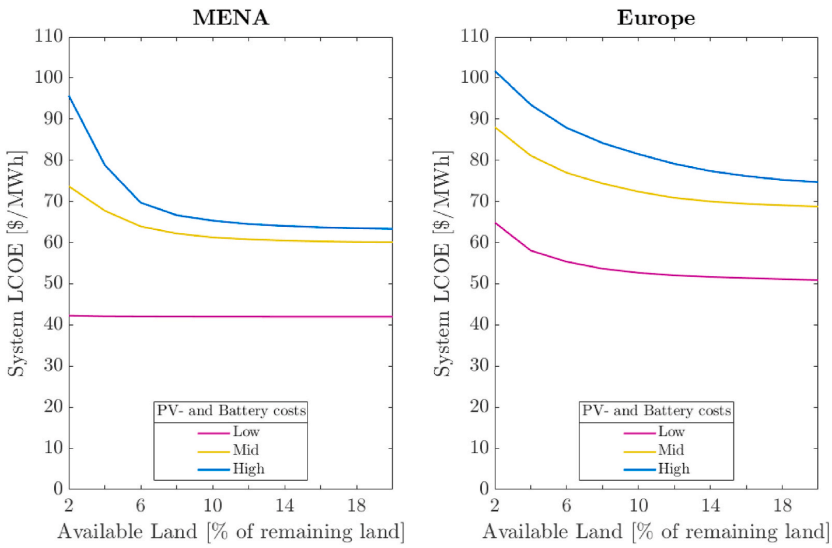

Fig. 4. System LCOE as a function of land available for PV and wind power for the cases of low, mid-range and high investment costs for PV and batteries.

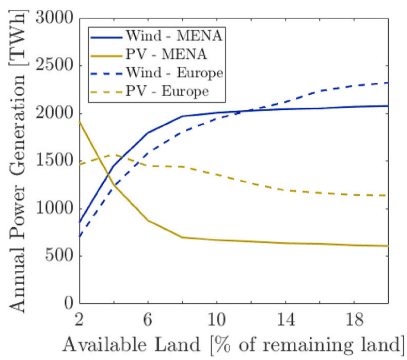

Fig. 5. Annual power generation from PV and wind power as a function of available land assuming mid-costs for PV and batteries.

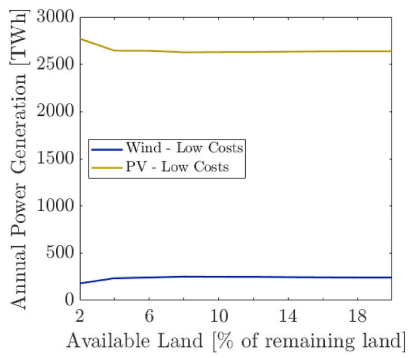

Fig. 6. Annual power generation from PV and wind power in MENA as a function of available land assuming low-costs for PV and batteries.

Schlachtberger et al. [4] reduces land available only for on-shore wind power, rather than for both on-shore wind- and solar power. This also applies to Bolwig et al. [43], who examine the effect of 'low social acceptance'[2] on consumer cost in the Nordic-Baltic region by increasing the investment cost for on-shore wind power. They find that the consumer cost for electricity could increase by up to 12% as a result of low social acceptance. They also find that solar PV occupies a larger share of the energy mix if there is low acceptance for wind power. Thus, these previous studies [4,43] have examined the effect of social acceptance for deployment of renewable energy by constraining on-shore wind power, while our study examines the possible effect of social acceptance by constraining both wind- and solar power. Our study shows that the effect of limiting available land for both wind- and solar power in MENA is highly dependent on solar and battery costs, while the effect of constraining available land in Europe depends to a lesser extent on future investment costs. In Europe, the impact on System LCOE of the assumptions on available land are of the same magnitude as the impact of allowing for inter-subregional transmission or nuclear power. In MENA, the effect of available land for wind-and solar farms is more significant than the effect of allowing for inter-subregional transmission or nuclear power. This suggests that land-availability assumptions should feature more prominently than currently in policy discussions and in the modeling community. The difference in System LCOE incurred by assumptions on available land could, for instance, be interpreted as an opportunity to give financial incentives to the part of the population negatively affected by the construction of wind and solar power.

3.3. Nuclear power option

Allowing for nuclear means expanding the available technology options, thus always inducing a decrease of System LCOE (or keeping the System LCOE at the same level as the base scenario). However, the resulting reduction of System LCOE is contingent on the costs of the alternative generation technologies, see Fig. 7. Two things stand out from the results: First, if the investment costs for PV and batteries are assumed to be low, allowing for nuclear power does not yield any reduction in System LCOE in MENA or Europe. Secondly, the cost reduction is smaller in MENA than it is in Europe. While the cost reduction in Europe is 11% and 19% for Mid and High investment costs for PV/batteries, respectively, the cost reduction in MENA is only a few percent, see Fig. 7.

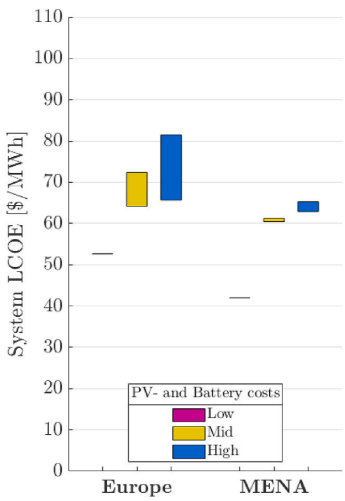

Fig. 7. Range of System LCOE between optimally installed nuclear power and no nuclear power for the cases of low, mid-range and high investment costs for PV and batteries.

The difference between MENA and Europe in the cost-reducing effect of allowing for nuclear (0–19% in Europe and 0–4% in MENA) may be explained by more favorable solar and wind resources in MENA. The abundance of solar and wind resources in MENA entails that a renewable system, including the necessary flexibility capacity (batteries and transmission), will out-compete nuclear in most subregions. In comparison, in Europe, there is less low-cost wind and solar resource in relation to its demand (see Fig. 1), which makes nuclear power relatively more competitive.

By modeling the power systems in MENA and Europe with and without the possibility of investing in nuclear power, we show that the impact from allowing for nuclear power on System LCOE may range between almost none to decrease System LCOE by about 20%. The effect of allowing for nuclear power is contingent on the supply of low-cost VRE resources (Fig. 1) as well as low-cost variation management resources (here battery storage). Thus, the higher-quality VRE resources in MENA, compared to Europe, entail that allowing nuclear power in the system has very little effect on System LCOE (the reduction in system cost is less than 4%, regardless of the cost assumptions for solar PV and batteries). In Europe, the benefit of including nuclear power is highly dependent on the cost assumptions, varying between 0% and 19% for the different cost assumptions for solar PV and battery investments. The System LCOE reductions that we find for Europe are in the low range of results in the literature, where e.g. Ref. [56] found a cost difference of between 11 and 44%, depending on the investment costs mainly for wind and solar. Reference [57] found only minor economic effects from allowing for nuclear in Switzerland. However, the literature also includes claims that decarbonizing without nuclear power (or other carbon-neutral thermal technologies such as coal wit CCS) is substantially more costly [17,55] than without those technologies. The main reason for these diverse conclusions in literature are likely different system boundaries, where regions are isolated and may not benefit from the flexibility provided by trade with other areas on a continental scale. In addition to this feature, which is also apparent in our study, we further nuance the potential cost benefit of nuclear to be contingent on resource quality and quantity in relationship to demand. Specifically, our study of MENA shows that the effect from allowing for nuclear power that was found in previous literature to be between 15% and 150%, depends on the regional characteristics of resource quality, availability of land and electricity demand. Thus, we argue that the results of comparative studies between CO_2 neutral power systems, such as [17,55–57]), should be interpreted bearing in mind the contingency both on method (isolated regions as in Ref. [17] or a larger connected region such as in Ref. [56]) as well as on the specific characteristics of the region, such as population density, electricity demand and availability of land for wind- and solar deployment.

Our results, which show that the reduction in System LCOE of allowing for nuclear power in MENA is very small, support strategies to decarbonize power systems in this region without investing in nuclear power and avoid associated concerns about safety and proliferation.

3.4. Transmission expansion

The present study investigated two scenarios regarding inter-subregional transmission capacity: an optimal expansion of the transmission capacity and a scenario excluding all transmission. We find an increase in System LCOE in both MENA and Europe when transmission is excluded, i.e., when subregions are isolated, see Fig. 8. The cost increase

[2] They formalize this concept by assuming a doubled investment cost for on-shore wind, thus reflecting increased cost for the entire building process.

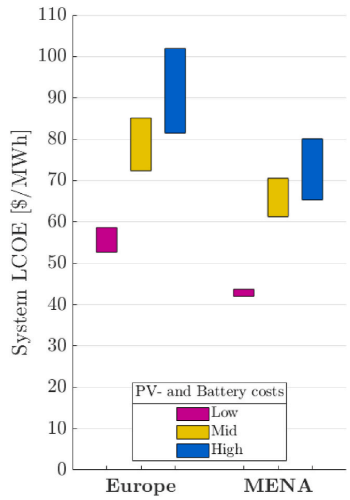

Fig. 8. Range of System LCOE between optimally installed transmission and no inter-subregional transmission for the cases of low, mid-range and high investment costs for PV and batteries.

is similar in both regions: 4–23% in MENA and 11–25% in Europe, depending on cost assumptions for PV and batteries.

Excluding inter-subregional transmission leads to a significantly higher System LCOE (23% and 25%, corresponding to a 15 $/MWh and 20 $/MWh cost increase respectively, for MENA and Europe), for high PV and battery investment costs, roughly corresponding to todayâ€™s PV and battery costs. Conversely, the effect of excluding transmission is less significant when costs for PV and batteries are low. At low costs for PV and batteries, the PV-dominated system in MENA suffers only a small increase (4%) in System LCOE from excluding transmission (the corresponding number for Europe is 11%). The explanation is two-fold: First, allowing for transmission is more important when wind power is a large part of the mix. Hence, the smaller effect of excluding transmission when PV and batteries are low-cost and thus form a more substantial part of the mix, see Fig. 3. Second, if batteries are cheap, especially in combination with cheap solar, allowing for trade (through transmission expansions) has a smaller effect. The cost increase caused by excluding transmission also depends on the cost of the alternative technology, which here is wind power. The spatially scattered high quality wind power sites can not be used as efficiently without transmission as with transmission, causing the higher cost. Hence, the more favorable solar and wind conditions in MENA (see Fig. 1 and S3 - S7) is the reason for the slightly lower cost increase in MENA compared to Europe despite the higher share of wind power in Europe's energy mix when PV and battery costs are mid- and high-cost.

We find that System LCOE increases by between 4 and 25% when inter-subregional transmission is excluded. Isolating subregions leads to over-investment in VRE capacity and more investment in storage and thermal generation capacity with potentially low full-load hours. This cost increase is consistent with results from other modeling studies [6,7,10,11,13,14,58,59], where the cost decrease due to large-scale transmission expansion is found to be between 10 and 30%. However, unlike the majority of these papers, we investigate how the benefit of optimal transmission expansion depend on the cost of solar PV and battery storage. The benefit of adding inter-subregional transmission is greater when investment costs for PV and batteries are high compared to when they are low. A similar result was found by Schlachtberger et al. [4]. The underlying mechanism is that increased transmission mainly benefits systems with a high share of wind power, and low-cost solar PV and batteries lead to a smaller share of wind power in the optimal generation mix. Low-cost solar PV and batteries systems instead rely on more battery storage. For example, the low investment cost case results in 5.4 *TWh* of battery storage in MENA, equivalent to about 65 million Tesla model S (85kwh) batteries. This quantity of batteries may have consequences in terms of the use of materials. On the other hand, a large-scale grid extension might not be feasible due to social acceptance issues [35,40–44] Thus, decarbonized power systems may entail hard-to-swallow features, such as large-scale transmission or large amounts of batteries or nuclear power.

3.5. Limitations

The main results of this paper are about how circumstances due to policy and public opinion (land for VRE, nuclear power, and the availability of transmission expansion) impact the cost of a CO_2-neutral power system, and how this impact may differ depending on regional resource endowment. The limitations of the model framework with potential consequences for this set of questions are:

1. The system boundary in this study is set around the electricity sector and does not include other sectors in the energy sector, such as heat, transportation, and industry. Besides, only one storage technology (lithium-ion batteries) is considered. This could have a bearing on the system cost difference between Europe and MENA. Sector coupling is likely to entail increased demand for electricity, both through electrification and the use of electro-fuels, thus increasing land scarcity for VRE farms. Thus, in the future, differences regarding the resource-to-demand relationship (Fig. 1) may be more considerable and have a more substantial effect on cost, thus increasing the cost in Europe compared to MENA. This would also impact the relative benefit of using nuclear for electricity generation, especially in Europe. Sector coupling increases the temporal flexibility of the system. In this sense, it resembles the effect of low-cost storage. Thus, if there is sector coupling, it is likely that the availability of other variation management strategies, such as transmission, becomes less consequential for System LCOE. Similarly, it would be comparatively less costly to integrate renewables, thus rendering the nuclear option less important for cost reduction. However, since sector coupling increases the demand for electricity, the land-availability issue becomes more pressing.
2. Political realities are not considered when modeling international transmission expansion, and only two cases are considered: no (international, i.e., inter-subregional) transmission and optimal transmission. These two extreme points of transmission expansion are both unlikely. In fact, transmission between subregions already exists in both Europe [90] and MENA [91]. The impact on System LCOE from extending transmission is in fact smaller than estimated in this paper, because the minimum amount of transmission is already greater than zero, and the maximum feasible transmission grid is likely smaller than the optimal grid.
3. We have not allowed for an expansion of hydropower. MENA exhibits a greater potential, compared to Europe, for expansion of hydropower. Allowing for expansion may therefore increase the difference in System LCOE between the regions.
4. We model every subregion as a copper plate, i.e., electricity transmission within each subregion is assumed to be unlimited. Due to this, internal transmission requirements are not considered. This assumption means that the cost for power systems is underestimated in general, and likely especially so in cases with large volumes of power traded between subregions. This model artifact could have a more significant effect on the cost estimate for MENA, since its model subregions are generally larger. This issue was addressed in Refs. [59], where it was seen that cost and capacity mix did not change significantly as the spatial resolution was gradually coarsened. However, it should be noted that the largest regional size in Ref. [59]

was still not as large as the regions in our study. The authors speculate that this is due to that, as the spatial becomes coarser, there are two mechanisms that counteract each other: the transmission needs are underestimated, but at the same time, the VRE resource is underestimated. This is due to that the method to estimate the VRE availability used in Ref. [59], entails that VRE resources are averaged, so that the best sites are no longer visible for larger regions. This latter is a trait which is less likely to interfere in the present study, since we employ wind- and solar classes in our model, thus capturing more of the resource heterogeneity compared with the method used in Refs. [59]. However, the lack of literature on the subject entails that we cannot be confident about the extent to which the large regions, and, especially, the unequal region size between Europe and MENA, impact the results. We believe that this topic merits more research in the future.

5. There are no ramping or start-and-stop costs for thermal power plants. Cebulla and Fichter [92] showed that including such constraints is of little consequence for predominantly renewable power systems.

We deem the first of these limitations as likely to have the largest effect on our results since it provides an alternative variation management strategy, which impacts the cost-effectiveness of nuclear as well as transmission expansion. Sector coupling also effectively increases the demand for electricity, putting more strain on land for power generation, which potentially increases the effect of less available land.

4. Conclusions

This paper investigates the effects of three socio-political factors on CO_2-neutral power system costs, the availability of: (i) nuclear power, (ii) international transmission, and (iii) land for wind and solar deployment. The analysis is applied to MENA and Europe separately, which allows for a comparison regarding how a priori conditions (such as population density, available land for RE and weather conditions) may be used to predict the cost and capacity mix of CO_2-neutral power systems. We find that:

- For any combination of assumptions on investment costs for solar PV and batteries, as well as transmission/nuclear/land availability, the system cost is lower in MENA than in Europe. This suggests that the lower system cost is linked to the better wind and solar resource quality.
- The cost for a CO_2-neutral power system ranges between 42 and 102 $/MWh in this study.
- Public acceptance of wind and solar farms may have a large impact on the cost of a CO_2-neutral power system. Our results indicate that a decrease of available land (from 10 to 2%) can increase system cost by about 50% in MENA and 25% in Europe for the case without nuclear but with the option of transmission expansion.
- Allowing for nuclear power reduces the system cost by 0–19% in Europe and 0–4% in MENA. The magnitude depends on investment costs for solar PV and batteries, resource quality, and the availability of land for wind and solar. Because these factors are more favorable in MENA, the availability of nuclear power has a greater impact on system cost in Europe than in MENA.
- Allowing for optimal transmission expansion decreases the system cost by between 5 and 25%. The highest cost decrease (25%) is found when PV and batteries are high-cost, due to a corresponding higher share of wind power which is favored by transmission, since it smooths out wind variations. The cost impact from optimal transmission is similar in Europe and MENA.

In summary, socio-political factors, here exemplified by whether nuclear power is included as a technology option, whether international transmission is possible, and the extent of land available for wind and solar farms, have markedly different impacts on results depending on the region (weather and demand conditions) and the cost of solar PV and storage capacity. Any judgment on the necessity of a specific socio-political factor for the realization of a decarbonized power system is contingent on assumptions regarding, for instance, investment costs and region. We also conclude that while the land available for wind and solar exploitation, which is affected by public acceptance issues, seems important for the system cost, this issue has not been investigated as thoroughly as other factors in model-based research. Future research could explore its importance in greater detail, with more realistic assumptions on restrictions for wind and solar expansion.

Author contribution

Hanna Ek Fälth: Conceptualization, Methodology, Formal analysis, Writing – original draft, Writing – review & editing. Dan Atsmon: Conceptualization, Methodology, Formal analysis, Writing – original draft. Lina Reichenberg: Conceptualization, Methodology, Writing – original draft, Writing – review & editing, Supervision. Vilhelm Verendel: Methodology, Writing – original draft

Declaration of competing interest

The authors declare that they have no known competing financial interests or personal relationships that could have appeared to influence the work reported in this paper.

Acknowledgements

The authors would like to acknowledge Niclas Mattsson for his generous help in using the GlobalEnergyGIS package.

Appendix A. Supplementary data

Supplementary data to this article can be found online at https://doi.org/10.1016/j.esr.2020.100590.

References

[1] Spm-Ipcc-Wgii, IPCC, 2014: Summary for Policymakers, in: Climate Change 2014, Mitigation of Climate Change, Climate change, 2014.
[2] C. Wolfram, O. Shelef, P. Gertler, How will energy demand develop in the developing world? J. Econ. Perspect. 26 (February 2012) 119–138.
[3] J.H. Williams, A. DeBenedictis, R. Ghanadan, A. Mahone, J. Moore, W.R. Morrow, S. Price, M.S. Torn, The Technology Path to Deep Greenhouse Gas Emissions Cuts by 2050: the Pivotal Role of Electricity, Science, 2011.
[4] D.P. Schlachtberger, T. Brown, M. Schäfer, S. Schramm, M. Greiner, Cost Optimal Scenarios of a Future Highly Renewable European Electricity System: Exploring the Influence of Weather Data, Cost Parameters and Policy Constraints, 2018 arXiv preprint arXiv:1803.09711.
[5] L. Reichenberg, F. Hedenus, M. Odenberger, F. Johnsson, "The marginal system lcoe of variable renewables–evaluating high penetration levels of wind and solar in europe, Energy 152 (2018) 914–924.
[6] T. Brown, D. Schlachtberger, A. Kies, S. Schramm, M. Greiner, Synergies of sector coupling and transmission reinforcement in a cost-optimised, highly renewable european energy system, Energy 160 (2018) 720–739.
[7] T. Tröndle, J. Lilliestam, S. Marelli, S. Pfenninger, Trade-offs between Geographic Scale, Cost, and Infrastructure Requirements for Fully Renewable Electricity in Europe, Joule, 2020.
[8] M. Child, C. Kemfert, D. Bogdanov, C. Breyer, Flexible electricity generation, grid exchange and storage for the transition to a 100% renewable energy system in europe, Renew. Energy 139 (2019) 80–101.
[9] A. Patt, N. Komendantova, A. Battaglini, J. Lilliestam, Regional integration to support full renewable power deployment for europe by 2050, Environ. Polit. 20 (5) (2011) 727–742.
[10] L.d.S.N. S. Barbosa, D. Bogdanov, P. Vainikka, C. Breyer, Hydro, wind and solar power as a base for a 100% renewable energy supply for south and central America, PloS One 12 (3) (2017), e0173820.
[11] D.P. Schlachtberger, T. Brown, S. Schramm, M. Greiner, The benefits of cooperation in a highly renewable european electricity network, Energy 134 (2017) 469–481.
[12] A.E. MacDonald, C.T. Clack, A. Alexander, A. Dunbar, J. Wilczak, Y. Xie, Future cost-competitive electricity systems and their impact on us co 2 emissions, Nat. Clim. Change 6 (5) (2016) 526.

[13] M. Haller, S. Ludig, N. Bauer, Decarbonization scenarios for the eu and mena power system: considering spatial distribution and short term dynamics of renewable generation, Energy Pol. 47 (2012) 282–290.

[14] D. Bogdanov, C. Breyer, North-east asian super grid for 100% renewable energy supply: optimal mix of energy technologies for electricity, gas and heat supply options, Energy Convers. Manag. 112 (2016) 176–190.

[15] A. Aghahosseini, D. Bogdanov, C. Breyer, Towards sustainable development in the mena region: analysing the feasibility of a 100% renewable electricity system in 2030, Energy Strategy Reviews 28 (2020) 100466.

[16] C. Breyer, D. Bogdanov, A. Aghahosseini, A. Gulagi, M. Child, A.S. Oyewo, J. Farfan, K. Sadovskaia, P. Vainikka, Solar photovoltaics demand for the global energy transition in the power sector, Prog. Photovoltaics Res. Appl. 26 (8) (2018) 505–523.

[17] N.A. Sepulveda, J.D. Jenkins, F.J. de Sisternes, R.K. Lester, The Role of Firm Low-Carbon Electricity Resources in Deep Decarbonization of Power Generation, Joule, 2018.

[18] M.Z. Jacobson, M.A. Delucchi, M.A. Cameron, B.V. Mathiesen, Matching demand with supply at low cost in 139 countries among 20 world regions with 100% intermittent wind, water, and sunlight (wws) for all purposes, Renew. Energy 123 (2018) 236–248.

[19] G. Pleßmann, M. Erdmann, M. Hlusiak, C. Breyer, Global energy storage demand for a 100% renewable electricity supply, Energy Procedia 46 (2014) 22–31.

[20] C. Breyer, D. Bogdanov, A. Gulagi, A. Aghahosseini, L.S. Barbosa, O. Koskinen, M. Barasa, U. Caldera, S. Afanasyeva, M. Child, et al., On the role of solar photovoltaics in global energy transition scenarios, Prog. Photovoltaics Res. Appl. 25 (8) (2017) 727–745.

[21] M.Z. Jacobson, M.A. Delucchi, Z.A. Bauer, S.C. Goodman, W.E. Chapman, M. A. Cameron, C. Bozonnat, L. Chobadi, H.A. Clonts, P. Enevoldsen, et al., 100% clean and renewable wind, water, and sunlight all-sector energy roadmaps for 139 countries of the world, Joule 1 (1) (2017) 108–121.

[22] A. Gulagi, D. Bogdanov, M. Fasihi, C. Breyer, Can Australia power the energy-hungry asia with renewable energy? Sustainability 9 (2) (2017) 233.

[23] A. Gulagi, D. Bogdanov, C. Breyer, A cost optimized fully sustainable power system for southeast asia and the pacific rim, Energies 10 (5) (2017) 583.

[24] G. Pleßmann, P. Blechinger, How to meet eu ghg emission reduction targets? a model based decarbonization pathway for europe's electricity supply system until 2050, Energy Strategy Reviews 15 (2017) 19–32.

[25] H.C. Gils, Y. Scholz, T. Pregger, D.L. de Tena, D. Heide, Integrated modelling of variable renewable energy-based power supply in europe, Energy 123 (2017) 173–188.

[26] E.H. Eriksen, L.J. Schwenk-Nebbe, B. Tranberg, T. Brown, M. Greiner, Optimal heterogeneity in a simplified highly renewable european electricity system, Energy 133 (2017) 913–928.

[27] A. Aghahosseini, D. Bogdanov, C. Breyer, A techno-economic study of an entirely renewable energy-based power supply for north America for 2030 conditions, Energies 10 (8) (2017) 1171.

[28] W.D. Grossmann, I. Grossmann, K.W. Steininger, Distributed solar electricity generation across large geographic areas, part i: a method to optimize site selection, generation and storage, Renew. Sustain. Energy Rev. 25 (2013) 831–843.

[29] M. Huber, A. Roger, T. Hamacher, Optimizing long-term investments for a sustainable development of the asean power system, Energy 88 (2015) 180–193.

[30] A. Blakers, B. Lu, M. Stocks, 100% renewable electricity in Australia, Energy 133 (2017) 471–482.

[31] M. Benasla, D. Hess, T. Allaoui, M. Brahami, M. Denaï, "The transition towards a sustainable energy system in europe: what role can north africa's solar resources play? Energy Strategy Reviews 24 (2019) 1–13.

[32] DESERTEC, "Desertec press archive." http://www.desertec.org/press. Date: [Dec. 18, 2018].

[33] A. Aghahosseini, D. Bogdanov, C. Breyer, The mena super grid towards 100% renewable energy power supply by 2030, in: 11th International Energy Conference, 2016, pp. 30–31.

[34] S. Batel, Research on the social acceptance of renewable energy technologies: past, present and future, Energy Research & Social Science 68 (2020) 101544.

[35] A. Battaglini, N. Komendantova, P. Brtnik, A. Patt, Perception of barriers for expansion of electricity grids in the European Union, Energy Pol. 47 (2012) 254–259.

[36] M. Harper, B. Anderson, P. James, A. Bahaj, Assessing socially acceptable locations for onshore wind energy using a gis-mcda approach, Int. J. Low Carbon Technol. (2019).

[37] G. Ellis, G. Ferraro, The Social Acceptance of Wind Energy: where We Stand and the Path Ahead, Jrc Science for Policy Report, European Commission, Joint Research Centre, Directorate for Nuclear Safety and Security, Brussels, 2016.

[38] P. Roddis, S. Carver, M. Dallimer, P. Norman, G. Ziv, The role of community acceptance in planning outcomes for onshore wind and solar farms: an energy justice analysis, Appl. Energy 226 (2018) 353–364.

[39] K. Borch, A.K. Munk, V. Dahlgaard, Mapping wind-power controversies on social media: facebook as a powerful mobilizer of local resistance, Energy Pol. 138 (2020) 111223.

[40] M. Neukirch, "Protests against German electricity grid extension as a new social movement? a journey into the areas of conflict," Energy, Sustainability and Society 6 (2016).

[41] Þorkell Stefánsson, A.D. Sæþórsdóttir, C.M. Hall, When tourists meet transmission lines: the effects of electric transmission lines on tourism in Iceland, Energy Research & Social Science 34 (2017) 82–92.

[42] P. Schmidt, J. Lilliestam, Reducing or fostering public opposition? a critical reflection on the neutrality of pan-european cost"benefit analysis in electricity transmission planning, Energy Research & Social Science 10 (2015) 114–122.

[43] S. Bolwig, T.F. Bolkesjø, A. Klitkou, P.D. Lund, C. Bergaentzlé, K. Borch, O.J. Olsen, J.G. Kirkerud, Y. kuang Chen, P.A. Gunkel, K. Skytte, Climate-friendly but socially rejected energy-transition pathways: the integration of techno-economic and socio-technical approaches in the nordic-baltic region, Energy Research & Social Science 67 (2020) 101559.

[44] V. Bertsch, M. Hall, C. Weinhardt, W. Fichtner, Public acceptance and preferences related to renewable energy and grid expansion policy: empirical insights for Germany, Energy 114 (2016) 465–477.

[45] X. Yuan, J. Zuo, R. Ma, Y. Wang, How would social acceptance affect nuclear power development? a study from China, J. Clean. Prod. 163 (2017) 179–186 (Achieving Low/no Fossil-carbon Economies based upon the Essential Transformations to Support them).

[46] B.B. Wittneben, The impact of the fukushima nuclear accident on european energy policy, Environ. Sci. Pol. 15 (1) (2012) 1–3.

[47] E.A. Rosa, R.E. Dunlap, Poll trends: nuclear power: three decades of public opinion, Publ. Opin. Q. 58 (2) (1994) 295–324.

[48] Y. Kim, M. Kim, W. Kim, Effect of the fukushima nuclear disaster on global public acceptance of nuclear energy, Energy Pol. 61 (2013) 822–828.

[49] Aljazeera, Jordan nuclear battle heats up. https://www.aljazeera.com/news/middleeast/2014/02/battle-heats-up-over-jordanian-nuclear-power-201422685957126736.html, 2014.

[50] E. Smith, H. Klick, Explaining nimby opposition to wind power, in: Annual Meeting of the American Political Science Association, 2007, pp. 1–19.

[51] J.E. Carlisle, S.L. Kane, D. Solan, M. Bowman, J.C. Joe, Public attitudes regarding large-scale solar energy development in the US, Renew. Sustain. Energy Rev. 48 (2015) 835–847.

[52] B.P. Heard, B.W. Brook, T.M. Wigley, C.J. Bradshaw, Burden of proof: a comprehensive review of the feasibility of 100% renewable-electricity systems, Renew. Sustain. Energy Rev. 76 (2017) 1122–1133.

[53] T. Brown, T. Bischof-Niemz, K. Blok, C. Breyer, H. Lund, B.V. Mathiesen, "Response to â€burden of proof: a comprehensive review of the feasibility of 100% renewable-electricity systems', Renew. Sustain. Energy Rev. 92 (2018) 834–847.

[54] J. Parsons, J. Buongiorno, M. Corradini, D. Petti, A Fresh Look at Nuclear Energy, 2019.

[55] S. Hong, S. Qvist, B.W. Brook, Economic and environmental costs of replacing nuclear fission with solar and wind energy in Sweden, Energy Pol. 112 (2018) 56–66.

[56] C. Jägemann, M. Fürsch, S. Hagspiel, S. Nagl, "Decarbonizing europe's power sector by 2050 analyzing the economic implications of alternative decarbonization pathways, Energy Econ. 40 (2013) 622–636.

[57] R. Pattupara, R. Kannan, "Alternative low-carbon electricity pathways in Switzerland and itâ€™s neighbouring countries under a nuclear phase-out scenario, Appl. Energy 172 (2016) 152–168.

[58] C.M. Grams, R. Beerli, S. Pfenninger, I. Staffell, H. Wernli, "Balancing europeâ€™s wind-power output through spatial deployment informed by weather regimes, Nat. Clim. Change 7 (8) (2017) 557–562.

[59] J. Hörsch, T. Brown, The role of spatial scale in joint optimisations of generation and transmission for european highly renewable scenarios, in: 2017 14th International Conference on the European Energy Market (EEM), IEEE, 2017, pp. 1–7.

[60] G. Brunekreeft, R. Meyer, Cross-Border Electricity Interconnectors in the EU: the Status Quo, Springer International Publishing, Cham, 2019, pp. 433–451.

[61] D. Ritter, R. Meyer, M. Koch, M. Haller, D. Bauknecht, C. Heinemann, Effects of a delayed expansion of interconnector capacities in a high res-e european electricity system, Energies 12 (16) (2019) 3098.

[62] National-Renewable-Energy-Laboratory, Annual Technology Baseline, 2018 Data, 2018. Okt. 18, https://atb.nrel.gov/. Date.

[63] W.J. Cole, C. Marcy, V.K. Krishnan, R. Margolis, Utility-scale lithium-ion storage cost projections for use in capacity expansion models, in: North American Power Symposium (NAPS), IEEE, 2016, pp. 1–6, 2016.

[64] World Energy Council, World Energy Resources — Hydropower, World Energy Council, 2016.

[65] N. Mattsson, V. Verendel, F. Hedenus, and L. Reichenberg, "An autopilot for energy models – automatic generation of renewable supply curves, hourly capacity factors and hourly synthetic electricity data for arbitrary world regions." Forthcoming. Energy Strategy Reviews.

[66] N. Mattson, "GlobalenergyGIS.jl - automatic generation of renewable energy input data for energy models in arbitrary world regions using public datasets." https://github.com/niclasmattsson/GlobalEnergyGIS.

[67] M. Berglund, P. Börjesson, Assessment of energy performance in the life-cycle of biogas production, Biomass Bioenergy 30 (3) (2006) 254–266.

[68] N. Scarlat, J.-F. Dallemand, F. Fahl, Biogas: developments and perspectives in europe, Renew. Energy 129 (2018) 457–472.

[69] H. Lorenz, P. Fischer, B. Schumacher, P. Adler, Current eu-27 technical potential of organic waste streams for biogas and energy production, Waste Manag. 33 (11) (2013) 2434–2448.

[70] P. Weiland, Biogas production: current state and perspectives, Appl. Microbiol. Biotechnol. 85 (2010) 849–860.

[71] IEA-ETSAP, Technology Brief Electricity Transmission and Distribution, Energy Technology Systems Analysis Program, Paris, 2014.

[72] National-Renewable-Energy-Laboratory, Jedi transmission line impact model. https://www.nrel.gov/docs/fy14osti/60250.pdf, 2013.

[73] ABB, Introducing HVDC, 2014.

[74] D. GarcÃ-a-Gusano, K. Espegren, A. Lind, M. Kirkengen, The role of the discount rates in energy systems optimisation models, Renew. Sustain. Energy Rev. 59 (2016) 56–72.
[75] C. For International Earth Science Information Network (CIESIN)â€"Columbia University, "Gridded Population of the World, Version 4 (Gpwv4): Population Density, 2016.
[76] M.A. Friedl, D. Sulla-Menashe, B. Tan, A. Schneider, N. Ramankutty, A. Sibley, X. Huang, Modis collection 5 global land cover: algorithm refinements and characterization of new datasets, Remote Sens. Environ. 114 (1) (2010) 168–182.
[77] V. Kapos, Unep-wcmc web site: mountains and mountain forests, Mt. Res. Dev. 20 (4) (2000), 378–378.
[78] C. Amante, B. Eakins, Etopo1 1 Arc-Minute Global Relief Model Procedures, Data Sources and Analysis: Noaa Technical Memorandum Nesdis Ngdc-24, vol. 10, National Geophysical Data Center, NOAA, 2009, p. V5C8276M.
[79] ECMWF, Ecmwf era5 reanalysis dataset, Feb. 19, https://www.ecmwf.int/en/forecasts/datasets/archive-datasets/reanalysis-datasets/era5. Date, 2019.
[80] The-World-Bank-Group, Global wind atlas, Feb. 19, https://globalwindatlas.info/. Date, 2019.
[81] D.E. Gernaat, P.W. Bogaart, D.P. van Vuuren, H. Biemans, R. Niessink, High-resolution assessment of global technical and economic hydropower potential, Nature Energy 2 (10) (2017) 821.
[82] B. Lehner, C.R. Liermann, C. Revenga, C. Vörösmarty, B. Fekete, P. Crouzet, P. Döll, M. Endejan, K. Frenken, J. Magome, et al., High-resolution mapping of the world's reservoirs and dams for sustainable river-flow management, Front. Ecol. Environ. 9 (9) (2011) 494–502.
[83] J.H. Friedman, Greedy function approximation: a gradient boosting machine, Ann. Stat. (2001) 1189–1232.
[84] K. Riahi, D.P. Van Vuuren, E. Kriegler, J. Edmonds, B.C. Oâ€™neill, S. Fujimori, N. Bauer, K. Calvin, R. Dellink, O. Fricko, et al., The shared socioeconomic pathways and their energy, land use, and greenhouse gas emissions implications: an overview, Global Environ. Change 42 (2017) 153–168.
[85] E. Doxsey-Whitfield, K. MacManus, S.B. Adamo, L. Pistolesi, J. Squires, O. Borkovska, S.R. Baptista, Taking advantage of the improved availability of census data: a first look at the gridded population of the world, version 4, Papers in Applied Geography 1 (3) (2015) 226–234.
[86] R. Gelaro, W. McCarty, M.J. Suárez, R. Todling, A. Molod, L. Takacs, C.A. Randles, A. Darmenov, M.G. Bosilovich, R. Reichle, et al., The modern-era retrospective analysis for research and applications, version 2 (merra-2), J. Clim. 30 (14) (2017) 5419–5454.
[87] Bp, Bp Statistical Review of World Energy 2016, 2018. London, UK.
[88] Y. Wan, Long-term Wind Power Variability, National Renewable Energy Lab. (NREL), Golden, CO (United States), 2012 tech. rep.
[89] C.M.S. Martin, J.K. Lundquist, M.A. Handschy, Variability of interconnected wind plants: correlation length and its dependence on variability time scale, Environ. Res. Lett. 10 (4) (2015), 044004.
[90] Entso-E, "Entso-e grid map." https://www.entsoe.eu/data/map/. Date: [June, 6, 2019].
[91] Arab Union of Electricity, "Electrical networks maps in arab countries." http://auptde.org/default.aspx?lang=en. Date: [Jan. 26, 2019].
[92] F. Cebulla, T. Fichter, Merit order or unit-commitment: how does thermal power plant modeling affect storage demand in energy system models? Renew. Energy 105 (2017) 117–132.

Paper B

Trade-offs between aggregated and turbine-level representations of hydropower in optimization models

Renewable and Sustainable Energy Reviews 183 (2023) 113406

Contents lists available at ScienceDirect

Renewable and Sustainable Energy Reviews

journal homepage: www.elsevier.com/locate/rser

Original research article

Trade-offs between aggregated and turbine-level representations of hydropower in optimization models

H. Ek Fälth *, N. Mattsson, L. Reichenberg, F. Hedenus

Department of Space, Earth and Environment, Chalmers University of Technology, Gothenburg, Sweden

ARTICLE INFO

Keywords:
Hydropower
Modeling
Aggregation
Head
River network
Turbine efficiencies
Energy system models

ABSTRACT

To model a future power system with high shares of variable renewables, it is essential to capture the flexibility of dispatchable technologies such as hydropower. However, the representation of hydropower is often oversimplified in energy system investment models, such that the flexibility of hydropower is significantly exaggerated. This suggests the need for improved representations of hydropower that capture physical river dynamics but are computationally efficient to maintain the tractability of large models. Here, we develop a series of hydropower optimization models for a single river with various levels of techno-physical detail to evaluate options for hydropower representations in energy system investment models. All models operate hourly over a full year with perfect foresight. We explore trade-offs between accuracy and computational time involved in including features such as the river network, head-dependent power production, and discharge-dependent turbine efficiencies. We find that the level of detail significantly affects the optimal production and confirm that a simplistic hydropower representation similar to those often used in investment models significantly overestimates the flexibility of hydropower. The most detailed nonconvex model includes a full river network, head-dependency, and turbine efficiencies and is solved in just one hour on a modern desktop computer. Furthermore, we linearize this detailed model, thereby reducing computation time to one minute while featuring production dynamics substantially more similar to the full nonconvex model than a naive linear network model. These contributions pave the way for improving hydropower representations in investment models to avoid overestimating the flexibility that hydropower may provide.

1. Introduction

Flexibility measures, such as transmission, storage, flexible renewable production, demand-side management, and sector-coupling, are essential components of a future renewable power system with high shares of variable renewables [1–4]. These strategies ensure that the demand can be met at all times despite variations in wind and solar power production levels. Reservoir hydropower[1] can be dispatchable on time scales from seconds to months and therefore serves as such a flexibility measure. Modeling hydropower with a realistic level of flexibility becomes more important when assessing its role in future renewable power systems as the share of variable renewables increases, since the level of flexibility afforded by hydropower affects the need for other variation management strategies. Hence, how hydropower is modeled is of interest to both the modeling community and policy-makers that use model results to inform their decisions on energy systems and their variation management strategies.

In a typical river hydropower system, there are usually several reservoirs and plants connected by waterways with delay times for the water flowing between the plants. For each plant along the river, environmental permits may constrain, for instance, how much water can or must be released at certain times, and they also often regulate the water levels in the reservoirs at different times of the year. The network structure of plants, reservoirs, and waterways within a river, the delay times, and the environmental constraints are referred to as the network effect in this study. Moreover, hydropower production is head-dependent, where the head[2] varies with the water levels, which in turn vary with power production and water inflow. Furthermore, each plant can contain one or more turbines, whereby the turbine efficiency varies with the discharge and head, depending on the design of the turbine.

However, due to computational limitations and a lack of available data, the representation of hydropower is often highly simplified in

* Corresponding author.
E-mail address: hanna.ek.falth@chalmers.se (H. Ek Fälth).

[1] Hereinafter, 'Reservoir hydropower' will simply be denoted as 'hydropower'. Note that it is always reservoir hydropower that is intended, i.e., hydropower plants connected to reservoirs, and never pumped hydropower or run-of-river hydropower.

[2] The height that the water drops, resulting in a loss of potential energy, which is converted to power via the turbines.

https://doi.org/10.1016/j.rser.2023.113406
Received 8 August 2022; Received in revised form 13 April 2023; Accepted 23 May 2023
Available online 12 June 2023

Nomenclature

Abbreviations

LP	Linear programming
NLP	Nonlinear programming
MIQP	Multi integer quadratic programming
RMSD	Root mean square deviation
PDC	Power duration curve

Indices

h	Hour
n	Hydropower plant
j	Turbine
l	Segments for effective discharge
un	Upstream plant to plant n
F	Forebay
T	Tailwater

Variables

R	Revenue from selling electricity [e]
P	Power production [Wh/h]
V	Reservoir content [HE][3] ([Wh] in Model E)
D	Discharge [m^3/s]
E	Effective discharge [Wh/h]
S	Spilled water [m^3/s] ([Wh/h] in Model E)
H	The height difference used for power production [m]
W	Water level at forebay and tailrace [m a s]

Parameters

p	Hourly power prices
$\hat{c}$	Maximum capacity of the river system in Model E [W]
$\hat{v}$	Reservoir content (volume) [HE] ([Wh] in Model E)
w	Minimum reservoir level according to environmental permits [m a s]
a	Reservoir surface area [HE/m]
η	Turbine efficiency
$\bar{\eta}$ and $\hat{\eta}$	Mean and maximum turbine efficiency
r	Regression parameters for tailrace functions
b	Break points for turbine efficiency curves [m^3/s]
k	Parameters for turbine efficiency curves
m	Large positive penalty constant
i	Inflow [m^3/s] ([Wh/h] in Model E)
ρ	Density of water [g/m^3]
g	Gravitational acceleration, 9.81, [m/s^2]
δ_n	The time it takes for the water to flow to plant n from its upstream plant [h]
$\bar{h}$	Mean head [m]
$\bar{d}$	Mean discharge [m^3/s]
$\bar{e}$	Mean effective discharge [m^3/s]
$f^{\min}$	Minimum forebay level according to environmental permits [m a s]
$f^{\max}$	Maximum forebay level according to environmental permits and dam construction [m a s]
$s^{\min}$	Minimum spillage according to environmental permits [m^3/s]
$d^{\min}$	Minimum flow through either turbine or spillway according to environmental permits [m^3/s]

energy system investment models. In these models, hydropower is usually represented as one power plant per modeled region with its aggregated installed capacity (in W) and reservoir volume (in Wh), together with an inflow profile to the reservoir (in Wh) [2,5–10]. In reality, the network effect, the head-dependency, and the turbine efficiency curves constitute physical and technical constraints imposed on the hydropower production of a river system. Thus, a model that does not incorporate these constraints overestimates the flexibility of hydropower and, thereby, the flexibility that it can provide for a system based on renewables.

There exist models for hydropower production planning that capture all or some of the above-listed characteristics (network effects, head-dependency, and turbine efficiency curves) [11–23]. These models aim to identify the optimal hourly production for a set of hydropower plants in a given energy system. This is achieved by either maximizing the hydropower revenue given a price signal or maximizing the hydropower energy output, depending on the market setting. Detailed representations of hydropower have also been included in models designed for hydro-thermal scheduling [24–28], in which the cost of operating the whole energy system is minimized. A common strategy in hydropower production planning and hydro-thermal scheduling is to use a less detailed model to find the optimal strategy for the reservoirs in the long term (years), which is subsequently used to establish boundary conditions for a more detailed hydropower model for short-term planning (days to a few weeks). The long-term models use a low time resolution and often disregard network effects and head-dependency. In contrast, the short-term models use a high temporal resolution and capture more of the characteristics of hydropower, albeit for only a short time horizon. To our knowledge, no models in the literature combine a detailed representation of the hydropower system with a high temporal resolution and long horizons.

In both production planning and hydro-thermal scheduling models, the installed generation, storage, and transmission capacities are assumed to be constant. In contrast, energy system investment models optimize investments in capacity and hourly operation of the system simultaneously. Therefore, for the purpose of quantifying the need for investments in flexible power production, transmission, and storage in a system with high shares of variable renewables, both a high temporal resolution and a long time horizon are prerequisites in investment models [29–31]. This motivates the investigation of hydropower models that operate with an hourly resolution for a full year.

There have been efforts in the literature to improve the endogenous hydropower representations in energy system investment models. Liu et al. [32] include the network effect, and Ramírez-Sagner and Muñoz [33] model one head-dependent hydropower plant. Stevanato et al. [34] improve an energy system optimization model by directly including the network effect and accounting for head-dependency by iteratively softlinking an external head calculation. Although alternative ways to represent hydropower in energy system models have been suggested, no systematic investigation of which characteristics to include has been reported in the literature. For this reason, we isolate hydropower and explore the full continuum between detailed and highly aggregated model versions. This lets us directly evaluate how including different characteristics contribute to a realistic assessment of the flexibility of hydropower, as well as trade-offs with computational effort. The overarching goal is to provide a stepping stone toward

[3] One HE, Hour Equivalent, corresponds to the volume of a flow of 1 m^3/s during 1 h, i.e., 1 HE = 3600 m^3.

finding hydropower representations suitable for implementation in energy system models.

In this study, we develop several different hydropower models for a single river, with varying degrees of physical and technological detail, and compare them to each other and to the simple aggregated approach used in investment models. These are all optimization models with hourly resolution over a full year that maximizes the revenue from the total production in one river, given exogenous prices and water inflow with perfect foresight. The most detailed model developed for this study includes (i) the network structure encompassing all the hydropower plants and waterways within a river, including the time that it takes for the water to flow between the different plants and the environmental constraints applied to each plant and reservoir; (ii) head-dependent power production; and (iii) nonconvex, discharge-dependent turbine efficiencies. The literature suggests various ways to model hydropower, with different choices regarding which constraints to include or exclude. However, no comparison of models that include or exclude these physical and technological details (i—iii) has been reported in the literature.

This work has the following research aims:

1. To examine the extent to which an aggregated hydropower model differs from a more physically sound model that includes network effects, head-dependency, and discharge-dependent turbine efficiencies. The goal here is to highlight the features of optimal hydropower generation that are omitted in typical formulations in investment models.
2. To explore the trade-offs between accuracy and computational time for different hydropower models, including various characteristics of hydropower. The goal is to evaluate the potential merits of using all the characteristics, rather than only a select few.
3. To evaluate the accuracy loss and computational gains of a novel linearization of head- and discharge-dependent hydropower production using Taylor approximation.

By addressing these three issues, this study takes a step toward finding a hydropower representation that captures a realistic level of flexibility while being computationally fast enough to potentially implement in energy system optimization models.

2. Method

This section provides an overview of all models developed and evaluated in this study, a presentation of the model formulations, and some comments on how we deal with nonconvexity. Lastly, a description of the river that was used as a test case is provided.

2.1. An overview of all models

We develop several hydropower models with various levels of physical and technological detail. Table 1 and Fig. 1 present a conceptual overview of all the models tested in this study. These models have in common exogenous deterministic water inflow and electricity prices, and the objective function to maximize the total revenue for the production from the river with perfect foresight. Models A, A:MIP, B, B:L, C, and D all include the network effect (river structure), i.e., they explicitly model all the power plants in a river, with each plant having one or more turbines. They differ in terms of whether or not power production in each turbine is head-dependent and in whether turbine efficiencies are nonconvex, convex or linear. In contrast, the least detailed model, Model E, which is designed to replicate the aggregated representations often used in investment models, consists of only one power plant and one reservoir. In Model E, the power production is constrained only by the reservoir content and the installed capacity.

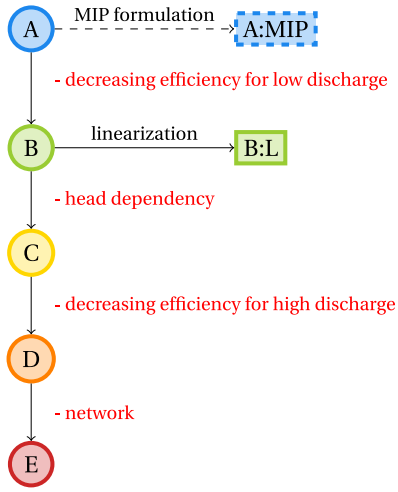

Fig. 1. Conceptual overview of the models, from most detailed (Model A) to the simplest (Model E). Red text indicates features that are removed between the model variants.

2.2. Main differences between the model variants

The power output (P) from a hydropower turbine is proportional to the head (H), discharge of water (D), and discharge-dependent turbine efficiency (η), as shown in Eq. (1).

$$P \propto H \cdot D \cdot \eta(D) \tag{1}$$

Our most detailed model (Model A) features the network effect, head-dependent production, and nonlinear discharge-dependent turbine efficiencies. A typical turbine efficiency curve is shown in the top panel of Fig. 2 (thick black line). Capturing the nonlinear shape of these efficiency curves while simultaneously allowing operation at zero discharge and zero power output necessarily introduces nonconvexity in Model A (see Section 2.3 for a description of how turbine efficiencies are implemented in the models). Another nonconvexity present in Model A is the power production equation itself (Eq. (1)), which can be rewritten as two bilinear functions by combining the discharge-dependencies, as described in Section 2.3.

In Model B, turbine efficiencies are relaxed and made convex (as described in Section 2.3). However, Model B remains nonconvex due to the nonconvex power production equation (Eq. (1)). Model B:L is a linearized version of Model B and represents a novel contribution of this study. Its purpose is to capture most of the complex dynamics of Models A and B, albeit with vastly reduced computational effort. We derive Model B:L by performing a Taylor expansion of the bilinear power equation and by replacing the convex turbine efficiency curve of Model B with multiple linear constraints. This results in a pure linear programming (LP) model. We evaluate the accuracy of the linearized model by comparing it with the bilinear Models A and B.

Model C is similar to Model B, although it eliminates the head-dependency by assuming a constant head. This also produces an LP model after applying the same linear representation of turbine efficiency as in Model B:L. Model D is further simplified by assuming constant turbine efficiencies.

In addition to these models, Model A:MIP (Fig. 1) is a mixed-integer quadratic program (MIQP) formulation of Model A, which arises because a bilinear product is a nonconvex quadratic function. Model A:MIP does not solve to optimum due to the size of the problem

Table 1
The seven hydropower models evaluated and compared in this study.

Model name	Network effect	Head-dependent	Turbine efficiency (see Fig. 2)	Aggregation level	Type
A	Yes	Yes	Nonconvex nonlinear	Turbine	NLP (nonconvex)
A:MIP	Yes	Yes	Nonconvex (multiple linear constraints)	Turbine	MIQP
B	Yes	Yes	Convex nonlinear	Turbine	NLP (nonconvex)
B:L	Yes	Yes (linearized)	Linear (multiple constraints)	Turbine	LP
C	Yes	No	Linear (multiple constraints)	Turbine	LP
D	Yes	No	Linear (single constant)	Turbine	LP
E	No	No	None	River	LP

(210,000 binary variables); in any case, it is not intended for use as a full model variant. The purpose of Model A:MIP is twofold. First, the LP root relaxation from the branch-and-bound algorithm (or subsequent integer solutions) can be used as a warm start to Model A. Second, the best integer solution of the branch-and-bound node tree produces an upper bound to the original problem, which is useful for evaluating locally optimal NLP solutions to Model A. Both of these areas of use are described in more detail in Section 2.5.

2.3. Turbine efficiency and effective discharge

In this study, turbine efficiencies (which are discharge-dependent[4] [16]) are incorporated into the variable effective discharge (E), which is defined as the product of discharge (D) and turbine efficiency (η):

$$E = D \cdot \eta(D) \tag{2}$$

The purpose of this substitution is to combine two discharge dependencies of Eq. (1) so the main power equation becomes bilinear instead of trilinear, c.f. its formulation in Model A (Eq. (4)). In this manner, the problem becomes quadratic, so quadratic solvers can be applied (e.g. to Model A:MIP); alternatively, further simplifications can make the model equations convex. However, Eq. (2) is not explicitly included in the models. Instead of using turbine efficiency curves, each model variant has its equation for discharge-dependent effective discharge (except Model E, which does not model water discharge explicitly).

The empirical relationship between each turbine's efficiency and discharge is established by analyzing historical data relating to discharge, head, and production for all turbines.[5] The efficiency reaches its maximum at a particular discharge level (different for each turbine in the river) and decreases for lower and higher levels of discharge. Fig. 2 illustrates the assumptions related to effective discharge (bottom panel) and the corresponding turbine efficiencies (top panel) for the various models. In Models A, A:MIP, B, B:L, and C, we model effective discharge as a second-degree polynomial of discharge for mid to high values of discharge, with coefficients estimated from historical data. In the models, operating at low discharge is endogenously discouraged because of low efficiency; in real-world turbines, cavitation and other physical effects can also restrict operation in this regime.

Model A captures the decreasing efficiency at higher and lower discharge levels than its point of maximum efficiency (see thick blue dashed line in Fig. 2). This results in a nonconvex constraint; the nonconvexity arises from the linear segment for low discharge levels, which excludes regions where the turbine curve polynomial would have negative efficiency (i.e., after it intersects the x-axis) but still allows zero discharge through the turbine. The reason for assuming a low arbitrary constant positive efficiency (30%) rather than zero is to ensure a downward slope for the effective discharge, so as to facilitate approaching the optimum for the solver.

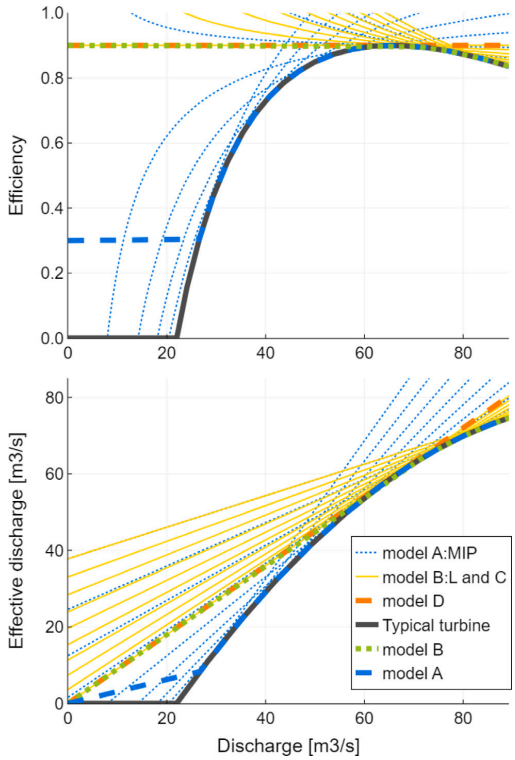

Fig. 2. Constraints for effective discharge (bottom panel) in the different model variants, and corresponding turbine efficiency (top panel). For models A:MIP, B:L, and C, linear constraints for effective discharge appear as curved lines in the top panel after dividing by the discharge to obtain the corresponding efficiency.

For Model A:MIP, effective discharge is modeled using multiple linear constraints (blue dotted lines, bottom panel) to approximate the turbine curves. Instead of the linear segment used in Model A, Model A:MIP uses logic implemented with binary variables to make the model choose between activating the linear constraints or operating at the origo, i.e., zero efficiency and zero discharge (turbine turned off).

For Model B (dotted green line), a high constant efficiency is assumed at low discharge levels, whereas the nonlinear curve of Model A is used at mid to high discharge levels. This is similar to the approach used in [17]. In Models B:L and C, we linearize the polynomial in Model B by approximating it with multiple linear constraints (yellow lines).

[4] Turbine efficiencies are also head-dependent, an aspect neglected in this study. However, for the river modeled in this study, the discharge dependency is much stronger than the head-dependency.

[5] Thus, the generator efficiency is also incorporated into what we call "turbine efficiency".

Finally, Model D uses a constant turbine efficiency for all discharge values (dashed orange line), as described previously [32,33].

2.4. Model formulations

This section gives an overview of the seven different model formulations implemented and compared in this study. With respect to notation, variables are written with an initial uppercase letter, and parameters are indicated with an initial lowercase letter. The nomenclature is found in the table at the beginning of the paper. All model implementations are publicly available at [35].

The objective function in all the models is to maximize revenue (R), given by the total hourly power production (P) multiplied by the hourly power price (p), as shown here. The indices h, n, and j correspond to hour, plant, and turbine, respectively.

$$R = \sum_{h,n,j} P_{h,n,j} \cdot p_h \tag{3}$$

2.4.1. Model A

Power production (P) in a hydropower plant is given by the change of potential energy of the water when it flows from a higher to a lower position (the height difference is called head, H), with a turbine-specific, discharge-dependent conversion efficiency [16]. We introduce a variable named effective discharge (E), which is the product of the discharge and the turbine efficiency (see Eq. (2) in Section 2.3). This allows us to express power production as follows (note that each hydropower plant can hold multiple turbines):

$$P_{h,n,j} \le E_{h,n,j} \cdot H_{h,n} \cdot \rho \cdot g \tag{4}$$

Effective discharge (E) is modeled (for each turbine within each hydropower plant) as a second-degree polynomial in the discharge variable (D), with an additional linear segment for low discharge levels (see dashed blue lines in Fig. 2).

$$E_{h,n,j} \le \begin{cases} k_{0,n,j} \cdot D_{h,n,j} & \text{if } D_{h,n,j} \le b_{n,j} \\ \sum_{i=1}^{3} k_{i,n,j} \cdot D_{h,n,j}^{i-1} & \text{if } D_{h,n,j} > b_{n,j} \end{cases} \tag{5}$$

Both constraints (4) and (5) are implemented as inequalities to improve the robustness of the nonlinear solver. However, they are pushed towards equality at optimum by profit maximization.

A water continuity equation balances reservoir content (V) and water flow between plants, similar to how it is modeled in [25,32,34]. The net water flow (for each hour and plant) is determined by inflow (i), discharge (D), delayed upstream discharge (D), spillage (S), and delayed upstream spillage (S). The index un represents the upstream plant to plant n. δ_n is the time it takes for the water to run from the upstream plant to plant n. The constant factor 1 converts units of flow during 1 h to volume.

$$V_{h,n} = V_{h-1,n} + 1 \cdot (i_{h,n} - \sum_j D_{h,n,j} - S_{h,n} + \sum_j D_{h-\delta_n,un,j} + S_{h-\delta_n,un}) \tag{6}$$

The reservoir content (V) is limited by its maximum capacity ($\hat{v}$).

$$0 \le V_{h,n} \le \hat{v}_n \tag{7}$$

We assume that the forebay level[6] ($W_{h,n}^F$) for a plant increases linearly with its reservoir content, as described in Eq. (8). The tailrace level[7] ($W_{h,n}^T$) depends on the design and geometry of the plant. Here we use linear regression to fit the tailrace water level to historical data on discharge and model it as in Eq. (9), see, e.g., Diniz and Maceira [26] for a similar approach.

$$W_{h,n}^F = w_n + \frac{V_{h,n}}{a_n} \tag{8}$$

$$W_{h,n}^T = r_{0,n} + r_{1,n} \cdot \sum_j D_{h,n,j} \tag{9}$$

Environmental regulations set time-specific limits on minimum spillage ($s^{\min}$), minimum flow ($d^{\min}$), and maximum and minimum forebay levels ($f^{\min}$, $f^{\max}$), as in Eqs. (10)—(12).

$$S_{h,n} \ge s_{h,n}^{\min} \tag{10}$$

$$\sum_j D_{h,n,j} + S_{h,n} \ge d_{h,n}^{\min} \tag{11}$$

$$f_{h,n}^{\min} \le W_{h,n}^F \le f_{h,n}^{\max} \tag{12}$$

The head (H) for each plant is modeled as the difference between the forebay and tailrace water levels, shown in Eq. (13). A similar approach is used in [13,22,26].

$$H_{h,n} = W_{h,n}^F - W_{h,n}^T \tag{13}$$

Since Eqs. (4) and (5) are nonlinear, Model A is a nonlinear program. It is also nonconvex due to the bilinear product of Eq. (4) and the slope of the first segment in Eq. (5).

2.4.2. Model A:MIP

Model A:MIP is a mixed-integer quadratic program. The only difference between Model A:MIP and Model A is the formulation of the effective discharge (see Section 2.3 and Fig. 2). For Model A:MIP, we construct ten linear constraints that approximate the second-degree polynomial for effective discharge. A binary variable is used to indicate if the turbine is on or off, and the "big M" method is used to switch on or off logical constraints, as shown in Eqs. (14) and (15). The first (ramping) segment in Model A is not used in Model A:MIP, as seen in Fig. 2.

$$E_{h,n,j} \le k_{0,n,j,l}^{A:MIP} + k_{1,n,j,l}^{A:MIP} \cdot D_{h,n,j} + m_{n,j} \cdot (1 - Z_{h,n,j}) \quad \forall l \tag{14}$$

$$E_{h,n,j} \le m_{n,j} \cdot (1 - Z_{h,n,j}) \tag{15}$$

Note that Model A:MIP is never solved to optimum. Instead, it is used to obtain an upper bound for Model A and as an alternative warm start to Model A (see Section 2.5).

2.4.3. Model B

The difference between Model A and Model B is that effective discharge (E) is modeled with a (coarse) convex approximation in Model B, where the efficiency is assumed to be constant for low discharge levels (see dotted green line in Fig. 2), following Blom et al. [17]. Thus, Eq. (5) in Model A is replaced with Eq. (16) in Model B. To make the feasible region convex, the first segment is chosen as the polynomial tangent that passes through origo. Note that Eqs. (5) and (16) are functionally identical, except for the breakpoint (b^B) and slope of the first segment (k_0^B).

$$E_{h,n,j} \le \begin{cases} k_{0,n,j}^B \cdot D_{h,n,j} & \text{if } D_{h,n,j} \le b_{n,j}^B \\ \sum_{i=1}^{3} k_{i,n,j} \cdot D_{h,n,j}^{i-1} & \text{if } D_{h,n,j} > b_{n,j}^B \end{cases} \tag{16}$$

Despite the convex effective discharge here, Model B is nonconvex due to the bilinear term in Eq. (4).

2.4.4. Model B:L

For this novel model, we linearize the power production equation of Model B using Taylor expansion. The bilinear product of the head (H) and effective discharge (E) in Eq. (4) is expanded around the mean head ($\bar{h}$) from historical data, and the mean effective discharge ($\bar{e}$), resulting in Eq. (17).

$$P_{h,n,j} \le (E_{h,n,j} \cdot \bar{h}_n + \bar{e}_{n,j} \cdot H_{h,n} - \bar{e}_{n,j} \cdot \bar{h}_n) \cdot \rho \cdot g \tag{17}$$

[6] The water level in the reservoir connected to each plant.
[7] The water level immediately downstream the power plant.

For simplicity (albeit not strictly correct), we calculate the mean effective discharge as the product of the mean discharge ($\bar{d}$) and mean efficiency ($\bar{\eta}$) (from historical data).

$$\bar{e}_{n,j} = \bar{d}_{n,j} \cdot \bar{\eta}_{n,j} \tag{18}$$

To linearize effective discharge, we replace the polynomial in Eq. (16) with ten linear constraints calculated from several of its tangents in a similar way as Eq. (14) for Model A:MIP. The feasible region is made convex using the same approach as in Model B, i.e., by extending the first segment through origo.

$$E_{h,n,j} \le k^{B:L}_{0,n,j,l} + k^{B:L}_{1,n,j,l} \cdot D_{h,n,j} \quad \forall l \tag{19}$$

In all other aspects, Model B:L is identical to Model B. Since all equations are linear, Model B:L forms a linear program.

2.4.5. Model C

In Model C, the head is considered constant, as in [18,24,25,28,32,36–39], and is set at the mean head ($\bar{h}$), retrieved from historical data. Thus, Eq. (4) is replaced with Eq. (20).

$$P_{h,n,j} \le E_{h,n,j} \cdot \bar{h}_{h,n} \cdot \rho \cdot g \tag{20}$$

Effective discharge is linearized as in Model B:L by incorporating Eq. (19). In all other aspects, this model is the same as Model B. Therefore, Model C is also a linear program.

2.4.6. Model D

In Model D, both the turbine efficiency and head are considered constant, as in [18,25,32]. We fix the turbine efficiency at its maximum value ($\hat{\eta}$), see the orange dashed line in Fig. 2, and the head at its mean value (from historical data). Thus, the effective discharge is proportional to discharge as described in Eq. (21). The power production equation is the same as in Model C, i.e., Eq. (20).

$$E_{h,n,j} \le D_{h,n,j} \cdot \hat{\eta}_{h,n,j} \tag{21}$$

2.4.7. Model E

The aggregated model (Model E) is designed to be similar to the hydropower models commonly used in investment models, e.g. the ones used in [2,5–10]. Instead of modeling separate hydropower plants, only one power plant and one reservoir are used to model the entire river, using the aggregated maximum turbine capacity (in W) and reservoir volume (in Wh) of all the plants in the river. Hourly power production (P) and reservoir content (V) are constrained by a maximum capacity ($\hat{c}$) and a maximum reservoir content $\hat{v}$, as expressed in Eqs. (22) and (23).

$$0 \le P_h \le \hat{c} \tag{22}$$

$$0 \le V_h \le \hat{v} \tag{23}$$

The maximum capacity is calculated by assuming maximum head and maximum effective discharge in all turbines simultaneously. The maximum reservoir content is converted from m^3 to Wh by calculating the potential energy of the water volumes in the reservoirs, using the height difference between each reservoir and the sea.

The water continuity equation in model E is shown in Eq. (24).

$$V_h = V_{h-1} + 1 \cdot (i_h - S_h - P_h) \tag{24}$$

The hourly inflow profile, i_h, to the aggregated reservoir is assumed to have the same shape as the aggregated inflows to all the considered plants and is given as the share of the total historical annual production by the river (in Wh).

2.5. Model implementation and dealing with nonconvexity

All the models are written in the Julia programming language using the JuMP extension for mathematical modeling [40], and are available at [35]. The Gurobi solver [41] was used for the MIQP Model A:MIP and the LP Models B:L, C, D and E. The NLP Models A and B were solved using IPOPT [42] with the MA86 linear solver [43]. We observed significant improvements in stability and solution times after replacing IPOPT's default linear solver MUMPS with MA86. Setting the IPOPT parameter "mu_strategy" to "adaptive" was also beneficial. The solution times for the various models reported in this research (e.g. in Fig. 7) were obtained by running the models on a desktop computer with an Intel Core i9 3.5 GHz processor and 64 GB RAM.

Large nonconvex optimization problems are notoriously difficult to solve, and with gradient-based solvers, there is no guarantee of finding the global optimum. Even in the case of Model A:MIP, for which the branch-and-bound algorithm theoretically converges to the global optimum, this is impossible in practice due to the large size of the problem (roughly 210,000 binary variables).

We use warm starts to facilitate the solver's search for local optima. For example, we warm start the convex NLP Model B with the solution to the LP Model B:L. This measure alone reduces solution times by more than a full order of magnitude compared to a cold start of Model B, and makes otherwise intractable problems solvable. Similarly, we warm start the nonconvex Model A with the solutions to Model B:L and Model C as well as the LP root relaxation from Model A:MIP. Multiple different warm starts were used in this case because warm starts increase the risk of locking the solver into a local optimum near the starting point. In the results described in Section 3, we present the solution that terminated with the best local optimum.

To increase confidence in the locally optimal solutions to Model A, we compare the objective values with the upper bounds obtained from the integer solutions of Model A:MIP returned by the Gurobi solver. Since Model A:MIP approximates the nonlinear turbine curves of Model A with multiple linear bounds constructed using tangents of those curves, the feasible region of Model A is a subset of that of Model A:MIP, which means that the upper bound for Model A:MIP is also an upper bound for Model A.

In several instances, we reformulated model equations to improve solver performance and stability. The most significant case was the choice of using effective discharge to simplify the power equation (see Section 2.3). Another example is the use of inequalities in Eqs. (4) and (5).

By applying the techniques described here to the model formulation in Section 2.4.1, we successfully solve the most detailed nonconvex model (Model A) with hourly resolution for a full year in roughly one hour. Deterministic hydropower models of similar complexity found in the literature have time horizons of two weeks or less and are used for short-term planning [11–14,16,17].

2.6. The modeled river

We test the models on the Skellefte River in Sweden. The river holds 15 hydropower plants with a total of 24 turbines, and 17 reservoirs connected by waterways, with a total installed capacity of about 1 GW. The distance from the uppermost reservoir to the last plant is about 410 km. The network structure is shown in Fig. 3, where blue boxes correspond to reservoirs and green boxes correspond to power stations (which can hold one or multiple turbines). We run the different models for 4 years separately (2016–2019) with hourly resolution.

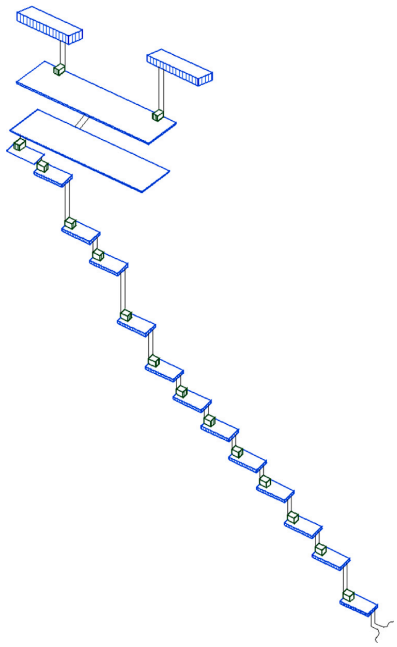

Fig. 3. Network structure of the Skellefte River.

2.6.1. Data and access

We received daily inflow data for each reservoir for 2004 to 2019, and these data were disaggregated into 24 uniform hourly inflow values for each day. We also obtained hourly historical plant-specific data on forebay levels, tailwater levels, discharge, and power output between 2004 and 2019. These data were used to construct turbine efficiency curves and to model tailwater levels as a function of discharge using linear regression (see Eq. (9)). The final analysis was limited to 2016–2019 because significant capacity and efficiency upgrades have occurred since 2004.

Historical hourly electricity prices were retrieved from NordPool. Historical data on production, water discharge, forebay levels and tailrace levels were kindly provided by Skelleftekraft, Vattenfall and Statkraft, and data on inflow, reservoir volumes and environmental constraints by Skellefteälvens vattenregleringsföretag and Energiföretagen. For reasons of confidentiality, the data are not shared alongside the model on GitHub.

3. Results

This section is structured around the three research aims posed in the Introduction (Section 1). Section 3.1 deals with research aim 1, and Section 3.2 is concerned with research aims 2 and 3.

3.1. Comparing the most simplified to the most detailed model

How does a simple hydropower model, similar to those included in full energy system models, differ from a more physically correct model? First, we compare optimized power production from the simplest model (E) with the most detailed model tested in this study (A). Fig. 4 shows the optimal hourly generation obtained from Models A and E compared to historical data on production over a full year. Similar figures for Models B, C, D, and B:L for four additional years may be found in the Supplementary material.

Comparing the hourly generation for Model E (red line in Fig. 4, bottom panel) with the historical production (dark-gray lines in Fig. 4), it is clear that Model E fails to capture the actual production pattern in the river. Instead, it shows a "flip-flop" behavior typical of linear optimization by constantly switching between maximum and minimum production depending on hourly electricity prices. This production pattern overestimates the flexibility of a real hydropower system. Model A (blue line in Fig. 4, top panel) matches the historical production pattern much more closely. Yet, there remains a significant discrepancy between Model A and the historical production. This discrepancy is expected, and may be explained by factors that are not included in Model A but are present in reality, see Section 4.2.

The most economically beneficial way to allocate water use over time would be to imitate the production pattern of Model E, producing at maximum capacity during hours with high prices and at zero when prices are low. This is more clearly evident in Fig. 5, which plots aggregate production as a function of electricity price for each hour. However, in reality, such a production pattern is impossible due to the physical constraints on river-based hydropower production that are captured in Model A. Note that Model A shows a similar dispersion in the correlation between production level and price to the historical data shown in Fig. 5.

In summary, we argue that: (i) Model A represents actual hydropower production significantly better than Model E; (ii) Model E overestimates the flexibility of hydropower, and consequently also overestimates the value of hydropower in a system with a large amount of solar and wind generation; (iii) and much of the error in Model E, comparing the optimized production and historical production levels, lies in excluding the techno-physical constraints included in Model A, i.e., the network effect, head-dependency, and turbine efficiency curves.

3.2. The trade-off between techno-physical accuracy and computational effort

The previous section discussed only the simplest (Model E) and the most detailed (Model A) hydropower models tested in this study. Here, we explore the trade-offs between accuracy and computation time for the models developed in this study (see Table 1 and Fig. 1). By comparing these models, we evaluate the merits of including all techno-physical characteristics rather than only a selection of the characteristics, which is the second research aim of this study.

The power duration curve (PDC), i.e., annual power production sorted from the hour with the highest production to the hour with the lowest production, provides a useful overview of the annual power generation profile. The PDCs for all the models are shown in Fig. 6 for the year 2019.[8] The PDC for Model E shows all-or-nothing dynamics, as noted in Section 3.1. Adding a representation of the river network (Model D) smooths and shifts the shape of the PDC roughly halfway towards that of the most detailed model (Model A). Next, adding partial discharge-dependent turbine efficiency reductions (Model C) reduces the incentive to produce near maximum discharge, thereby shifting some hours from high to intermediate power output. By introducing head-dependent production, Model B further smooths the PDC. Finally, Model A, which adds the decreasing efficiency for low discharge levels, shifts some hours from low to intermediate power output. As noted in Section 3.1, there remains a significant discrepancy between the optimized power from Model A and the historical production profile; this discrepancy will be revisited in Section 4.2.

The difference in maximum output between the models in Fig. 6 is noteworthy (see top-left corner). Since aggregated representations, such

[8] PDCs for the years 2016–2018 are found in the Supplementary material.

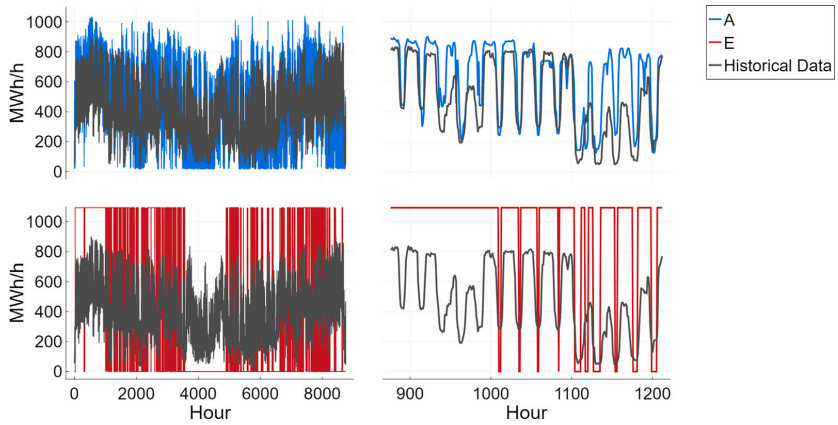

Fig. 4. Optimal aggregated hourly hydropower production (in MWh/h) from the Skellefte River for Models A and E compared with the historical production level in 2019.

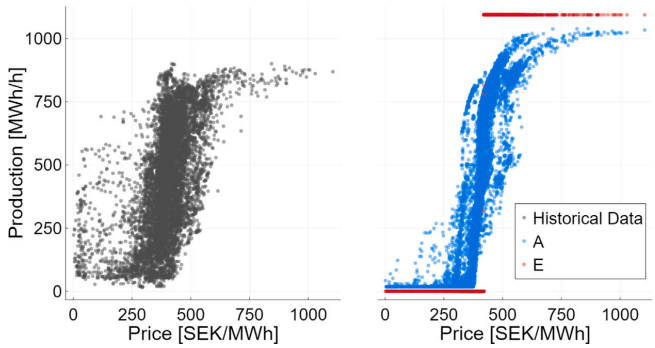

Fig. 5. Power production [MWh/h] as a function of the spot prices [SEK/MWh] for Models A and E, and historical data.

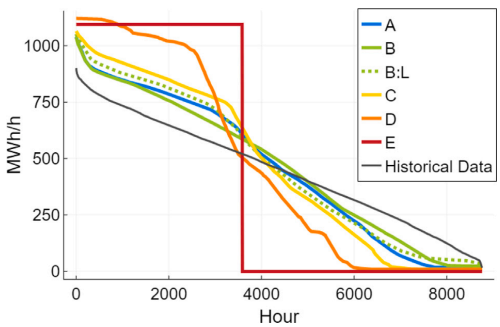

Fig. 6. Power duration curves for all the models in 2019, i.e., the annual production profile sorted by decreasing hourly power generation.

as Model E, have no representation of the river network, the maximum power output of the river system is an exogenous input parameter. Estimating its value is nontrivial due to the many interdependent variables that determine hydropower output (discharge, head, turbine efficiency). To some extent, the choice is arbitrary because it is usually impossible to maximize all variables simultaneously for all plants. In this study, we set the aggregated maximum capacity in Model E to its theoretical maximum, calculated assuming all plants were running with maximum head and effective discharge simultaneously, although this is impossible in practice. Model D has a higher maximum capacity than Model E (see the top left corner of Fig. 6) because Model D uses a constant maximum efficiency and discharge with these values selected individually, thus overestimating the maximum effective discharge which takes interplay of efficiency and discharge into account. An alternative method to find the maximum capacity for Model E could be to extract the maximum output from historical data, which, as we see here, yields a lower capacity than all the models. The results show that some of the reasons for the historical data having lower maximum output than the aggregated installed capacities are the network effect, head-dependency, and turbine efficiency curves (which creates soft upper-limits on turbine capacity, determined endogenously by efficiency loss).

A metric that we use to evaluate the accuracy of the models is the root-mean-square deviation (RMSD) of hourly production, comparing each model with Model A. The rationale is that Model A is the most advanced deterministic model that we can construct. In Section 4.2, we expand on why this comparison is more valid for evaluating model variants than comparing with historical data. The RMSD is defined as follows:

$$RMSD = \sqrt{\frac{\sum_{h=1}^{H}(a_h - m_h)^2}{H}} \tag{25}$$

where H is the number of hours, m_h is the hourly production obtained by the model, and a_h is the hourly production obtained by Model A.

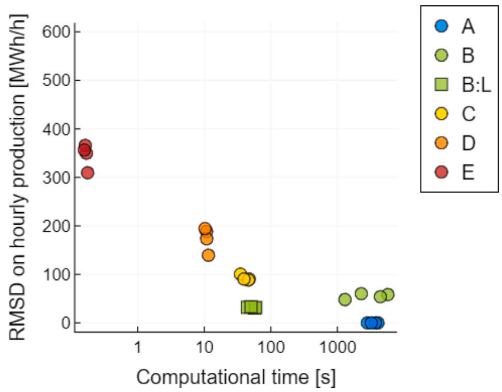

Fig. 7. The trade-off between model complexity and computation time. RMSD of hourly production for each model compared to Model A and computation time for four years of runs (2016–2019). For reference, the installed capacity in the river is about 1000 MW. The RMSD for all Model A runs is zero by definition. See Fig. 1 and Table 1 for a reminder of how the models are constructed.

The RMSD is shown as a function of computation time in Fig. 7. For reference, the installed capacity in the river is about 1 GW. As expected, increased model complexity generally results in a lower value of RMSD for all the modeled years (2016–2019). For comparison, the RMSD of hourly production comparing Model A with historical data is between 237 and 380 MWh/h (23%–36% of maximum production) for the modeled years.

However, with higher model complexity comes longer computation times. Fig. 7 shows that the computation time indeed increases with model complexity, with the exception that Model B takes about the same time to solve as Model A. The most accurate model (Model A) successfully solves in about one hour and the simple aggregated model solves in less than a second. Fig. 7 also presents the evaluation of the novel linearized model, thereby addressing the third research aim of this study. The linearized model, Model B:L, performs surprisingly well in terms of both accuracy and computation time. The RMSD of hourly production for Model B:L, compared to Model A, is on average about 3% of the installed capacity for the modeled years. Fig. 8 illustrates its accuracy by showing the hourly production obtained for models A and B:L for two representative weeks out of the 8760 modeled hours. While maintaining a high level of accuracy, Model B:L reduces the computation time by a factor of 60, from around one hour (Model A) to one minute (Model B:L) as shown in Fig. 7.

4. Discussion

4.1. Comparison with other studies

In energy system investment models, hydropower is often modeled similarly to the aggregated model (Model E) [2,5–9]. By comparing the optimal hourly production between the most detailed model (Model A) and the aggregated model (Model E), we show that Model E overestimates the flexibility of hydropower (see Fig. 4), with the RMSD of hourly production at 345 MWh/h, or 33% of the installed river capacity (see Fig. 7). Overestimating the flexibility of hydropower has, in turn, an effect on the system operation cost [25]. Härtel and Korpås [25] compared two hydropower representations with and without the network effect, in a power system dispatch model for Europe with a hydropower share of 8% of installed capacity, and discovered that a model that neglects the network effect underestimates the system operation cost by 6%. A difference in system operation cost of 6% might not be highly significant. However, this study indicates that their calculated cost increase may be regarded as a low estimate of what may be expected if dispatch models incorporate characteristics of hydropower other than only the network effect, namely the head-dependency and efficiencies, both of which are shown here to have a significant impact on the optimized production (see Fig. 7).

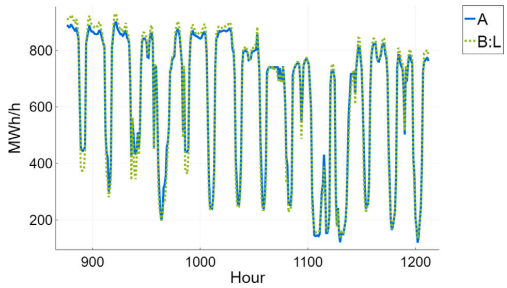

Fig. 8. Hourly production in Models A and B:L for two representative weeks of 2019.

By adding decreased turbine efficiency for high discharge levels (Fig. 2), i.e., moving from Model D to Model C in our framework, we see that this feature also has a considerable impact on model accuracy. This more realistic representation of turbine efficiency improves the accuracy of the production profile, decreasing the RMSD of hourly production from, on average, 17% to 9% of installed capacity (from 174 to 93 MWh/h) (see Fig. 7). Increasing energy losses at high discharge levels reduces the incentive to produce at high levels during periods of high prices, and has a substantial impact on the power duration curve, as noted in Section 3.2. This finding is similar to that reported by Diniz et al. [44]. They showed that production decreased during high-load hours in short-term planning when real efficiency curves, rather than average constant efficiencies, were used. However, Diniz et al. [44] also concluded that the increased accuracy conferred by the more realistic depiction of turbine efficiency may not be worth the increase in computational effort. While Diniz et al. [44] applied the entire efficiency curve all at once, in this study we introduce the efficiency curve in two steps. The first step, introducing the convex part of the discharge-dependent efficiency while going from Model D to Model C, increases accuracy with a much smaller increase in computation time (from 10 to 40 s) than if the full efficiency curves would have been implemented at once.

The merits of including head-dependent production are explored by comparing Models C and B in our framework. Head-dependent production is added in Model B (see Fig. 1) and is found to increase accuracy, decreasing the RMSD of hourly production by about 41% (Fig. 7), from on average 9% to 5% of installed capacity (93 to 55 MWh/h). The effect of head-dependent hydropower production in investment models has been investigated by Ramírez-Sagner and Muñoz [33] by extending the aggregated model (Model E) with head-dependency, i.e., they represent hydropower as one aggregated plant with head-dependent production. They show that neglecting the head-dependency leads to more investments in solar and wind power and a lower system cost than if head-dependent production is considered. Whereas they model only one power plant and, thus, do not evaluate the network effect, we show that the network effect significantly affects optimal production (compare Models E and D in Figs. 6 and 7). In addition, turbine efficiencies are assumed to be constant by Ramírez-Sagner and Muñoz [33] whereas this study shows that representing efficiency curves does affect the production pattern (compare Model C with Model D, and Model A with Model B in Fig. 7). Therefore, if in addition to the head-dependency the network effect and turbine efficiency curves for hydropower would be represented in an investment model, the cost increase and the change in energy mix would be larger than that described in the paper by Ramírez-Sagner and Muñoz [33].

4.2. Discrepancy between the results from the most detailed model and the historical data

The aim of this study was to explore how techno-physical constraints in a hydropower system affect the optimal production profile, rather than attempting any replication of the historical production. Historical production is only used to verify that the model results become generally more realistic when techno-physical constraints are represented (see Figs. 4 and 6). Comparing Model A with the historical data, the RMSD of hourly production is between 237 and 380 MWh/h (23%–36% of maximum production) for the modeled years. However, the extent to which it is meaningful to compare the models to the historical production is limited, since there are factors that are not included even in the most detailed model. The discrepancy observed between the historical data and the results from Model A has three principal sources: (i) uncertainties related to inflow and prices; (ii) market settings; and (iii) technical limitations not included in this study.

Starting with uncertainties, Belsnes et al. [15] showed that for one week, planning with a stochastic model increases the average revenue by up to 9% compared to using a deterministic model. They also showed that using a stochastic model, rather than a deterministic model, yields a higher production level for the modeled week, i.e., a stochastic model tends to use water now rather than saving it for later use. While further research is needed to understand fully how a stochastic formulation would play out in the model settings in this research, it is clear that the estimated revenue would decrease, and thereby become more similar to that of the historical data, due to imperfect information.

Our models also have a simplified representation of power markets. Market settings play a role in hydropower planning since owners collect revenue not only from the day-ahead market (which is the only market we model) but also from the balancing market. Thus, production planners have incentives not only to act on the spot prices but also to save capacity and keep the turbines running to act on the balancing market. Thus, if the balancing market were to be included in the model, the number of hours with maximum as well as minimum production in Fig. 6 could decrease, which in turn would affect the hourly production pattern. Another type of market that could have a similar effect is a capacity market. Such markets exist in many countries but not in Sweden. The effects of capacity markets on hydropower planning have been investigated by Helseth et al. [39], who concluded that including the capacity market results in a more smooth power duration curve, due to the need to save capacity for up- and down-regulation. This type of modulation of the power duration curve of the historical data compared to Model A is what we see in the results when we compare production profiles for Model A and historical data (see Fig. 6).

One technical limitation not included in this study is the availability of hydropower plants. In all models, availability is assumed to be 100%, while in reality, availability is lower due to periods of scheduled maintenance or malfunction. Therefore, the annual production and profit profiles are overestimated in Model A. Consequently, this affects the production pattern and the RMSD of hourly production between Model A and the historical data. Other technical factors not included are forbidden discharge zones due to e.g. cavitation, although low discharge is strongly discouraged in Model A due to low efficiency.

4.3. Negative production using the Taylor approximation

To linearize the power equation, in Model B:L, we use a Taylor expansion around mean head and mean effective discharge. Model B:L performs with an average error of 32 MWh/h (3% of the installed capacity), measured in RMSD of hourly production, as compared to the most detailed model (Model A). The error increases with the deviation in head and discharge from the mean head and mean effective discharge. Thus, if the variations in head and discharge were greater, e.g., for another river system, the Taylor approximation would perform less effectively than in this study. One drawback associated with the Taylor approach is that the production can become negative for some combinations of values of discharge and head, for instance when discharge is zero and the head is lower than the mean-head (see Eq. (17)). Negative production of small magnitude can be seen in the results for a few hours for some turbines; this could be a problem if the production levels of each turbine are important. However, for the aggregated river, which is what interests us here, negative production is never observed (see Fig. 6).

4.4. Limitation of this study

The analysis in this study is performed on one river that has 15 hydropower plants, 24 turbines, and 17 reservoirs. The configuration of this river is close to linear, i.e., the plants are mostly sequentially connected (see Fig. 3). In the Swedish context, this is a less complex configuration than is seen in most rivers with hydropower. It is possible that the network effect will be even more pronounced for more complex river structures. More research is needed to confirm that the computation time and the ranking of models with regards to the trade-off between accuracy and computation time (as in Fig. 7) hold true for other river structures.

4.5. Candidates for implementation in energy system models

We show that an aggregated representation of hydropower is inadequate if capturing flexibility is essential. Some hydropower representations in investment models or dispatch models include additional characteristics (head-dependency, the network effect, or both) compared to the aggregated approach [25,32–34]. These studies demonstrate that varying the assumptions on flexibility of hydropower affects high-level features, such as overall system cost and capacity mix [25,33,34]. We show that including multiple characteristics yields a more realistic production profile, and that this can be done at relatively low computational cost (see Figs. 6 and 7). An alternative to modeling the characteristics of hydropower explicitly is to develop multi-station equivalents [17,36–38]. These equivalents are simplified river structures with artificial ramping constraints, parameterized using a detailed model (similar to Model B) for one week. Running for only one week could lead to a poor parameterization of a hydropower representation intended to perform for a full year of analysis in investment models.

A relatively fast solve time for the hydropower module is essential to maintain tractable energy system investment models. Fig. 7 shows the accuracy levels and computation times for the models evaluated in this study. Models A, B:L, and D have a higher level of accuracy for the expended computation time than Models B and C. We judge that the computation time associated with including all the characteristics (Model A) makes direct implementation in investment models impractical. In contrast, the performance of the Taylor approximation model (Model B:L) is close to that of Model A but uses only 1.5% of the computation time (about one minute compared to one hour). Therefore, we deem it a potentially viable option to implement Model B:L in an investment model. Only including the network effect (Model D), which has been successfully implemented in investment models by Liu et al. [32], is an option that has a shorter computation time than Model B:L (about 10 s compared to 60 s) albeit with about fourfold higher RMSD of hourly production (see Fig. 7). Thus, it would be of interest to test a hydropower representation such as B:L in investment models.

Stevanato et al. [34] improve an energy system optimization model by including both head-dependency and the network effect while keeping constant turbine efficiencies. However, they model head-dependency by iterating between the optimization model and an external calculation of the head to keep the model linear. This softlinking approach gives a feasible solution but does not guarantee a global

optimum. In that respect, implementing Model B:L in an energy dispatch model may be a further improvement since it would guarantee global optimum (subject to the linear approximation) while capturing decreasing turbine efficiencies for high values of discharge.

However, energy system investment or dispatch models typically model large regions holding multiple rivers, and since this study is performed only on one river, the analysis does not evaluate how the computation time scales with multiple rivers that are to be optimized together in an energy system model. In addition, a remaining challenge is the significant amount of data needed to use a full network model like Model B:L in investment models for regions that contain multiple rivers. Therefore, further research is needed to evaluate whether B:L is a viable option for direct implementation in investment models. As an alternative to implementing Model B:L directly in an investment model, Model A or B:L could be used to parameterize a model similar to Model E with artificial constraints, thereby creating a more realistic production profile, which is a possible direction for future research.

5. Conclusion

Traditionally, the representation of hydropower has been highly simplified in investment models, aggregating all the power plants and reservoirs in a region into one of each. By comparing the optimal hourly production between a simple aggregated model and more detailed models developed in this study, we show that a simple representation of hydropower significantly overestimates the flexibility of hydropower and, thus, the flexibility that it can provide in a future renewable power system. Therefore, using an oversimplified representation of hydropower in energy system models is likely to underestimate the system cost and the need for other types of flexibility in the energy system.

The most detailed model developed in this study (Model A) has an hourly resolution for a full year and includes the three following hydropower characteristics: (i) the network effect, (ii) head-dependency, and (iii) turbine efficiency curves. By reformulating model equations using effective discharge and by warm-starting from a linear model, we solve this detailed nonlinear model in about one hour on a modern desktop computer for a river with 24 turbines. We show that this model (Model A) yields an hourly production level closer to the historical data than the aggregated model (Model E).

In addition to the aggregated and detailed models, we develop models of intermediate complexity to explore the merits of including all the abovementioned characteristics (i-iii) of hydropower and to identify candidates that display high accuracy but require less computational effort. We find that each of the characteristics significantly affects the optimal hourly hydropower production, and evaluate the trade-off between accuracy and computational time for different models.

Our novel Taylor expansion model (Model B:L) renders the full nonlinear detailed model completely linear by linearizing the head-dependent power equation and assuming a convex discharge-dependent turbine efficiency. The performance of Model B:L is promising since it reduces computation time to about one minute (as compared to one hour) while maintaining an hourly production profile that is very similar to the full nonlinear model (Model A).

In summary, the main contributions of this study are:

- a highly detailed hydropower model (Model A), including its formulation and solution procedure that allows it to successfully solve in one hour
- a linearized model (Model B:L), which greatly reduces computation time while maintaining a high level of accuracy
- an evaluation of how the level of detail incorporated in hydropower models affects accuracy and computational time

Concerning recommendations and future research direction, the inaccuracy of the aggregated model demonstrated in this study suggests that modelers who use an aggregated representation of hydropower need to be aware of its limitations and potentially consider alternative representations. This is especially relevant for renewable energy systems where hydropower serves as a significant flexibility measure. As a step towards an improved representation, we show that the performance of the linearized model (Model B:L) could make it attractive for endogenous implementation in energy system models. However, a remaining challenge is the significant amount of data needed to model all rivers with this level of detail. Alternatively, a simpler hydropower representation could be used in energy system models, perhaps with artificial constraints, to make the production profile more realistic. In such a case, the linearized model (Model B:L), or the most detailed model (Model A), could be used as reference models for parameterization of the simpler hydropower representations due to their high performance levels for a full year.

CRediT authorship contribution statement

H. Ek Fälth: Conceptualization, Methodology, Software, Formal analysis, Writing – original draft, Writing – review & editing, Visualization, Funding. **N. Mattsson:** Methodology, Software, Formal analysis, Writing – original draft, Writing – review & editing, Supervision. **L. Reichenberg:** Conceptualization, Writing – review & editing, Supervision. **F. Hedenus:** Conceptualization, Writing – review & editing, Supervision, Project administration, Funding acquisition.

Declaration of competing interest

The authors declare that they have no known competing financial interests or personal relationships that could have appeared to influence the work reported in this paper.

Data availability

The code is openly available at GitHub. Regarding the data, the authors do not have permission to share it.

Acknowledgments

The authors gratefully acknowledge Åforsk grant 20-513 for funding, and Skellefteälvens vattenregleringsföretag, Skellefteå kraft, Vattenfall and Statkraft, for providing all the data that made this study possible and for sharing their technical experience related to running the hydro plants. We also thank Vincent Collins for proofreading the article and his excellent writing advice.

Appendix A. Supplementary data

Supplementary material related to this article can be found online at https://doi.org/10.1016/j.rser.2023.113406.

References

[1] Johansson V, Göransson L. Impacts of variation management on cost-optimal investments in wind power and solar photovoltaics. Renew Energy Focus 2020;32:10–22, URL https://www.sciencedirect.com/science/article/pii/S1755008419302017.

[2] Child M, Kemfert C, Bogdanov D, Breyer C. Flexible electricity generation, grid exchange and storage for the transition to a 100% renewable energy system in Europe. Renew Energy 2019;139:80–101, URL https://www.sciencedirect.com/science/article/pii/S0960148119302319.

[3] Rodríguez RA, Becker S, Andresen GB, Heide D, Greiner M. Transmission needs across a fully renewable European power system. Renew Energy 2014;63:467–76, URL https://www.sciencedirect.com/science/article/pii/S0960148113005351.

[4] Kirkerud JG, Bolkesjø TF, Trømborg E. Power-to-heat as a flexibility measure for integration of renewable energy. Energy 2017;128:776–84, URL https://www.sciencedirect.com/science/article/pii/S0360544217305479.

[5] Hoersch J, Hofmann F, Schlachtberger D, Brown T. PyPSA-Eur: An open optimisation model of the European transmission system. Energy Strategy Rev 2018;22:207–15, arXiv:1806.01613.

[6] Schlachtberger DP, Brown T, Schramm S, Greiner M. The benefits of cooperation in a highly renewable European electricity network. Energy 2017;134:469–81, URL https://www.sciencedirect.com/science/article/pii/S0360544217309969.

[7] Brown T, Schlachtberger D, Kies A, Schramm S, Greiner M. Synergies of sector coupling and transmission reinforcement in a cost-optimised, highly renewable European energy system. Energy 2018;160:720–39, URL https://www.sciencedirect.com/science/article/pii/S036054421831288X.

[8] Tröndle T, Lilliestam J, Marelli S, Pfenninger S. Trade-offs between geographic scale, cost, and infrastructure requirements for fully renewable electricity in Europe. Joule 2020;4(9):1929–48, URL https://www.sciencedirect.com/science/article/pii/S2542435120303366.

[9] Jacobson MZ, Delucchi MA, Cameron MA, Mathiesen BV. Matching demand with supply at low cost in 139 countries among 20 world regions with 100% intermittent wind, water, and sunlight (WWS) for all purposes. Renew Energy 2018;123:236–48, URL https://www.sciencedirect.com/science/article/pii/S0960148118301526.

[10] Hirth L. The benefits of flexibility: The value of wind energy with hydropower. Appl Energy 2016;181:210–23, URL https://www.sciencedirect.com/science/article/pii/S0306261916309801.

[11] Borghetti A, D'Ambrosio C, Lodi A, Martello S. An MILP approach for short-term hydro scheduling and unit commitment with head-dependent reservoir. IEEE Trans Power Syst 2008;23(3):1115–24, Conference Name: IEEE Transactions on Power Systems.

[12] Mariano SJPS, Catalão JPS, Mendes VMF, Ferreira LAFM. Optimising power generation efficiency for head-sensitive cascaded reservoirs in a competitive electricity market. Int J Electr Power Energy Syst 2008;30(2):125–33, URL https://www.sciencedirect.com/science/article/pii/S0142061507000853.

[13] Lima RM, Marcovecchio MG, Novais AQ, Grossmann IE. On the computational studies of deterministic global optimization of head dependent short-term hydro scheduling. IEEE Trans Power Syst 2013;28(4):4336–47, Conference Name: IEEE Transactions on Power Systems.

[14] Catalão JPS, Mariano SJPS, Mendes VMF, Ferreira LaFM. Nonlinear optimization method for short-term hydro scheduling considering head-dependency. Eur Trans Electr Power 2010;20(2):172–83, URL https://onlinelibrary.wiley.com/doi/abs/10.1002/etep.301. _eprint: https://onlinelibrary.wiley.com/doi/pdf/10.1002/etep.301.

[15] Belsnes MM, Wolfgang O, Follestad T, Aasgård EK. Applying successive linear programming for stochastic short-term hydropower optimization. Electr Power Syst Res 2016;130:167–80, URL https://www.sciencedirect.com/science/article/pii/S0378779615002576.

[16] Finardi EC, Silva ELd, Sagastizábal C. Solving the unit commitment problem of hydropower plants via Lagrangian relaxation and sequential quadratic programming. Comput Appl Math 2005;24(3):317–42, URL http://www.scielo.br/scielo.php?script=sci_abstract&pid=S1807-03022005000300001&lng=en&nrm=iso&tlng=en. Publisher: Sociedade Brasileira de Matemática Aplicada e Computacional.

[17] Blom E, Söder L, Risberg D. Performance of multi-scenario equivalent hydropower models. Electr Power Syst Res 2020;187:106486, URL https://www.sciencedirect.com/science/article/pii/S0378779620302893.

[18] Pereira MVF, Pinto LMVG. Stochastic optimization of a multireservoir hydroelectric system: A decomposition approach. Water Resour Res 1985-06;21(6):779–92, URL http://doi.wiley.com/10.1029/WR021i006p00779.

[19] Ellis JH, ReVelle CS. A separable linear algorithm for hydropower optimization1. JAWRA J Am Water Resour Assoc 1988;24(2):435–47, URL https://onlinelibrary.wiley.com/doi/abs/10.1111/j.1752-1688.1988.tb03003.x. _eprint: https://onlinelibrary.wiley.com/doi/pdf/10.1111/j.1752-1688.1988.tb03003.x.

[20] Finardi EC, Silva ELd, Sagastizábal C. Solving the unit commitment problem of hydropower plants via lagrangian relaxation and sequential quadratic programming. Comput Appl Math 2021;24:317–42, Publisher: Sociedade Brasileira de Matemática Aplicada e Computacional. http://www.scielo.br/scielo.php?script=sci_abstract&pid=S1807-03022005000300001&lng=en&nrm=iso&tlng=en. (Dec. 2005).

[21] Zhao Z, Cheng C, Yan L. An efficient and accurate Mixed-integer linear programming model for long-term operations of large-scale hydropower systems. IET Renew Power Gener Place: Hertford Publisher: Inst Engineering Technology-Iet WOS:000621962000001.

[22] Barros MTL, Tsai FT-C, Yang S-l, Lopes JEG, Yeh WW-G. Optimization of large-scale hydropower system operations. J Water Resour Plann Manag 2003;129(3):178–88, URL https://ascelibrary.org/doi/abs/10.1061/%28ASCE%290733-9496%282003%29129%3A3%28178%29. Publisher: American Society of Civil Engineers.

[23] Wen X, Zhou J, He Z, Wang C. Long-term scheduling of large-scale cascade hydropower stations using improved differential evolution algorithm. Water 2018;10(4):383, URL https://www.mdpi.com/2073-4441/10/4/383. Number: 4 Publisher: Multidisciplinary Digital Publishing Institute.

[24] Helseth A, Mo B, Lote Henden A, Warland G. Detailed long-term hydro-thermal scheduling for expansion planning in the Nordic power system. IET Gener Transm Distrib 2018;12(2):441–7, URL https://onlinelibrary.wiley.com/doi/abs/10.1049/iet-gtd.2017.0903. _eprint: https://onlinelibrary.wiley.com/doi/pdf/10.1049/iet-gtd.2017.0903.

[25] Härtel P, Korpås M. Aggregation methods for modelling hydropower and its implications for a highly decarbonised energy system in Europe. Energies 2017;10(11):1841, URL https://www.mdpi.com/1996-1073/10/11/1841. Number: 11 Publisher: Multidisciplinary Digital Publishing Institute.

[26] Diniz AL, Maceira MEP. A four-dimensional model of hydro generation for the short-term hydrothermal dispatch problem considering head and spillage effects. IEEE Trans Power Syst 2008;23(3):1298–308, Conference Name: IEEE Transactions on Power Systems.

[27] Rashid AHA, Nor KM. An algorithm for the optimal scheduling of variable head hydro and thermal plants. IEEE Trans Power Syst 1993;8(3):1242–9, Conference Name: IEEE Transactions on Power Systems.

[28] Helseth A, Jaehnert S, Diniz AL. Convex relaxations of the short-term hydrothermal scheduling problem. IEEE Trans Power Syst 2021;36(4):3293–304, Conference Name: IEEE Transactions on Power Systems.

[29] Reichenberg L, Siddiqui AS, Wogrin S. Policy implications of downscaling the time dimension in power system planning models to represent variability in renewable output. Energy 2018;159:870–7, URL https://www.sciencedirect.com/science/article/pii/S0360544218312258.

[30] Reichenberg L, Hedenus F. The error induced by using representative periods in capacity expansion models. 2020, URL https://www.preprints.org/manuscript/202012.0229/v1. Publisher: Preprints.

[31] Mallapragada DS, Papageorgiou DJ, Venkatesh A, Lara CL, Grossmann IE. Impact of model resolution on scenario outcomes for electricity sector system expansion. Energy 2018;163:1231–44, URL https://www.sciencedirect.com/science/article/pii/S0360544218315238.

[32] Liu H, Brown T, Andresen GB, Schlachtberger DP, Greiner M. The role of hydro power, storage and transmission in the decarbonization of the Chinese power system. Appl Energy 2019;239:1308–21, URL https://www.sciencedirect.com/science/article/pii/S0306261919302995.

[33] Ramírez-Sagner G, Muñoz FD. The effect of head-sensitive hydropower approximations on investments and operations in planning models for policy analysis. Renew Sustain Energy Rev 2019;105:38–47, URL https://www.sciencedirect.com/science/article/pii/S1364032118308177.

[34] Stevanato N, Rocco MV, Giuliani M, Castelletti A, Colombo E. Advancing the representation of reservoir hydropower in energy systems modelling: The case of Zambesi River Basin. PLoS One 2021-12-02;16(12):e0259876, URL https://journals.plos.org/plosone/article?id=10.1371/journal.pone.0259876. Publisher: Public Library of Science.

[35] Ek Fälth H, Mattsson N. Rivermodel. 2022, GitHub Repository. https://github.com/hannaekfalth/Rivermodel-Public.

[36] Brandão JLB. Performance of the equivalent reservoir modelling technique for multi-reservoir hydropower systems. Water Resour Manag 2022;24:3101–14, http://dx.doi.org/10.1007/s11269-010-9597-9. (Sept. 2010).

[37] Risberg D, Söder L. Hydro power equivalents of complex river systems. In: 2017 IEEE manchester PowerTech. 2017, p. 1–6.

[38] Shayesteh E, Amelin M, Söder L. Multi-station equivalents for short-term hydropower scheduling. IEEE Trans Power Syst 2016;31(6):4616–25, Conference Name: IEEE Transactions on Power Systems.

[39] Helseth A, Fodstad M, Mo B. Optimal medium-term hydropower scheduling considering energy and reserve capacity markets. IEEE Trans Sustain Energy 2016;7(3):934–42, Conference Name: IEEE Transactions on Sustainable Energy.

[40] Dunning I, Huchette J, Lubin M. JuMP: A modeling language for mathematical optimization. SIAM Rev 2017;59(2):295–320.

[41] Gurobi Optimization, LLC. Gurobi optimizer reference manual. 2022, URL https://www.gurobi.com.

[42] Wächter A, Biegler LT. On the implementation of an interior-point filter line-search algorithm for large-scale nonlinear programming. Math Program 2006;106(1):25–57.

[43] HSL. A collection of Fortran codes for large scale scientific computation. URL https://www.hsl.rl.ac.uk/ipopt/.

[44] Diniz AL, Esteves PPI, Sagastizabal CA. A mathematical model for the efficiency curves of hydroelectric units. In: 2007 IEEE power engineering society general meeting. 2007, p. 1–7, ISSN: 1932-5517.

Paper C

Through energy droughts: Hydropower's ability to sustain a high output

Renewable and Sustainable Energy Reviews 214 (2025) 115519

Contents lists available at ScienceDirect

Renewable and Sustainable Energy Reviews

journal homepage: www.elsevier.com/locate/rser

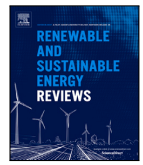

Original Research Article

Through energy droughts: Hydropower's ability to sustain a high output

Hanna Ek Fälth [a,*], Fredrik Hedenus [a], Lina Reichenberg [a], Niclas Mattsson [b]

[a] Department of Space, Earth and Environment, Division of Physical Resource Theory, Chalmers University of Technology, Gothenburg, Sweden
[b] Department of Space, Earth and Environment, Division of Energy Technology, Chalmers University of Technology, Gothenburg, Sweden

ARTICLE INFO

Keywords:
Hydropower
Modelling
Energy systems
Energy droughts
Dunkelflaute
Resilience
Sustained output
Renewables

ABSTRACT

Previous research has highlighted concerns about week-long energy droughts in renewables-based energy systems. Reservoir hydropower could offer a viable solution to mitigate such energy shortfalls. However, current energy systems models often oversimplify hydropower by assuming it can operate continuously at maximum output. This study investigates the ability of reservoir hydropower to sustain a high output and thereby mitigate energy droughts. In contrast to most energy system models, the hydropower model used in this study includes cascading, head dependency, turbine efficiency curves and environmental constraints. We estimate that Swedish hydropower can sustain between 77% and 96% of its installed capacity for one week, with the higher end of this range achievable during spring. This range in sustained output is equivalent to about 3 GW, or about 20% of average demand in Sweden, which underscores the importance of understanding the operational limitations of hydropower. Our findings indicate that river bottlenecks, primarily due to regulations on maximum flows, are the main factor limiting hydropower's ability to sustain higher outputs. With the upcoming renewal of environmental permits for hydropower plants in Sweden, these findings provide valuable insights for policymakers. The importance of analysing hydropower's ability to sustain high outputs is not unique to Sweden; the method proposed in this study can serve as a critical tool for similar assessments in other hydro-rich countries. Moreover, the sustained output capabilities demonstrated in this study challenge the prevalent simplified representations of hydropower in energy models, highlighting the need for more sophisticated modelling approaches.

1. Introduction

Variation management strategies are essential in renewables-based energy systems to ensure that the demand can be met at all times despite variations in wind and solar power production. Energy storage, expansion of transmission grids, demand-side management, and dispatchable generation technologies are the key strategies discussed in the literature [1–9]. Furthermore, reservoir hydropower has been argued to provide flexibility in renewables-based systems [10–16]. In this study, we analyse the ability of reservoir hydropower to provide capacity during a sustained period of low availability of supply relative to demand, a so-called *energy drought*.

In contrast to many other variation management strategies, hydropower has been used in power systems for decades, and has long been recognised for its operational flexibility. In Sweden, hydropower has contributed significantly to system flexibility by providing diurnal production to follow load, seasonal storage capabilities, and grid stability. However, the shift towards renewable energy systems could alter the way in which hydropower is optimally utilised. A recent study by Öberg et al. [17] has revealed a notable shift in hydropower's operational dynamics, in that the conventional daily production cycle is becoming less pronounced, influenced by the increasing integration of wind power into the electricity system. This trend suggests a re-evaluation of hydropower's role, which may be transitioning from its traditional focus on meeting intra-day demand fluctuations to accommodating the variability of renewable energy sources on different time-scales.

Energy systems that have a large share of renewables face numerous challenges related to variability, ranging from short-term issues such as maintaining frequency control and adapting to hourly load changes to persistent supply shortages due to factors such as low-wind periods or technology failures. Researchers have explored hydropower's role in addressing these challenges across different time-scales. Phillips et al. [15] have developed a framework to assess hydropower's potential for enhancing short-term grid resilience after a disturbance, highlighting reservoir hydropower's critical role in managing disruptions. Yang et al. [18] have quantified the quality of short-term regulation of hydropower and the burden placed on generation equipment, and they have also evaluated burden relief strategies under different future

* Corresponding author.
E-mail address: hanna.ek.falth@chalmers.se (H.E. Fälth).

https://doi.org/10.1016/j.rser.2025.115519
Received 14 August 2024; Received in revised form 2 February 2025; Accepted 17 February 2025
Available online 3 March 2025

variable renewable energy (VRE) scenarios. Extending the research to intra-day variations, Thapa et al. [16] have examined the capacity of a cascaded reservoir hydropower system to meet daily demand peaks under various operational constraints, and they have identified some key factors influencing intra-day flexibility. However, hydropower's potential to mitigate week-long energy droughts is poorly explored. Such droughts can result from, for instance, weather phenomena [19–24], technical failures in transmission lines [25,26], and emergency shutdowns of nuclear power plants [27,28].

This study fills the knowledge gap by evaluating hydropower's ability to sustain a high output over extended periods, thereby assessing its capacity to counteract energy droughts. Rather than relying on historical data, which are insufficient because the demand for a high output for long periods of time has not been pressing enough, we employ a model. As has been advocated both by the International Energy Agency (IEA) and the National Renewable Energy Laboratory (NREL), energy system models have too simple a representation and cannot accurately assess hydropower's flexibility [29,30]. Hence, this study employs a detailed model of the hydropower infrastructure to offer insights into its potential to maintain a high level of output for 1–3 weeks. In addition, we investigate the extent to which this ability depends on limitations on how much water can be released through, or passing, each plant. These flow limitations can be due to regulations, technical capacities, or hydrological factors, some of which may be subject to change depending on their impact on energy performance and environmental concerns. We also map seasonal patterns, exploring the relationship between variations in the ability to sustain output at different times of the year and energy drought occurrences.

This study focuses on Sweden as a case study, but the importance of such an analysis extends globally, especially to regions that are heavily dependent upon reservoir hydropower, like South America, Canada, China, Central Africa, and parts of the USA and Europe.

2. Methods

The goal of this work was to determine the maximum possible output that hydropower plants across multiple rivers can sustain simultaneously for 1–3 weeks in the presence of strong economic incentives. To assess this ability, we use a detailed hydropower optimisation model that maximises profits. We simulate high-demand conditions by introducing high market prices and thereby mimicking real-world economic incentives for increased production.

The remainder of the Methods section is organised as follows. First, we introduce and define two key metrics — *Sustained capacity* and *Sustained production* — to quantify sustained output (Section 2.1). Next, we provide an overview of the detailed hydropower optimisation model that we use for the analysis (Section 2.2). We then explain how energy droughts are represented and how the study is designed to test hydropower's ability to sustain high output for different lengths of energy drought periods at different times of the year (Section 2.3). Subsequently, we explain water flow limitations in rivers and how that is implemented in the model (Section 2.4). Next, we present three flow limitation scenarios that we introduce to explore how limits on flows passing each power plant could affect hydropower's performance (Section 2.5). Finally, we summarise the test design and all model runs conducted in this study (Section 2.6).

2.1. Measuring sustained output

To address energy droughts effectively, we require technologies that can meet the demand throughout these critical periods. This study introduces two metrics to evaluate the ability to sustain a high output: *Sustained capacity* and *Sustained production*.

- *Sustained capacity* is defined as the consistent power output that hydropower plants can guarantee throughout a specified period. This metric is measured as a percentage of the maximum capacity of the plants.

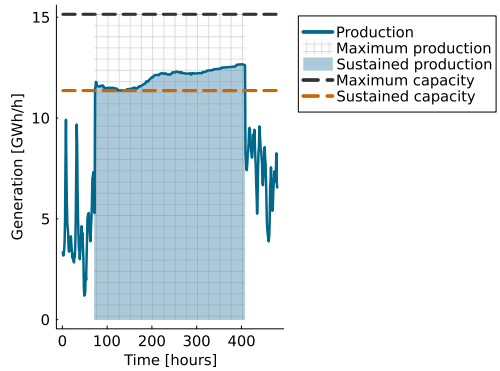

Fig. 1. Illustration of the definitions of the *Sustained capacity* and *Sustained production* metrics. The figure depicts hydropower production levels over a 20-day period, highlighting the metrics during a simulated 14-day energy drought.

- *Sustained production* is defined as the total electrical energy generated during a specific period. This metric is expressed as the percentage of the maximum possible production, i.e., the total production from hydropower plants running at maximum capacity throughout this period.

Fig. 1 shows the hydropower production profile over 20 days with a simulated 14-day energy drought in the middle and shows the metrics of *Sustained capacity* and *Sustained production* applied to this example.

2.2. Model overview

The methodology we use to represent hydropower in a detailed manner is derived from the approach outlined previously by Ek Fälth et al. [31] (described as model B:L in that paper). Briefly, it is a linear optimisation model that maximises profit for a set of hydropower plants subjected to deterministic spot prices over a full year with hourly resolution. The model represents each component of the river systems, including reservoirs, flow paths with their respective flow times, and individual turbines at each power plant with their respective efficiency curves. Turbine efficiencies are modelled using piece-wise linear approximations of actual non-linear efficiency curves, while the head-dependent production is linearised via a Taylor approximation. Furthermore, the model incorporates environmental constraints, such as minimum flow requirements and seasonally dependent minimum and maximum water levels.

To ensure the accuracy of the linear model used in this study for evaluations of sustained output, we conducted a sensitivity analysis using a full non-linear model without linearisations of head-dependency and efficiency curves (described as model A in [31]). This sensitivity analysis confirmed that the linearised model used in this study accurately replicates the results regarding the ability to sustain high output levels, as compared to using a full non-linear model. Figure A.6 in the Supplementary material presents this sensitivity analysis.

In addition to the technical features in the original model described in [31], we implemented, for the purpose of this study, more realistic constraints on the allowed water flow at each hydropower plant. These constraints are dictated by regulations (due to ecological and social considerations) and technical capacities, thus enhancing the model's realism. Moreover, as will be demonstrated in this study, the constraints on water flow rates significantly impact the potential for sustained hydropower output, underscoring their importance in accurately addressing the main research question. Further details of these water flow limitations are presented in Section 2.4.

The next section details the geographic scope of the model, which includes a majority of Sweden's hydropower capacity.

Table 1
The modelled Swedish hydropower capacity, presented as the percentages of total installed capacity in Sweden, both in aggregate and by Nord Pool price area.

	Total	SE1	SE2	SE3	SE4
Share [%]	92	98	99	72	0
Modelled capacity [GW]	15.13	5.24	7.99	1.90	0
Installed capacity [GW] [32]	16.40	5.36	8.08	2.64	0.32

2.2.1. Geographic coverage of the modelled hydropower

The installed hydropower capacity in Sweden is about 16 GW, and in 2022 about 70 TWh of the Swedish electricity generation originated from hydropower, corresponding to 41% of the total electricity production [32]. Our model covers 92% (about 15 GW) of the hydropower capacity in Sweden, encompassing nine major rivers (Luleälven, Skellefteälven, Umeälven, Indalsälven, Ångermanälven, Ljungan, Ljusnan, Dalälven and Göta älv, including Klarälven + Uvån + the stretch below Vänern), incorporating around 240 reservoirs and power plants, each of which is equipped with 1–10 turbines. Table 1 presents the geographic coverage of the modelled hydropower, segmented by Nord Pool price area.

2.2.2. Data overview

For the parameterisation of our model across the nine rivers, we employed an extensive data set spanning from Year 2016 to Year 2020. This data set includes the hourly production levels, water levels at both the intake and outlet, turbine discharge rates, and spillage across the 240 reservoirs and power plants included in our analysis. All the companies that own these facilities provided the data under confidentiality agreements.

The input data for the parameterised model include the spot prices for each bidding area from Year 2016 to Year 2020, sourced from Nord Pool, and the hourly site-specific water inflow data for all rivers, as provided by the Swedish Meteorological and Hydrological Institute (SMHI) and the Water Regulation companies (Vattenregleringsföretagen), also under confidentiality agreements. In addition, the hourly intake water levels were used to determine the start and end reservoir levels for each model run.

2.3. Representing energy droughts in the model

To evaluate the ability of hydropower to sustain high outputs during periods of energy droughts, we simulated conditions of high demand by incorporating constant high market prices into historical price profiles. This method allows us to mimic the economic signals that would trigger hydropower plants to operate at increased output levels, mimicking real-world energy droughts.

2.3.1. Drought duration scenarios

To examine how the ability to sustain high output varies with different durations of energy droughts, we modified historical price profiles to include *one, two* or *three* consecutive weeks at a constant high price. These three drought duration scenarios are visualised as "Drought duration scenarios" in dark orange in Fig. 5.

The price at the high-price weeks was set at 5000 SEK/MWh (approximately 430 €/MWh). This pricing level was selected as a substantial incentive for high production levels; for reference, the peak price on the Swedish spot market in Year 2023 was 3760 SEK/MWh. Fig. 2 demonstrates an example.

We conducted a sensitivity analysis to confirm that the price level of 5000 SEK/MWh effectively motivates maximum sustained output during these high-price intervals. The findings, detailed in Figure A.6 in the Supplementary material, reveal that even a significantly higher price of 50,000 SEK/MWh did not increase the sustained output. This result confirms that our chosen price level effectively encourages Swedish hydropower plants to maximise their outputs during critical high-demand periods, assuming that prices during the remainder of the year align with the historical levels recorded between 2016 and 2020.

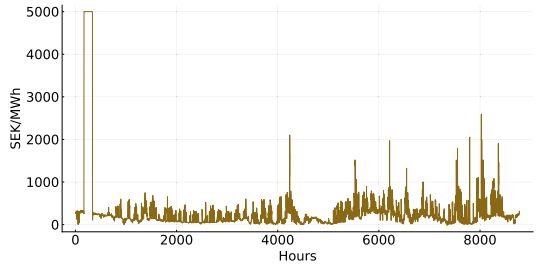

Fig. 2. Example of a price profile with an introduced high-price period of 1 week in region SE3 in January 2020.

We utilised a model that has perfect foresight, incorporating deterministic water inflows and spot prices. To reduce the risk of overestimating the sustained outputs – a consequence of using a model that is capable of precisely planning water releases and levels with complete foresight – we strategically introduced the high-price period just 1 week after the initial modelled hour. This approach restricts the model's ability to optimise water levels in advance, thus enhancing the realism of our results for sustained output.

2.3.2. Droughts at different times of the year

To investigate how timing influences the sustained output capabilities of Swedish hydropower, we simulated energy droughts in each month individually. To cover differences in annual inflow between years, we conducted one full-year model run for each month (as the start month) for four different years (2016–2019). To clarify, we modelled January 2016 to January 2017 with the high-price period in January 2016 and replicated this for all months and years up to December 2019 to December 2020. This methodological approach enabled us to assess how the timing of energy drought periods affects sustained production levels, as influenced by variations in inflow and initial reservoir levels. These are visualised as "Time periods" in light blue in Fig. 5.

2.4. Water flow limitations

Water flow limitations due to regulations, technical capacities, or hydrological factors can create bottlenecks at specific points along the river, significantly affecting the abilities of the hydropower plants in that river to sustain high outputs, as demonstrated by the findings of this study. This section provides an overview of how we define river bottlenecks and how they impact the ability to sustain high output levels. It further explains how water flow limitations were integrated into our model. Section 2.5 details the three flow limitation scenarios analysed in this study.

2.4.1. Bottlenecks affecting the ability of hydropower to sustain a high output

River flow rates typically increase as one moves downstream, due to the convergence of tributaries as the river progresses towards the sea. However, the larger reservoirs in Swedish river systems, which serve as substantial seasonal water storage facilities, are predominantly located upstream. In contrast, some downstream reservoirs can only hold enough water for a few days of full-capacity generation. Therefore, sustaining high production levels at downstream plants for prolonged periods requires the release of water from these larger upstream reservoirs, so as to compensate for the limited capacities of

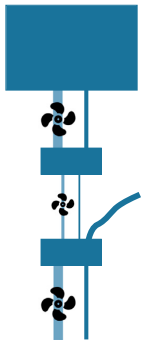

Fig. 3. Conceptual representation of a river system, illustrating the concept of bottlenecks that can exist at various points along a river. The diagram depicts a series of reservoirs and turbines, with a large upstream reservoir followed by smaller ones downstream. It highlights how varying turbine capacities can create bottlenecks, particularly when a lower-capacity turbine is situated between higher-capacity turbines. Given the present regulatory frameworks and infrastructure, whereby the allowed flow through a plant (either through the turbine or in the spillway) generally is limited to the maximum flow capacity of the plant's turbines, these bottlenecks diminish the ability to sustain high levels of hydropower production.

smaller downstream reservoirs.

Bottlenecks arise where the allowed water flow rate of one plant is lower than others upstream or downstream, impeding water transfer. Fig. 3 conceptually illustrates such a bottleneck. Consider a river system with a large upstream reservoir connected to a turbine and spillway with high-flow capability. Further downstream lies a smaller reservoir with a turbine and spillway that is capable of lower flows, followed by another small reservoir that is equipped with a high-flow turbine because it receives additional water from a tributary. The most-downstream turbine cannot sustain maximum capacity without rapidly depleting its reservoir, because even if ample water remains upstream, it cannot bypass the bottleneck (the middle turbine) quickly enough. Moreover, the most-upstream turbine cannot run at full capacity indefinitely without risking an overflow at the intermediary reservoir.

2.4.2. Flow limits in the model

The permit under which hydropower plants operate can limit the amount of water that they can release through turbines or in spillways, as well as the rate at which they can change water flows. For instance, some power plants can operate with so-called *short-term regulation*, i.e., frequently changing the water flows withdrawn from their closest reservoir, while others do not.

Since some plants have the right to conduct short-term regulation, whereas some can only change their water flows at a limited rate of change, we introduced two variables to represent the flow constraints in our model: long-term spillage, $L_{t,p,p2}$; and short-term spillage, $S_{t,p,p2}$. The long-term spillage has the upper bound $l_{t,p,p2}$, as in Eq. (1). The right to regulate water in the short term includes both spillage and the water released in the turbines. Thus, we set the sum of the short-term spillage, $S_{t,p,p2}$, and the turbine discharge, $D_{t,p,p2}$, to be below the upper bound for short-term regulation, $s_{t,p,p2}$, as in Eq. (2). Index t represents time, and the indices p and $p2$ represent the passage from plant p to downstream plant $p2$.

$$L_{t,p,p2} \leq l_{t,p,p2} \tag{1}$$

$$S_{t,p,p2} + D_{t,p,p2} \leq s_{t,p,p2} \tag{2}$$

To restrict the rate of change in long-term spillage, we introduced constraints that limit the increase and decrease of long-term spillage from hour to hour. The parameter i represents the allowed increase each hour, and d represents the allowed decrease each hour.

$$L_{t,p,p2} \leq L_{t-1,p,p2} + i_{t,p,p2} \tag{3}$$

$$L_{t,p,p2} \geq L_{t-1,p,p2} - d_{t,p,p2} \tag{4}$$

In our flow limitation scenarios, we applied either short-term spillage or long-term spillage to each plant. In reality, it could be that one is allowed to release water above the limit for short-term regulation if that water release is carried out with slow changes to the flow. However, allowing for both long-term and short-term spillage in our model requires some model development since the current implementation would lead to the possibility of having short-term spillage on top of the long-term spillage, thereby changing the flow rates faster than is allowed above the upper limit for short-term regulation.

2.5. Flow limitation scenarios

To explore the impacts of bottlenecks on sustained output, we examined the following three scenarios with different upper bounds on spillage: *Present regime*, *Reduced bottlenecks*, and *Unrestricted*. These three scenarios are visualised as "Flow limitation scenarios" in light orange in Fig. 5.

2.5.1. Present regime scenario

Sweden's current regulatory framework for hydropower production involves the issuing of specific permits for each plant. These permits typically impose restrictions on permissible water flow rates at specific points along the river. Some power plants can operate with short-term regulation, while others do not. For instance, reservoirs that are not directly linked to power plants frequently lack such permissions. Based on discussions with specialists from power production companies and water regulation authorities in Sweden, we conclude that power plants that are authorised to engage in short-term regulation are generally permitted to adjust flows rapidly between any minimum flow requirement and the maximum capacity of their installed turbines. In this study, for the *Present regime* scenario, we have assumed that all reservoirs that are connected directly to power plants are entitled to regulate their water flows on a short-term basis. We have further assumed that flows that exceed the maximum capacity of the installed turbines, plus any mandatory minimum spillage requirements, are not permitted except during periods when the inflow exceeds the turbine's maximum flow capabilities. Consequently, for these reservoirs, the upper limit on short-term regulation [s in Eq. (2)] is set each hour by the greater of the maximum flow capacity of installed turbines or the present inflow to that reservoir. Furthermore, the upper limit on long-term spillage [l in Eq. (1)] is set at zero.

For reservoirs that are not directly connected to a power plant, we set the short-term regulation [s in Eq. (2)] to zero and permit long-term spillage [l in Eq. (2)] every hour, equal to either the maximum inflow recorded that calendar month during the period of 2016–2020 or the mean inflow for the same period, whichever is greater during that hour.

2.5.2. Reduced bottlenecks scenario

In this scenario, we identified all power plants in which the maximum flow capacity of the installed turbines was lower than that of any of the upstream plants. Following this approach, approximately 30% of all power plants were classified as bottlenecks. For these identified bottlenecks, we increased the allowed short-term regulation [s in Eq. (2)] to match the maximum flow capacity of the turbines in the upstream plant. This adjustment resulted in an average increase of 20% in the maximum water flows at these plants. When comparing these

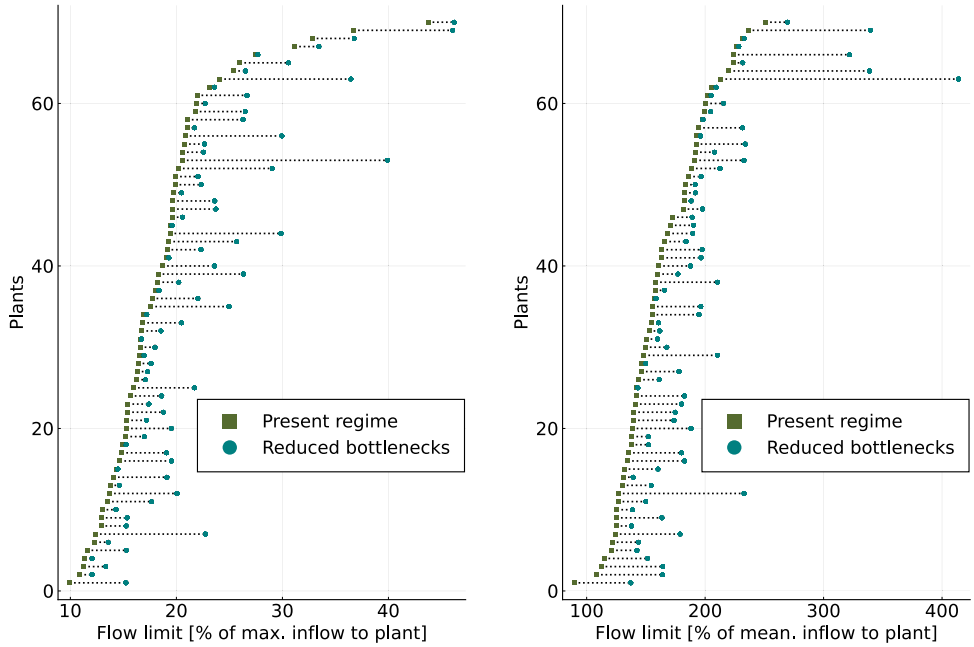

Fig. 4. Overview of the 70 hydropower plants (out of approximately 240) identified as bottlenecks. The figure compares flow rate limitations at bottleneck sites under the *Present regime* and *Reduced bottlenecks* scenarios, highlighting adjustments made to improve performance during energy droughts. The left panel presents flow rate limits as a percentage of the maximum inflow to the plant, while the right panel shows them as a percentage of the mean inflow.

revised flow rate limits to the maximum recorded inflow for each plant (including the inflow to all upstream plants) over the period of 2016–2020, we found that the limits increased from an average of 18% to 22% of the maximum inflow. Similarly, when compared to the average inflow during the same period, the spillage limits rose from an average of 163% to 194% of the mean inflow. Details of these adjustments to the flow rate limits, in relation to both the maximum and average inflows, are illustrated in Fig. 4.

2.5.3. Unrestricted scenario

In the *unrestricted* scenario, the upper limits on short-term regulation [s in Eq. (2)] were removed for all power plants and reservoirs. Thus, all the plants, including reservoirs without directly connected power plants, were allowed to regulate water without an upper limit. Note that we retained the upper limits on turbine discharge. Thus, we effectively increased the spillage limits.

2.6. Test setup

The test setup integrates the various elements described in the Methods section to systematically evaluate hydropower's ability to sustain high output under different conditions. An overview of the setup is presented in Fig. 5.

The study focuses on three key factors that influence sustained hydropower production:

- **Energy drought duration** – The impact of drought length is assessed through three scenarios, representing one-, two-, and three-week energy droughts.
- **Timing of energy droughts** – To investigate seasonal differences in the ability of hydropower to sustain high output, we assess energy droughts in each of the 12 months. To account for inter-annual variability, we repeat the analysis for four different years, resulting in 48 distinct time periods.
- **Flow limitations** – The role of flow bottlenecks is analysed through three flow limitation scenarios:
  - *Present Regime* (existing constraints on water flows),
  - *Reduced Bottlenecks* (relaxed constraints to enhance sustained output), and
  - *Unrestricted* (no flow limitations).

The study includes assessments for nine different river systems. In total, more than 5000 model runs were carried out, covering all combinations of drought durations, time periods, and flow limitation scenarios. This setup allows for a detailed examination of how hydropower's ability to sustain high output is influenced by drought conditions and operational constraints.

In addition to these scenario-based runs, baseline runs were conducted to establish reference points for annual energy production and maximum capacity, as described in the following section.

2.6.1. Baseline runs as reference points for energy production and capacity

To establish reference points for energy production, baseline runs were conducted using original historical spot prices. These runs were performed for all flow limitation scenarios, time periods, and rivers, aligning with each drought duration scenario (see the topmost white dashed box in Fig. 5). Comparing these with the energy drought runs allowed us to quantify the annual production loss resulting from sustaining high output during energy droughts. This loss is caused by spillage at bottlenecks, which occurs to sustain high production during high-price energy drought weeks, as this yields higher overall profits than reducing spillage.

Maximum turbine capacities are not directly specified in our model but are inferred from several factors: the maximum turbine flows, the varying head levels derived from intake and outlet elevations, and the configuration of the turbine efficiency curves. To determine the

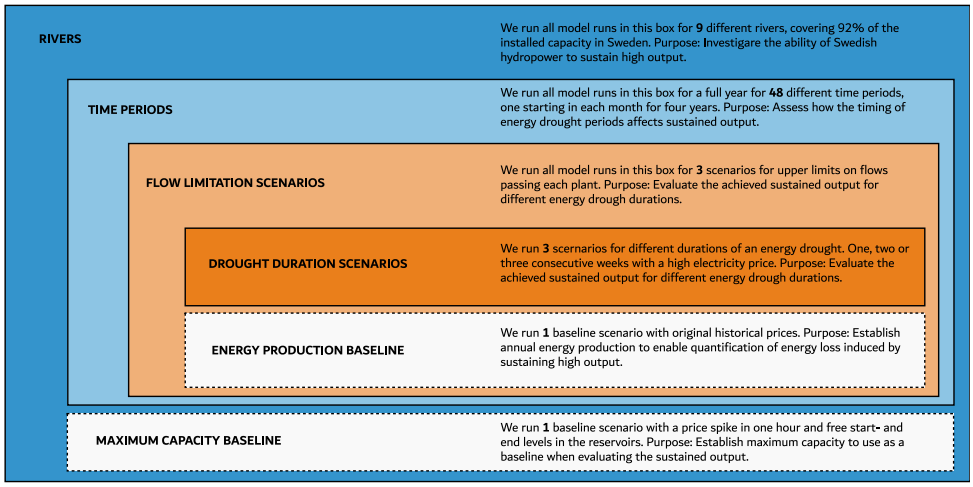

Fig. 5. A summary of all the model runs conducted in this study. The innermost box represents 3 Drought duration scenarios (one, two and three weeks; dark orange), each applied under 3 Flow limitation scenarios—*Present Regime*, *Reduced Bottlenecks*, and *Unrestricted* (light orange). These scenarios were tested across 48 time periods (12 months × 4 years; light blue) for 9 different rivers (dark blue). Baseline runs, conducted to establish reference points for annual energy production and maximum capacity, are visualised in white dashed boxes. In total, this results in over 5000 model runs.

maximum capacity for each river, we ran the model with a short high-price period lasting only one hour, allowing for optimised initial and final reservoir levels. This approach provides a meaningful reference for comparing the *Sustained Capacity* during high-price weeks to the maximum possible capacity.

Baseline runs for energy production and maximum capacity are represented by white dashed boxes in Fig. 5.

3. Results & discussion

3.1. Hydropower capacity can be sustained at high levels over several weeks

Our findings reveal that hydropower can sustain high production levels over several weeks. Under current infrastructure and regulatory conditions, the Sustained capacity of Swedish hydropower ranges from 67% to 96%, depending on the time of year and the durations of high-price periods. On average, across all months spanning the period of 2016–2019, the Sustained capacity for a 1-week period was 84%, decreasing to 78% for a 3-week period. Regardless of the season or year, Swedish hydropower consistently maintained at least 67% of its total capacity for up to 3 weeks. These results are illustrated in Fig. 6 for the *Present regime* scenario, which showcases hydropower's Sustained capacity over one to three consecutive weeks. The results obtained for Sustained production are very similar to those for Sustained capacity and are, therefore, not shown here, although they are provided in Figure A.1 in the Supplementary material. Furthermore, the results for the sustained output divided according to Nord Pool price areas in Sweden are presented in Figures A.2 and A.3 in the Supplementary material.

Further examination of Fig. 6 indicates that the variation in hydropower's ability to sustain output over 1 week versus 3 weeks is less significant than the variation observed across different months and years, as highlighted by the magnitudes of the variability within each violin. This suggests that the timing of energy droughts plays a more critical role than drought duration in determining hydropower's capacity to maintain output during these periods.

We have modelled and analysed 92% of Sweden's installed hydropower capacity, focusing on the largest and most flexible river systems. Since the remaining capacity primarily consists of plants with

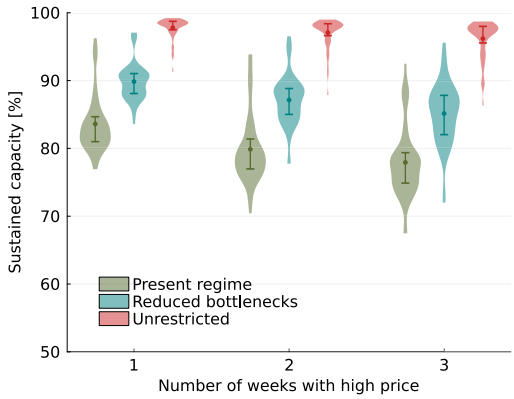

Fig. 6. An illustration of the Sustained capacity of hydropower over a period of one to three consecutive weeks of high electricity prices for three different operational flow limitation scenarios. Each violin shows the results for each month over four different years. The dots represent the mean values, while the lines extending from the dots indicate the 25th to 75th percentile range. The colour-coding corresponds to the following operational flow limitation scenarios: *Present regime* with current regulations and infrastructure (green); *Reduced bottlenecks* with a higher upper limit on spillage in bottlenecks (blue); and *Unrestricted*, with unrestricted spillage (red). The different scenarios highlight the influences of operational constraints on the ability of hydropower to sustain a high output during energy droughts. The results shown are based on approximately 5000 model runs. Refer to Section 2.6 for details of the test setup.

lower levels of operational flexibility, the results for sustained output should not be extrapolated to this remaining capacity. It is also worth noting that we assumed that all power plants would be available for production at all times. In reality, owing to planned and unplanned shutdowns for maintenance and failures, the actual sustained production may occasionally be lower than is indicated by our results.

Furthermore, the unpredictable natures of the inflow and prices pose challenges for production planning, limiting the flexibility of hydropower compared to the deterministic model's idealised approach used in this study. For instance, deterministic models may completely empty or fill reservoirs with confidence because they know precisely when new water will arrive and when a high-price period will appear. This cannot be accomplished in practice, as it may lead to exceeding the upper and lower bounds of reservoir content due to incorrect inflow forecasts. We introduced the high-price period only 1 week after the initial modelled hour, to reflect more accurately the actual conditions and to reduce the over-estimation of flexibility from the deterministic model. This adjustment restricts the model's ability to optimise the water levels before encountering the high-price period. Nevertheless, even with this modelling approach, using a deterministic model still somewhat over-estimates the possibilities for hydropower to sustain output.

3.2. Adjusting the allowed water flows at bottlenecks enhances hydropower output during energy droughts

The current regulatory regime for hydropower production in Sweden includes limitations on allowed water flow rates in different sections along the river. The regulations generally permit operators to run water through or bypass power plants up to the maximum flow capacity of the installed turbines, except during high-inflow periods when more-significant water flow rates are allowed or forced. Bottlenecks arise when the maximum flow capacity of the turbines in a power plant is lower than that of plants upstream or downstream, thereby impeding water transfer. For more details on bottlenecks, see Section 2.4 *Water flow limitations*.

To explore the impacts of bottlenecks on sustained output, we examined two alternative scenarios, as detailed in Section 2.5. First, we analysed an *Unrestricted* scenario, in which the upper limits on water flow rates were removed at each hydropower plant, while maintaining maximum turbine flows, thereby effectively increasing the spillage limits. Allowing unrestricted spillage throughout the river could raise the sustained output to > 95% on average for periods of up to 3 weeks (illustrated by the red violins in Fig. 6), as compared to 77% under current regulatory regimes (green violins in Fig. 6). However, unrestricted spillage entails severe risks, such as flooding and erosion. Although unrealistic, this scenario indicates the impact of current water flow rate limits on sustained output and serves as an upper bound on the possibilities for sustained output.

Second, we evaluated a more targeted approach that allowed water flows to exceed the turbine flow capacities at identified bottleneck sites. The adjustments to the allowed water flows were made without increasing the maximum turbine flow capacities, thus only increasing the spillage limits. Sections 2.4 and 2.5 describe how and why flow limits were expanded at bottlenecks, and Fig. 4 shows adjustments to the flow rate limits as shares of both the maximum and average inflows.

In this *Reduced bottlenecks* scenario, Sustained capacity averages 90% for 1 week and 85% for 3 weeks (blue violins in Fig. 6). This marked improvement over the *Present regime* scenario demonstrates that adjusting spillage regulations at bottlenecks notably enhances hydropower's performance during energy droughts. Nevertheless, while the benefits of increasing flow limits are clear, they must be carefully balanced against potential environmental and social impacts, which could have negative effects on the river ecosystems and the communities that depend on them.

Our analysis did not capture all the complexities related to spillage, since we were constrained by data limitations. Each power plant operates under individual permits that regulate the release of water. We generalised these regulations by setting the upper limits on water flows through the turbines or in spillways to be equal to the maximum installed turbine flow. This assumption is based on consultations with experts from power production companies and water regulation authorities. Furthermore, water flows are restricted during wintertime due to ice formation in rivers and the risk of mechanical issues, likely resulting in a reduced ability to sustain output during the colder months. Given the generalisation of permits and the omission of the ice-related problems, our results should be viewed as indicative of the potential for sustained high output in Swedish hydropower rather than definitive calculations.

Furthermore, it is important to note that achieving sustained high-level production in rivers fundamentally depends on maintaining high flow rates throughout the entire river system. Our approach focused on increasing the spillage limits to improve flow at bottlenecks. Another effective solution could be to expand the turbine flow capacity by installing additional turbines at these critical points. Such an expansion would enhance the river system's ability to sustain high output and increase capacity while avoiding the increased annual energy losses associated with higher spillage.

3.3. Higher sustained hydropower capacity can be obtained during periods of high natural inflow and high reservoir levels

Our findings reveal notable variability in the sustained output across the *Present regime* and *Reduced bottlenecks* scenarios, as illustrated by the green and blue violins, respectively, in Fig. 6. Fig. 7 shows the 1-week Sustained capacity by month for three operational scenarios: *Present regime*, *Reduced bottlenecks*, and *Unrestricted*. The *Unrestricted* scenario consistently demonstrates sustained capacities >98%, except from March to May. This decrease can be explained by current operational practices, whereby reservoir levels are typically at their lowest before the spring run-off due to intentional winter draw-downs to meet the high demand and to accommodate anticipated spring recharge. Consequently, diminished reservoir volumes limit the capacity for full output over 1 week, and reduced head heights in plants with significant reservoir level variability decrease the energy potential, thereby affecting the power output. This also explains the downward trend in Sustained capacity observed from November to March in both the *Present regime* and *Reduced bottlenecks* scenarios (Fig. 7).

In addition, Fig. 7 charts the total natural inflow to the modelled rivers over the year as a percentage of the maximum observed, illustrating the correlation between inflow and Sustained capacity. A fluctuating inflow throughout the year affects the permitted spillage levels, as high-level spillage is only allowed during periods of naturally high inflow, such as during snowmelt or consistent rainfall, as detailed in Section 2.4. Consequently, the potential for high sustained output is greater during these high-inflow periods, as is evident in both the *Present regime* and the *Reduced bottlenecks* scenarios. This pattern arises from the design of the spillage constraints; natural inflow typically exceeds turbine capacity mainly in the springtime and occasionally in autumn, dictating spillage limits only during these periods. Allowing higher flows leads to a higher Sustained capacity because it enables water to bypass bottlenecks, and downstream plants can maintain high production levels using water from upstream reservoirs. For the same reasons, months with higher variability in terms of inflow also exhibit greater variability of Sustained capacity. Notably, the sustained output in April appears low despite there being a high inflow. This discrepancy is due to two factors: (1) the peak inflows typically occur at the end of April, whereas we introduced the high price period in the middle of the month; and (2) as discussed above, reservoir levels are generally lower before the spring run-off due to the high demand during wintertime and the anticipated recharge.

Thus, two primary factors determine the ability of hydropower to sustain a high hydropower output: (1) the water levels in the reservoirs; and (2) more critically, the permitted flow rates. These factors contribute to significant variability in hydropower's ability to sustain a high output throughout the year and across different years, as illustrated in Fig. 7. However, it is important to consider that future changes in inflow patterns driven by climate change, as well as adjustments made to reservoir management in response to these inflows and evolving energy demands, will alter the yearly differences in hydropower's potential to sustain output.

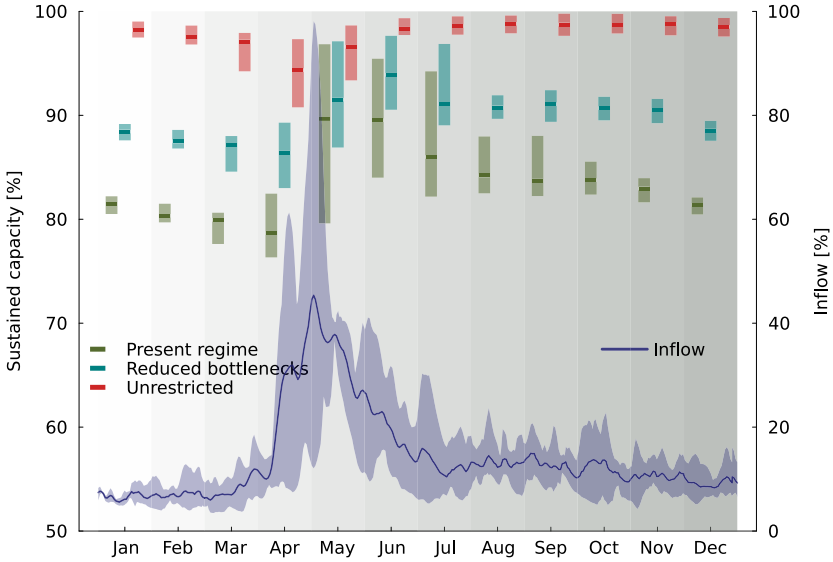

Fig. 7. A comparison of the monthly Sustained capacity of Swedish hydropower under three operational scenarios and the natural inflow throughout the year, illustrating how today's hydrological cycle influences hydropower's ability to sustain a high output. The Sustained capacity values under the *Present regime* (green), *Reduced bottlenecks* (blue), and *Unrestricted* (red) scenarios are shown in box plots, which display the range and mean values for each month. The line graph represents the total inflow as a percentage of the maximum recorded. The shaded area behind the line graph indicates the variability of the inflow for the modelled period of 2016–2020.

3.4. High sustained capacity creates annual energy losses

Achieving a high sustained hydropower capacity inevitably reduces the annual energy output, primarily due to increased spillage at bottlenecks and, to a lesser extent, reduced turbine efficiencies at maximum flows. Fig. 8 illustrates the annual production losses that are entailed by a high Sustained capacity, contrasting the outputs from scenarios involving elevated market prices with scenarios that have historical price levels. In the *Unrestricted* scenario (Fig. 6), sustaining an average capacity of 96%–98% results in a loss of about 0.8% of the annual production for each week of sustained high output, as depicted by the red violins in Fig. 8. Meanwhile, with the current regulations and infrastructure, an average Sustained capacity of 78%–84% is achievable (as shown in the *Present regime* scenario in Fig. 6), with a corresponding lower loss of about 0.2% of yearly production per week.

In summary, sustaining a high output from hydropower, so as to counteract energy droughts, leads to some energy losses, amounting to 0.2%–0.8% of annual production for each week of sustained output. This should be considered within the broader context of energy system needs. While losing renewable energy might appear to be negative in terms of the pursuit of a transition to a carbon-neutral energy system, the flexibility provided by hydropower is critical for renewables-based energy systems. It is generally more challenging to find renewable sources that offer this level of flexibility than to generate renewable energy in bulk.

3.5. What does hydropower's sustained capacity, as measured in this study, imply for the management of energy droughts?

Our analysis demonstrates that Swedish hydropower can deliver between 67% and 96% of its installed capacity during critical periods of 1–3 weeks. This capability under-scores the significant potential of hydropower to ensure the energy supply during multi-week energy droughts. However, evaluating the adequacy of this sustained output requires the consideration of several key factors.

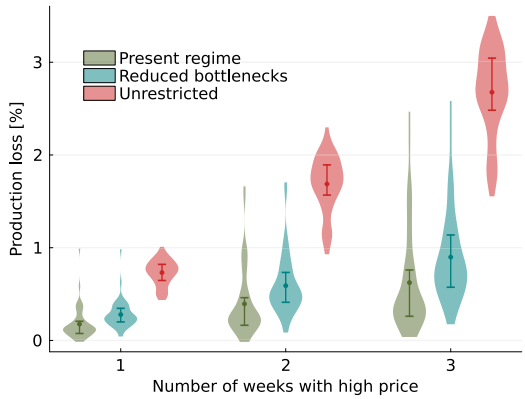

Fig. 8. Losses in yearly production associated with sustaining high output levels, comparing the yearly production obtained with elevated market prices with the yearly production obtained with historical price levels. Each violin represents the results for each month over 5 different years. The dots represent the mean values, while the lines extending from the dots indicate the 25th to 75th percentile range. The colour-coding corresponds to the following operational scenarios: *Present regime*, with the current regulations and infrastructure (green); *Reduced bottlenecks*, with a higher upper limit on spillage in bottlenecks (blue); and *Unrestricted*, with unrestricted spillage (red).

First, the relevance of sustained hydropower output depends on its share of the energy mix. In Sweden, the lowest observed sustained output of 67%, approximately 10 GW, can fulfil about 40% of the peak electricity demand and 68% of the average electricity demand. At the higher end, a Sustained capacity of 96%, equivalent to 14.5 GW, could meet almost 60% of the peak demand and almost 100% of the average electricity demand. These values highlight the significant role that hydropower plays in enhancing the resilience of a renewable

energy system, although they also point to the need for additional energy sources during severe energy droughts. The broad range of observed sustained outputs, with a 4.5 GW difference between the highest and lowest outputs – equivalent to the capacity of three to four Swedish nuclear reactors – underlines the need to evaluate carefully hydropower's sustained output capabilities when developing strategies to counteract energy droughts.

Moreover, Sweden's energy system's interconnection with the rest of Europe adds complexity to the assessment. While this interconnectivity often acts as a buffer against local shortages by enabling trade in energy, it also poses risks when energy droughts occur simultaneously across the continent, thereby amplifying the demand for reliable back-up solutions.

Second, the timing and seasonality of the hydropower output relative to energy droughts are crucial. Energy droughts are more likely to occur during the wintertime in today's European electricity system [20,22,23], and this trend may intensify with climate change [24]. Moreover, historical data indicate that the winter months (December to February) are the periods of peak demand in Sweden [33], due to the use of electric heating. Our findings reveal that the ability of Swedish hydropower to sustain a high output is weakest during the winter months (November to March). This observation aligns with periods identified in recent literature as most susceptible to energy droughts. Unfortunately, this means that the seasons with the highest risk of energy shortages coincide with the periods during which there is a reduced capacity for hydropower to deliver high outputs.

3.6. Understanding hydropower's role in future energy systems

While our study does not directly evaluate the role of hydropower in future energy systems by integrating a detailed representation within an energy system model, it offers valuable insights that can facilitate such assessments in future research. Our findings can be used to establish more realistic assumptions regarding hydropower's ability to sustain a high output, compared to those used in the simplified representations that are commonly found in existing energy system models.

Energy system model studies have shown that reservoir hydropower can provide important flexibility in renewables-based systems [10,11]. However, these models often assume that hydropower's Sustained capacity is 100% as long as there is water in the reservoirs. Our research indicates that the actual capacity to sustain high output can sometimes be as low as 67%. Models that over-simplify hydropower's capabilities may thus overestimate the resilience provided by hydropower and underestimate the need for additional assets that can provide backup during energy droughts.

In contrast, some models that explore renewable energy systems use historical hydropower data to parameterise their representations. Such data have not historically shown the high sustained outputs that our study suggests are possible, due to the lack of economic incentives for such performance in previous energy systems. Therefore, relying on historical data to predict hydropower's operation in future energy systems will likely under-estimate its flexibility.

The influences of economic incentives on sustained output are significant, as sustaining a high output involves a trade-off between maximising output during high-price periods and saving water for hours with lower prices. In addition, as we have shown, sustaining a high output entails a reduction of annual production, adding to this trade-off. We conducted a sensitivity analysis to determine whether the price level used in our study (5000 SEK/MWh, approximately 430 €/MWh) effectively encourages maximising the sustained output during high-price periods. This analysis demonstrated that even at a substantially higher price of 50,000 SEK/MWh, the sustained output did not increase, thereby affirming that our chosen price point efficiently motivates Swedish hydropower plants to reach maximum output during these critical periods, given that prices during the remainder of the year align with the historical levels recorded from 2016 to 2020. Details of this sensitivity analysis are depicted in Figure A.6 in the Supplementary material.

Flow rate limitations in the rivers are crucial when considering periods of elevated market prices. Interestingly, limits on flow rates had a marginal impact when only historical prices were considered, as in the past there were limited incentives for hydropower plants to sacrifice water to sustain high output. This represents a critical takeaway message with respect to the use of historical data for model validation: factors that may seem to be irrelevant under the conditions of current energy systems and price structures could take on importance as new incentives emerge in future energy systems.

3.7. Policy implications and future research

Sweden is initiating a comprehensive process of reissuing environmental permits for approximately 2000 hydropower plants across the country, starting in Year 2024 [34,35]. Our study highlights the critical role of bottlenecks in influencing hydropower's ability to sustain high output and, consequently, the hydropower sector's capacity to mitigate energy shortages during periods of low wind or other critical phases for the energy system. While discussions surrounding the new environmental permits often revolve around how to regulate minimum flows to facilitate fish migration, among other things, this study underlines the importance of also discussing upper flow limits. We highlight the potential to enhance hydropower's ability to sustain high output through updates to environmental permits, particularly by allowing increased spillage or maximum turbine flows. However, these considerations must be carefully balanced against the risks of significant environmental consequences.

Given that hydropower constitutes a significant share of the energy system in many parts of the world, it is important to understand whether hydropower can sustain output at, for example, 50% or close to 100%, so as to evaluate the need for other types of back-up assets to ensure the supply during energy droughts. However, generalising the results of this study to other hydro-rich nations requires careful consideration, as each region presents unique technical and environmental challenges that affect the ability to sustain high output levels. Therefore, further studies of other regions are warranted to generate more robust conclusions about the broader applicability of our findings.

4. Conclusions

This study provides a comprehensive analysis of Swedish hydropower's ability to sustain high output levels during extended periods of energy droughts, offering valuable insights for both national and global energy systems. In summary, the main contributions of this study are:

- Swedish hydropower can sustain between 67% and 96% of its installed capacity over 1 to 3 weeks. The variation in the ability to sustain output over the year identified in this study is equivalent to the capacity of three to four Swedish nuclear reactors, highlighting the need to understand hydropower's operational limits when developing strategies to address energy droughts.
- River bottlenecks, which result from regulations, technical capacities, or hydrological factors that restrict maximum flow rates, pose a major constraint on the ability of hydropower to sustain high output. Adjusting regulations or technical capacities, particularly by increasing spillage limits at critical bottleneck locations, can significantly improve hydropower performance during energy droughts.
- Under the present regime of flow limits at hydropower plants, the ability to sustain output is strongly influenced by seasonal variations in natural inflow. Higher sustained output is more achievable during periods of increased inflow.

Looking forward, the findings of this study can be applied in three key ways. First, the upcoming renewal of environmental permits for hydropower plants in Sweden presents a timely opportunity for policymakers to revise regulations on maximum flow rates, potentially enhancing hydropower's ability to sustain output during critical periods. Second, the common assumption in current energy models that hydropower can sustain maximum output as long as water is available in reservoirs is challenged by our findings, which demonstrate that sustained output can be significantly lower. This underscores the need for more detailed hydropower modelling and regulatory considerations in energy system planning, both in Sweden and globally. Third, the methodology developed in this study offers a valuable tool for future research, enabling the exploration of operational limits regarding sustained output in other hydro-rich nations, thereby contributing to a more comprehensive understanding of hydropower's role in mitigating energy droughts.

Declaration of competing interest

The authors declare that they have no known competing financial interests or personal relationships that could have appeared to influence the work reported in this paper.

Acknowledgements

We thank the Swedish water regulation authorities and power production companies for valuable discussions and information regarding Sweden's river infrastructures and hydropower regulatory frameworks. Special thanks to Anna Hedström Ringvall at Vattenregleringsföretagen and Emma Wikner at Statkraft for their contributions. We also thank Vattenfall, Statkraft, Skelleftekraft, Jämtkraft, Fortum and Energiföretagen for providing the data used in this study.

This research was funded by faculty resources. Co-funding from the Swedish Energy Agency, Sweden P2022-00768 is acknowledged.

Appendix A. Supplementary data

Supplementary material related to this article can be found online at https://doi.org/10.1016/j.rser.2025.115519.

Data availability

The authors do not have permission to share data.

References

[1] Sinsel SR, Riemke RL, Hoffmann VH. Challenges and solution technologies for the integration of variable renewable energy sources—a review. Renew Energy 2020;145:2271–85, (2024). https://www.sciencedirect.com/science/article/pii/S0960148119309875.

[2] Kirkerud JG, Bolkesjø TF, Trømborg E. Power-to-heat as a flexibility measure for integration of renewable energy. Energy 2017;128:776–84, (2024). https://www.sciencedirect.com/science/article/pii/S0360544217305479.

[3] Rodríguez RA, Becker S, Andresen GB, Heide D, Greiner M. Transmission needs across a fully renewable European power system. Renew Energy 2014;63:467–76, (2024). https://www.sciencedirect.com/science/article/pii/S0960148113005351.

[4] Child M, Kemfert C, Bogdanov D, Breyer C. Flexible electricity generation, grid exchange and storage for the transition to a 100% renewable energy system in Europe. Renew Energy 2019;139:80–101, (2024). https://www.sciencedirect.com/science/article/pii/S0960148119302319.

[5] Lund PD, Lindgren J, Mikkola J, Salpakari J. Review of energy system flexibility measures to enable high levels of variable renewable electricity. Renew Sustain Energy Rev 2015;45:785–807, (2024). https://www.sciencedirect.com/science/article/pii/S1364032115000672.

[6] Johansson V, Göransson L. Impacts of variation management on cost-optimal investments in wind power and solar photovoltaics. Renew Energy Focus 2020;32:10–22, (2024). https://www.sciencedirect.com/science/article/pii/S1755008419302017.

[7] Ruhnau O, Qvist S. Storage requirements in a 100% renewable electricity system: extreme events and inter-annual variability. Environ Res Lett 2022;17(4):044018. http://dx.doi.org/10.1088/1748-9326/ac4dc8, (2023). Publisher: IOP Publishing.

[8] Kondziella H, Specht K, Lerch P, Scheller F, Bruckner T. The techno-economic potential of large-scale hydrogen storage in Germany for a climate-neutral energy system. Renew Sustain Energy Rev 2023;182:113430, (2023). https://www.sciencedirect.com/science/article/pii/S1364032123002873.

[9] Söder L, et al. A review of demand side flexibility potential in Northern Europe. Renew Sustain Energy Rev 2018;91:654–64, (2024). https://www.sciencedirect.com/science/article/pii/S1364032118302053.

[10] Hirth L. The benefits of flexibility: The value of wind energy with hydropower. Appl Energy 2016;181:210–23, (2022). https://www.sciencedirect.com/science/article/pii/S0306261916309801.

[11] Dimanchev EG, Hodge JL, Parsons JE. The role of hydropower reservoirs in deep decarbonization policy. Energy Policy 2021;155:112369, (2023). https://www.sciencedirect.com/science/article/pii/S0301421521002391.

[12] Owolabi OO, et al. A robust statistical analysis of the role of hydropower on the system electricity price and price volatility. Environ Res Commun 2022;4(7):075003. http://dx.doi.org/10.1088/2515-7620/ac7b74, (2024). Publisher: IOP Publishing.

[13] Liu H, Brown T, Andresen GB, Schlachtberger DP, Greiner M. The role of hydro power, storage and transmission in the decarbonization of the Chinese power system. Appl Energy 2019;239:1308–21, (2024). https://www.sciencedirect.com/science/article/pii/S0306261919302995.

[14] Zhao Z, et al. The importance of flexible hydropower in providing electricity stability during China's coal phase-out. Appl Energy 2023;336:120684, (2023). https://linkinghub.elsevier.com/retrieve/pii/S030626192300048X.

[15] Phillips T, et al. A metric framework for evaluating the resilience contribution of hydropower to the grid. In: 2020 resilience week. RWS, Salt Lake City, UT, USA: IEEE; 2020, p. 78–85, (2024). https://ieeexplore.ieee.org/document/9241249/.

[16] Thapa S, Magee T, Zagona E. Factors that affect hydropower flexibility. Water 2022;14(16):2563, (2023). https://www.mdpi.com/2073-4441/14/16/2563, Number: 16 Publisher: Multidisciplinary Digital Publishing Institute.

[17] Öberg S, Göransson L, Ek Fälth H, Rahmlow U. Evaluation of hydropower equivalents in electricity capacity expansion models. Preprint. Available At SSRN: https://papers.ssrn.com/sol3/papers.cfm?abstract_id=5013603.

[18] Yang W, et al. Burden on hydropower units for short-term balancing of renewable power systems. Nat Commun 2018;9(1):2633, (2024). https://www.nature.com/articles/s41467-018-05060-4, Publisher: Nature Publishing Group.

[19] Staffell I, Pfenninger S. The increasing impact of weather on electricity supply and demand. Energy 2018;145:65–78, (2024). https://www.sciencedirect.com/science/article/pii/S0360544217320844.

[20] Li B, Basu S, Watson SJ, Russchenberg HWJ. A brief climatology of dunkelflaute events over and surrounding the North and Baltic Sea Areas. Energies 2021;14(20):6508, (2024). https://www.mdpi.com/1996-1073/14/20/6508, Number: 20 Publisher: Multidisciplinary Digital Publishing Institute.

[21] Raynaud D, Hingray B, François B, Creutin JD. Energy droughts from variable renewable energy sources in European climates. Renew Energy 2018;125:578–89, (2024). https://www.sciencedirect.com/science/article/pii/S0960148118302829.

[22] Most LVD, Wiel KVD, Gerbens-Leenes W, Benders RR, Bintanja R. Temporally compounding energy droughts in European electricity systems with hydropower. preprint, In Review; 2024, (2024). https://www.researchsquare.com/article/rs-3796061/v1.

[23] Otero N, Martius O, Allen S, Bloomfield H, Schaefli B. A copula-based assessment of renewable energy droughts across Europe. Renew Energy 2022;201:667–77, (2024). https://www.sciencedirect.com/science/article/pii/S0960148122015841.

[24] Kapica J, et al. The potential impact of climate change on European renewable energy droughts. Renew Sustain Energy Rev 2024;189:114011, (2024). https://www.sciencedirect.com/science/article/pii/S1364032123008699.

[25] Stankovski A, Gjorgiev B, Locher L, Sansavini G. Power blackouts in Europe: Analyses, key insights, and recommendations from empirical evidence. Joule 2023;7(11):2468–84, (2024). https://www.sciencedirect.com/science/article/pii/S2542435123003665.

[26] Fotis G, Vita V, Maris TI. Risks in the European transmission system and a novel restoration strategy for a power system after a major blackout. Appl Sci 2023;13(1):83, (2024). https://www.mdpi.com/2076-3417/13/1/83, Number: 1 Publisher: Multidisciplinary Digital Publishing Institute.

[27] Ahmad A. Increase in frequency of nuclear power outages due to changing climate. Nat Energy 2021;6(7):755–62, (2024). https://www.nature.com/articles/s41560-021-00849-y, Publisher: Nature Publishing Group.

[28] Jeong M, You JS. Estimating the economic costs of nuclear power plant outages in a regulated market using a latent factor model. Renew Sustain Energy Rev 2022;166:112582, (2024). https://www.sciencedirect.com/science/article/pii/S1364032122004786.

[29] Huertas-Hernando D, et al. Hydro power flexibility for power systems with variable renewable energy sources: an IEA Task 25 collaboration. WIREs Energy Environ 2017;6(1):e220, (2024). https://onlinelibrary.wiley.com/doi/abs/10.1002/wene.220, _eprint: https://onlinelibrary.wiley.com/doi/pdf/10.1002/wene.220.

[30] Stoll B, Andrade J, Cohen S, Brinkman G, Brancucci Martinez-Anido C. Hydropower modeling challenges. Tech. rep. NREL/TP–5D00-68231, 1353003, 2017, (2024). NREL/TP–5D00–68231, 1353003, http://www.osti.gov/servlets/purl/1353003/.

[31] Ek Fälth H, Mattsson N, Reichenberg L, Hedenus F. Trade-offs between aggregated and turbine-level representations of hydropower in optimization models. Renew Sustain Energy Rev 2023;183:113406, (2024). https://www.sciencedirect.com/science/article/pii/S1364032123002630.

[32] Bruttoproduktion, installerad effekt samt antal anläggningar fördelat på elområde. år 2015 - 2022 sv. 2024, http://www.statistikdatabasen.scb.se/pxweb/sv/ssd/START_EN_EN0105_EN0105A/AnlInstEffBrProd/.

[33] Topplasttimmen sv. 2024, (2024). https://www.svk.se/om-kraftsystemet/kraftsystemdata/topplasttimmen/.

[34] Moderna miljövillkor - Nationella planen sv. 2024, https://www.domstol.se/amnen/mark-och-miljo/miljotillstand/moderna-miljovillkor---nationella-planen/.

[35] Regeringskansliet Ro. Omprövning av vattenkraftverkens miljötillstånd pausas 12 månader sv. 2022, Text. (2024) https://www.regeringen.se/pressmeddelanden/2022/12/omprovning-av-vattenkraftverkens-miljotillstand-pausas--12-manader/, Publisher: Regeringen och Regeringskansliet.

Paper D

Balancing Rivers and Grids: Electricity System Impacts of Environmental Hydropower Regulation

Balancing Rivers and Grids: Electricity System Impacts of Environmental Hydropower Regulation

Manuscript

Hanna Ek Fälth [1,*], *Lina Reichenberg* [1], *Holger Johansson* [1], *Simon Öberg* [2], *Fredrik Hedenus* [1]

1 Department of Space, Earth and Environment, Division of Physical Resource Theory, Chalmers University of Technology, Gothenburg, Sweden

2 Department of Space, Earth and Environment, Division of Energy Technology, Chalmers University of Technology, Gothenburg, Sweden

* *hanna.ek.falth@chalmers.se*

Abstract

Hydropower provides dispatchable generation capacity and large-scale energy storage through reservoir operations, but its operations alter river flow regimes and obstruct fish migration. Using a Northern European dispatch model with detailed plant-level hydropower representation, we quantify the electricity system consequences of two categories of environmental constraints: connectivity measures (mandatory bypass flows for fish passage) and hydropeaking limitations (constraining daily flow variation). Our analysis yields three main findings. First, connectivity measures reduce annual hydropower production but preserve operational flexibility, whereas the hydropeaking scenario has only minor production effects but directly reduces intraday balancing capacity; this distinction determines how the system responds and which resources compensate. Second, contrary to common assumptions emphasizing hydropower's flexibility value, connectivity constraints impose larger system cost increases than hydropeaking constraints in todays electricity system: energy removed through bypass flows must be replaced by higher-cost thermal generation, whereas the flexibility loss can be partially compensated by other flexible resources in the interconnected system. Third, costs fall primarily on the regions where constraints are imposed. Among market actors within these constrained regions, regulated hydropower producers bear the largest losses, while a modest electricity price increase creates limited cost increases for consumers and benefits non-constrained generators.

Keywords

Hydropower, Electricity systems, Environmental regulations, River ecosystems

1 Introduction

Decarbonizing the electricity system while maintaining reliability and affordability represents one of the central challenges of the energy transition. Hydropower has long been viewed as an essential enabler of this transition, providing both dispatchable generation capacity and large-scale energy storage through reservoir operations. Its flexibility allows the integration of variable renewable energy sources such as wind and solar power [1–3], which are necessary to cost-effectively decarbonize electricity production. However, hydropower operations, particularly hydropeaking (rapid flow variations), altered flow regimes, and obstructed fish migration, have significant negative impacts on river ecosystems [4, 5]. This creates a fundamental tension between two critical environmental objectives: decarbonization of the electricity system through renewable energy, and the restoration and protection of aquatic ecosystems and biodiversity.

This tension is not unique to any single country but represents a global challenge facing all nations with significant hydropower resources. In the European Union, this conflict manifests in the simultaneous pursuit of carbon-neutral electricity production under the European Green Deal [6] and the restoration towards "good ecological status" for water bodies under the EU Water Framework Directive [7]. Sweden and Norway provide timely examples where comprehensive regulatory processes are currently underway to revise environmental permits for existing hydropower facilities [8, 9]. In Sweden, failure to comply with the EU Water Framework Directive's requirements has led to repeated infringement proceedings by the European Commission, resulting in governmental commitments to revise environmental permits for all hydropower plants, a large-scale process currently being implemented through environmental courts [10].

There are a limited amount of studies that consider both changing environmental constraints and evaluate the consequences of these for the system value of hydropower [11–19]. Across the studies, a consistent picture emerges: tighter environmental constraints on hydropower reduce production [11–13, 18, 19] and operational flexibility [11, 12, 14, 15, 17–19]. The environmental constraints considered may be divided into those that increase connectivity [11–13, 16, 18, 19] and those that limit the hydropeaking [11, 14, 16–19]. It seems that connectivity constraints mainly affect the production volume [11–13, 16, 18, 19], while ramping constraints (to limit hydropeaking) mainly affect the flexibility [11, 14, 17–19].

The studies that evaluate the economic effects of future, more stringent environmental constraints for hydropower operation use models that are motivated by exogenous prices [13, 15–19], dispatch models [11, 12], or investment models [14]. The significance of this methodological difference for the results is fundamental: exogenous prices cannot capture the dynamic effects of other generation "stepping in" when hydropower capacity is effectively temporarily withdrawn, which is the effect of more stringent environmental constraints. Such dynamics are essential to capture cases where total hydropower operation is affected enough to have a significant effect on power prices in the price area or region. In other words: if the goal is to assess new environmental constraints for a hydropower plant that is much smaller than the total capacity in the price region, approaches using exogenous prices may be relevant. However, if the plant is relatively large compared to the sum of other flexible generation in the price region, such approaches are likely to overestimate the decrease in revenue for hydropower plants due to the new environmental constraints. The dynamics affect both consumer surplus, through power prices, and producer surplus, through both prices and changes in dispatch. The latter is illustrated by the somewhat counter-intuitive result that total revenues slightly increased for the hydropower producers affected by the environmental constraints in [11]. The reason is that the decrease in capacity due to the environmental constraints changed the merit order in such a way that power prices increased and compensated for the production loss.

Despite a growing literature on the environmental impacts of hydropower and its role in low-carbon electricity systems, three critical gaps remain.

First, existing studies typically assess specific sets of environmental regulations or case-specific permit revisions, making it difficult to generalize results across regulatory designs. In particular, the literature does not clearly distinguish between different categories of environmental constraints, such as connectivity measures (fish passage flows) versus hydropeaking limitations (flow variation constraints), and separately analyze their respective impacts on electricity systems. This limits the transferability of findings across regulatory contexts.

Second, many system-level assessments rely on exogenous electricity prices. Such approaches cannot capture market feedback effects whereby reduced hydropower availability alters the merit order, changes electricity prices, and induces compensating responses from other generation technologies. As a result, they risk misrepresenting both the magnitude and the incidence of economic impacts, particularly when hydropower constitutes a large share of regional flexibility.

Third, while several studies estimate changes in system costs or producer revenues, as far as we know none examine how the economic burden of environmental regulations is distributed across market actor groups, including consumers, regulated hydropower producers, other generators, and transmission system

operators.

Addressing these gaps requires combining detailed plant-level hydropower modeling with large-scale electricity system representation. On one hand, implementing and evaluating plant-specific environmental constraints demands high-resolution cascade modeling that captures water travel times, reservoir storage dynamics, and individual turbine characteristics. On the other hand, quantifying system-wide consequences and identifying which alternative generation technologies substitute for constrained hydropower requires modeling the broader interconnected electricity system with sufficient geographical scope. While recent studies of Norwegian hydropower have approached this level of integration [11, 12], comparable detailed system-wide analyses for Swedish hydropower are absent from the literature.

This paper addresses these gaps by examining environmental constraints as conceptual categories rather than policy-specific packages. We focus on two categories currently being discussed in regulatory processes: connectivity measures (requiring mandatory fish passage flows at dam sites) and hydropeaking limitations (constraining flow variation rates to reduce downstream impacts). These categories address fundamentally different ecological stressors; connectivity restores migratory pathways for fish, while hydropeaking limitations reduce harmful flow fluctuations in downstream ecosystems, and comprehensive river restoration will generally require a combination of both. We categorize them not to suggest that one could replace the other, but to distinguish their respective effects on electricity generation, operational flexibility, and electricity system economics. This categorical approach yields generalizable insights transferable to other hydropower systems facing similar regulatory pressures. We evaluate their consequences using an integrated multi-region electricity system model with endogenous price formation and detailed plant-level cascade representation, enabling us to quantify both aggregate efficiency losses and their distribution across regions and market actors.

Specifically, we address three research objectives:

1. To quantify and compare the effects of two categories of environmental constraints (connectivity measures and hydropeaking limitations) on hydropower generation and operational flexibility, and the resulting system-level impacts on the broader electricity system.

2. To assess how the system-level costs are distributed geographically, distinguishing between impacts borne by constrained regions and spillover effects on neighboring interconnected regions.

3. To evaluate how the economic impacts of environmental constraints are distributed across market actor groups, including consumers, regulated hydropower producers, other producers, and transmission system operators.

2 Methods

The objective of this study is to quantify how different types of environmental constraints (connectivity measures, hydropeaking limitations, and natural flow requirements) on hydropower operations affect the broader electricity system. We examine impacts on total system costs, electricity prices, and the distribution of economic effects across regions and among market actor groups (consumers, hydropower producers, other producers, and TSOs). To address this, we designed seven environmental constraint scenarios representing different regulatory approaches, ranging from removing existing constraints to imposing natural flow operations (see Section 2.2), and analyzed their impacts using detailed energy system modeling over Northern Europe.

For this analysis, we employ RAPID (River and Power System Integrated Dispatch), a continental-scale electricity system optimization model with detailed hydropower cascade modeling (see Section 2.1). The model determines cost-minimizing hourly electricity system operation across Northern Europe while representing Swedish hydropower at individual plant and turbine resolution. This enables explicit implementation of plant-specific environmental constraints and tracking of how these constraints propagate through river cascades to affect the broader electricity system.

2.1 Model description

This section describes the RAPID model structure, covering the optimization framework and the general representation of different generation technologies. RAPID belongs to the class of large-scale techno-economic dispatch models with endogenous price formation, similar to commercial models such as PLEXOS, PROMOD, and BID3. However, it extends this class by embedding detailed plant-level hydropower cascade modeling within a multi-region electricity system framework. Compared to detalied hydropower scheduling models, such as those described by Jafari Aminabadi *et al.* [20], which focus on water value optimization under exogenous prices, RAPID captures detailed hydropower representation with full electricity system interactions and

market feedback effects. It is therefore most closely related to recent integrated hydropower system studies (e.g. [11, 12]) using the FanSI [21] and EMPS [22] models. This section provides an overview of RAPID, and the full mathematical formulation of is found in the Supplementary material S.1.

2.1.1 Optimization framework

RAPID is formulated as a linear programming problem that minimizes total electricity system cost across all modelled regions $r \in \mathscr{R}$ and hours $t \in \mathscr{T}$, subject to physical and operational constraints. The objective function is:

$$\min \sum_{r \in \mathscr{R}} \left[\sum_{p \in \mathscr{P}^{\text{th}},\, t \in \mathscr{T}} \frac{E_{r,p,t}}{\eta_p} \cdot c_p^{\text{fuel}} + \sum_{p \in \mathscr{P},\, t \in \mathscr{T}} E_{r,p,t} \cdot c_p^{\text{var}} + \sum_{p \in \mathscr{P}^{\text{th}},\, t \in \mathscr{T}} C_{r,p,t}^{\text{cyc}} + \Gamma_r \cdot c^{\text{CO}_2} \right] \tag{1}$$

where $E_{r,p,t}$ is the electricity generation from technology $p \in \mathscr{P}$ in region r at hour t (MWh/h), η_p is the fuel-to-electricity efficiency, Γ_r is the total regional CO_2 emissions and c_p^{fuel}, c_p^{var} and c^{CO_2} are fuel, variable O&M, and carbon emission costs respectively. $C_{r,p,t}^{\text{cyc}}$ captures cycling costs for thermal technologies $p \in \mathscr{P}^{\text{th}}$ (see Eq. 14).

The model determines optimal hourly dispatch of all generation units, transmission flows between regions, and energy storage operations given the regional energy balance constraint:

$$\sum_{p \in \mathscr{P}} E_{r,p,t} - B_{r,t}^{\text{ch}} - Z_{r,t}^{\text{ch}} / \eta^{\text{pump}} + \sum_{r' \in \mathscr{R}} \left[T_{r',r,t} - (1 + \gamma_{r,r'}) \cdot T_{r,r',t} \right] = \ell_{r,t} \quad \forall\, r, t \tag{2}$$

where $B_{r,t}^{\text{ch}}$ and $Z_{r,t}^{\text{ch}}$ are battery charging and pumped hydro pumping, $T_{r',r,t}$ is the power flow from region r' to r, $\gamma_{r,r'}$ is the transmission loss factor, and $\ell_{r,t}$ is electricity demand.

Electricity prices emerge endogenously as the dual variables (shadow prices) $\lambda_{r,t}$ of this regional energy balance constraint. The endogenous price formation is important since it enables us to capture how different environmental constraint scenarios affect market equilibrium by altering the merit order, the temporal allocation of hydropower, and the need for alternative generation.

2.1.2 Technology representation

The model represents the diverse operational characteristics of generation technologies across Northern Europe, capturing differences in cost structure, flexibility, and technical constraints that determine how environmental regulations on hydropower propagate through the electricity system. Figure 1 shows the merit order of generation technologies in the modelled system, ordered by marginal cost with bar widths corresponding to installed capacity in 2024. Thermal technologies (lignite, hard coal, oil, CHP, and CCGT) appear twice due to an assumed 50/50 split between old and new plants, where old plants have been appointed a 20% lower efficiency. Detailed technology and cost assumptions are provided in Supplementary Material S.2.1 and S.2.2.

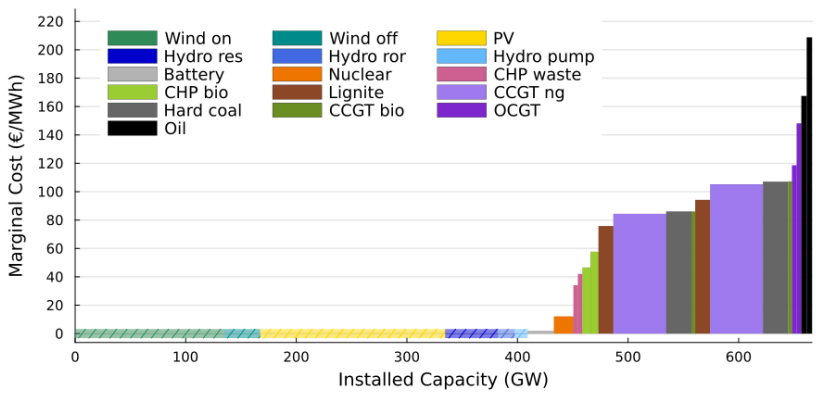

Figure 1: Merit order of electricity generation technologies. Technologies are ordered by marginal cost (€/MWh), with bar widths corresponding to total installed capacity in all modelled regions. Marginal costs include variable O&M, fuel costs, and CO_2 emission costs (cycling costs are not included). Note that technologies with zero marginal costs (wind, PV, hydro) are marked in the plot with hatched bars and that their hight are not corresponding to marginal costs.

The merit order illustrates the fundamental dispatch logic: generation technologies are deployed in order of increasing marginal cost until demand is met in each hour. However, physical and operational constraints can override this economic ordering. Storage technologies (hydropower reservoirs, pumped hydro, batteries) can shift energy across time, thermal plants face technical constraints on ramping and minimum operation levels, and variable renewables produce according to weather conditions rather than economic signals. These operational characteristics determine which technologies can substitute for reduced hydropower production and flexibility when environmental constraints are imposed. Below, we describe broadly the representation of each technology category.

Reservoir hydropower (detailed): Swedish hydropower in bidding zones SE1-SE3, covering 98% of Sweden's installed hydropower capacity, is represented at individual plant and turbine resolution using the FORSA (Flow Optimization for River Systems Analysis) framework (extending on model B:L in [23]), characterizing 33 reservoir-only facilities and 219 power plants with 421 individual turbines across nine major river systems[1]. The core equation governing each facility is the water balance. For each river $ri \in \mathcal{V}$, hydropower plant $pl \in \mathcal{H}_{ri}$, and hour t:

$$\begin{aligned} V_{ri,t,pl} = V_{ri,t-1,pl} + i_{ri,t,pl} - \sum_{j \in \mathcal{J}_{ri,pl}} Q^{\mathrm{d}}_{ri,t,pl,j} - \sum_{pl' \in \mathcal{D}^{\mathrm{b}}(pl)} Q^{\mathrm{b}}_{ri,t,pl,pl'} - \sum_{pl' \in \mathcal{D}^{\mathrm{sp}}(pl)} Q^{\mathrm{sp}}_{ri,t,pl,pl'} \\ + \sum_{pl' \in \mathcal{U}^{\mathrm{d}}(pl)} \sum_{j \in \mathcal{J}_{ri,pl'}} Q^{\mathrm{d}}_{ri,t-\tau^{d},pl',j} + \sum_{pl' \in \mathcal{U}^{\mathrm{b}}(pl)} Q^{\mathrm{b}}_{ri,t-\tau^{b},pl',pl} + \sum_{pl' \in \mathcal{U}^{\mathrm{sp}}(pl)} Q^{\mathrm{sp}}_{ri,t-\tau^{sp},pl',pl} \end{aligned} \tag{3}$$

where V is the stored water ($\mathrm{m}^3/\mathrm{s{\cdot}h}$), Q^{d}, Q^{b}, and Q^{sp} are turbine discharge for each turbine $j \in \mathcal{J}$, bypass flow (fish passage), and spillway flow. $\mathcal{U}^{\mathrm{d/b/sp}}(pl)$ and $\mathcal{D}^{\mathrm{b/sp}}(pl)$ are the upstream and downstream neighbours by flow pathway, with pathway-specific time delays τ.

An effective discharge, $D_{ri,t,pl,j}$, is calculated using the efficiency-weighted turbine discharge. It is bounded by piecewise-linear segments fitted to each turbine's individually calibrated (with historical production data) efficiency–discharge curve:

$$D_{ri,t,pl,j} \leq \left(k^{s}_{ri,pl,j} \cdot Q^{\mathrm{d}}_{ri,t,pl,j} + m^{s}_{ri,pl,j}\right) \cdot \sigma_{ri,t,pl,j} \quad \forall\, s \in \mathcal{S} \tag{4}$$

where $k^{s}_{ri,pl,j}$ and $m^{s}_{ri,pl,j}$ are the slope and intercept of efficiency segment s. The piecewise-linear upper bound ensures that at any discharge level, the effective discharge equals the minimum across all segments, correctly approximating a concave efficiency curve. In addition, $\sigma_{ri,t,pl,j} \in \{0,1\}$ indicates whether the turbine is available, accounting for stop hours for maintenance that are incorporated based on estimates from power companies.

Power production at each turbine, $P_{ri,t,pl,j}$, is linearized around the mean head $\overline{h}_{pl}$:

$$P_{ri,t,pl,j} \leq \left[\overline{h}_{pl} \cdot D_{ri,t,pl,j} + H_{ri,t,pl} \cdot d^{*}_{pl,j} \cdot \eta^{*}_{pl,j} - \overline{h}_{pl} \cdot \eta^{*}_{pl,j} \cdot d^{*}_{pl,j}\right] \cdot g \cdot \rho \cdot 10^{-6} \tag{5}$$

$$H_{ri,t,pl} = W^{\mathrm{f}}_{ri,t,pl} - W^{\mathrm{t}}_{ri,t,pl} \tag{6}$$

where H is the hydraulic head (forebay water level minus tailrace water level, see S.1.4 for how water levels are modelled), and $d^{*}_{pl,j}$ is the best-efficiency discharge with corresponding efficiency point $\eta^{*}_{pl,j}$ for turbine j.

Multiple diverse environmental constraints are modelled for individual plants (see 2.2 and Supplementary Material S.1). Environmental constraints can act on water flows (*b* - bypass, *sp* - spillway, *tot* - discharge+bypass+spillway) or forebay water levels/reservoir volume. Below follows the most used constraints; the full list is found in the Supplementary material S.1.5.

Each flow pathway is bounded and hourly ramp limits constrain the rate of change:

$$\underline{q}^{\mathrm{tot}}_{ri,t,pl,pl'} \leq Q^{\mathrm{tot}}_{ri,t,pl,pl'} \leq \overline{q}^{\mathrm{tot}}_{ri,t,pl,pl'} \quad \forall\, ri,t,pl,pl' \tag{7}$$

$$Q^{\mathrm{tot}}_{ri,t,pl,pl'} - Q^{\mathrm{tot}}_{ri,t-1,pl,pl'} \leq \delta^{\uparrow,\mathrm{tot}}_{ri,t,pl,pl'} \tag{8}$$

$$Q^{\mathrm{tot}}_{ri,t,pl,pl'} - Q^{\mathrm{tot}}_{ri,t-1,pl,pl'} \geq -\delta^{\downarrow,\mathrm{tot}}_{ri,t,pl,pl'} \tag{9}$$

[1] Luleälven, Skellefteälven, Umeälven, Ångermanälven, Indalsälven, Ljungan, Ljusnan, Dalälven, and Götaälv (including Klarälven)

with analogous bounds on Q^{b} and Q^{sp}.

Variation within periods (*per*) like days or weeks on forebay levels is constrained using auxiliary variables that track the maximum and minimum within each period:

$$\max_{t \in per} W^{\mathrm{f}}_{ri,t,pl} - \min_{t \in per} W^{\mathrm{f}}_{ri,t,pl} \leq \overline{\delta}^{\mathrm{f,per}}_{ri,d,pl} \tag{10}$$

with analogous bounds on Q^{tot}, Q^{b}, and Q^{sp}

Reservoir hydropower (aggregated): Hydropower in non-SE regions uses a two-storage representation distinguishing between long-term seasonal storage and short-term regulation, i.e each region is modelled with one large and one small reservoir. The large reservoir is dimensioned according to data on aggregated reservoir capacity, and the small reservoir is dimensioned to hold on average one week of the yearly inflow. Generation draws from the short-term reservoir, which is replenished by local inflow and transfers from the long-term reservoir:

$$S^{\mathrm{sh}}_{r,t} \leq S^{\mathrm{sh}}_{r,t-1} + i^{\mathrm{sh}}_{r,t} + \Phi_{r,t} - E_{r,\mathrm{Hydro},t} \tag{11}$$

$$S^{\mathrm{lo}}_{r,t} \leq S^{\mathrm{lo}}_{r,t-1} + i^{\mathrm{lo}}_{r,t} - \Phi_{r,t} \tag{12}$$

where $i^{\mathrm{sh}}_{r,t}$ and $i^{\mathrm{lo}}_{r,t}$ are inflows to each reservoir and $\Phi_{r,t} \leq \overline{\phi}_r$ is water transferred from long-term to short-term storage, bounded by the region's installed hydropower capacity. The inequality form allows for spillage when reservoirs are full.

The assumed inflow split varies by region, where regions with large scale hydropower is allocated up to 70% to long-term storage and 30% to short term while regions with more run-of-river character is allocated down to 20% to long-term-storage and 80% to long term (see Supplementary Table S.11). This two-storage approach reduces the overestimation of flexibility that would result from assuming that all inflow can be stored in large reservoirs.

Thermal generation: Thermal power plants, including lignite, hard coal, oil, combined-cycle gas turbines, open-cycle gas turbines, combined heat and power plants, and nuclear plants, are modelled using a two-variable approach [24, 25] that captures unit commitment effects without binary variables. This representation is critical for our analysis, as overestimating thermal plant flexibility would bias the estimated cost of reduced hydropower flexibility.

For each hour, the model determines both the committed ("hot") capacity $K_{r,p,t}$ and actual generation $E_{r,p,t}$:

$$\mu_p \cdot K_{r,p,t} \leq E_{r,p,t} \leq K_{r,p,t} \tag{13}$$

where μ_p is the minimum stable generation level as a fraction of committed capacity. Changing committed capacity incurs cycling costs:

$$C^{\mathrm{cyc}}_{r,p,t} \geq \Delta K_{r,p,t} \cdot c^{\mathrm{start}}_p + \left(K_{r,p,t} - E_{r,p,t}\right) \cdot c^{\mathrm{partload}}_{p,r} \tag{14}$$

where $\Delta K_{r,p,t}$ captures capacity increases (start-ups) and c^{start}_p and $c^{\mathrm{partload}}_{p,r}$ are start-up and part-load costs. The increase in committed capacity is bounded by the start-up time τ_p: a plant can only recommit capacity that has been cold for at least τ_p hours (see Eqs. S.34–S.35). This means that technologies with long start-up times, such as coal plants, are physically prevented from cycling rapidly regardless of the cost incentive, while fast-starting technologies such as open-cycle gas turbines face no such restriction. See Supplementary Table S.5 for parameter values.

For **nuclear** plants, availability is additionally constrained through two complementary mechanisms to capture unplanned and planned outages. First, unplanned outages are imposed on each individual reactor based on historical patterns from the IAEA PRIS database (2016-2024), with reactor-specific average unplanned outage hours (see Supplementary Table S.10). $\alpha^{\mathrm{uo}}_{r,t}$ represents an unplanned outages set which is zero for specific regions and hours based on the historical patterns, which limits nuclear power production, $E_{r,\mathrm{Nuclear},t}$ to:

$$E_{r,\mathrm{Nuclear},t} \leq \kappa_{nuc,r} \cdot \alpha^{\mathrm{uo}}_{r,t} \tag{15}$$

where $\kappa_{nuc,r}$ is the installed regional nuclear capacity.

Second, total annual generation is constrained (see Supplementary Table **??**), capturing both unplanned and planned maintenance requirements, so that the model can optimally choose when to schedule additional downtime (representing planned maintenance), allowing this to occur during periods of low system value rather than at fixed times.

$$\sum_{t \in \mathcal{T}} E_{r,\text{Nuclear},t} \leq \kappa_{\text{nuc},r} \cdot \alpha_r \cdot |\mathcal{T}|/8760 \tag{16}$$

where α_r is the availability factor, i.e the maximum full load hours obtainable based on historical unplanned and planned outages.

Transmission: Inter-regional electricity trade is modelled using a transport model with Net Transfer Capacity (NTC) bounds from the ENTSO-E Transparency Platform (2024 data):

$$0 \leq T_{r,r',t} \leq \overline{v}_{r,r',t} \quad \forall\, r, r' \in \mathcal{R},\, t \in \mathcal{T} \tag{17}$$

where $\overline{v}_{r,r',t}$ is the net transfer capacity between bidding zones. Transmission losses of 5% per 1000 km are applied (see the loss term $(1+\gamma_{r,r'})$ in Eq. 2). Each bidding zone is treated as a copperplate.

Variable renewables: Wind and solar power production is modelled using hourly capacity factors derived from the Global Energy GIS package [26, 27]. Capacity factors are multiplied by installed capacity from national transmission system operators and ENTSO-E statistics (2024) to determine hourly generation potential. Technology-specific and region-specific scaling factors (0.7-0.9) adjust the capacity factors for modelled production to match actual reported generation in 2024, accounting for non-ideal siting, old fleets etc.

Energy storage: Battery storage is modeled with region-specific power and energy capacities. Pumped hydro storage is modeled as closed-loop systems with region-specific production capacity, pump capacity, and storage reservoir size (see Supplementary Table S.7).

2.1.3 Data sources

Generation capacity data by technology and region for 2024 is mostly obtained from the ENTSO-E Transparency Platform [28], supplemented with national sources (UK [29], SE [30]). Nuclear availability data comes from the IAEA PRIS database [31]. Electricity demand profiles use historical hourly load data from ENTSO-E [32]. Fuel prices are from [33, 34]. Carbon prices reflect EU ETS allowance prices for 2024. Technology-specific costs are from [35].

2.2 Environmental constraint scenarios

We design seven environmental constraint scenarios containing some of the measures currently under discussion in the process of Swedish environmental permit revisions following the EU Water Framework Directive implementation.

The baseline scenario (*Current*), represents existing plant-specific environmental court rulings in Swedish hydropower, including for instance minimum flow or bypass flow requirements, reservoir level restrictions, and limits in variation of flow and levels on different time scales, that vary by plant and season. Table 1 provides an overview of all modelled scenarios and their key characteristics. The connectivity and hydropeaking categories address fundamentally different ecological stressors and comprehensive river restoration will generally require a combination of both. We separate them here to distinguish their respective effects on the electricity system, not to suggest that one could substitute for the other.

The *No env. constraints* scenario (Table 1) removes all existing environmental constraints that currently regulate Swedish hydropower operations. This scenario serves as a theoretical upper bound for hydropower operational flexibility and production, representing conditions where plants face no flow restrictions, reservoir level limitations, or ramping constraints beyond physical and technical equipment capabilities. While this scenario does not represent a realistic policy option, it provides an essential reference point for quantifying the total opportunity cost of current environmental regulations. By comparing this unconstrained scenario with the *Current* baseline, we can measure how much operational flexibility and economic value has already been foregone under today's regulatory framework, contextualizing the incremental impacts of proposed additional constraints.

Table 1: Overview of the seven environmental constraint scenarios analyzed in this study. The scenarios target different ecological stressors: connectivity measures address river fragmentation and fish migration barriers, hydropeaking measues adresses impacts on downstream ecosystems and natural flow scenarios are there to illustrate the most extreme scenario where the hydropower plants would be operated as no regulation of the water was allowed. For reference, a scenario removing today's permits is included and called *No env. constraints*

Scenario name	**Category**	**Description**
No env. constraints	Unconstrained	Removed existing plant-specific environmental constraints including current minimum flows, bypass flows, reservoir level restrictions, and flow/level variation limits as stipulated in environmental court rulings.
Current	Baseline	Existing plant-specific environmental constraints including current minimum flows, bypass flows, reservoir level restrictions, and flow/level variation limits as stipulated in environmental court rulings.
+ Connectivity 1	Connectivity	Mandatory bypass flow of 1 m^3/s at all plants, added to the other types of existing constraints in the *Current* scenario.
+ Connectivity 5	Connectivity	Mandatory bypass flow of 5 m^3/s at all plants, added to the other types of existing constraints in the *Current* scenario.
- Hydropeaking	Hydropeaking	Constrains maximum daily flow variation to limit hydropeaking, added to the existing constraints in the *Current* scenario.
Natural flow	Natural flow regime	Operations must follow natural inflow patterns within narrow bands (90-110% of natural inflow), approximating run-of-river operation. Existing constraints in the *Current* scenario are removed.
Natural flow + Connectivity	Natural flow regime	Combines natural flow constraints (90-110% of natural inflow) with mandatory 5 m^3/s bypass flows at all plants. Existing constraints in the *Current* scenario are removed.

The *Current* scenario (Table 1) represents the baseline condition with existing plant-specific environmental constraints as stipulated in current environmental court rulings. These constraints vary substantially across plants and river systems, reflecting site-specific ecological conditions. Typical constraints include minimum flow requirements, bypass flow obligations, reservoir level restrictions that limit drawdown rates and mandate minimum water levels during critical seasons, and operational constraints on flow variations over different time scales (hourly, daily, weekly, and seasonal). Additionally, we assume that weekly flow variations through bypass outlets (spillways not used for power generation) are limited to 10% of the weekly mean flow to reflect typical operational practices that avoid rapid fluctuations in these controlled releases (see Eq. 10). This heterogeneous regulatory landscape reflects the historical development of Swedish environmental law and provides the baseline against which we evaluate proposed additional measures from the EU Water Framework Directive implementation. Based on the permit data compiled for this study, spillage flow requirements exist at 34 of 254 river stretches modeled across SE1–SE3 (13%), with year-round requirements at 22 of these and seasonal requirements at the remaining 12. Where such requirements exist, required flows range from 0.05 to 40 m^3/s, with a median of approximately 2.5 m^3/s. The connectivity scenarios modeled here therefore represent both a substantial expansion in spatial coverage and, for many plants, an increase in required bypass flow magnitude relative to current conditions.

The + *Connectivity* scenarios (Table 1) impose mandatory flow through fish passages in all 252 facilities to restore connectivity for migratory fish species, addressing one of the primary ecological impacts of river fragmentation by hydropower dams. This is modeled via Eq.7 for bypass flows (Q^b). The required flow for effective fish passages is very location specific, and requires minimum flows to provide hydraulic cues and sufficient water depth for migration. Due to the lack of data on appropriate fish passage flow rates for all Swedish hydropower plants, a uniform flow is assumed across all passages, and two scenarios are analysed: 1 m^3/s and 5 m^3/s.

The - *Hydropeaking* scenario (Table 1) limits daily total flow fluctuations at each plant, to reduce hydropeaking, by constraining the maximum daily flow change to 50% of each plant's LLQ (Lowest Low flow across all years of historical data). This is modelled via Eq.10 for total flow (Q^{tot}) For example, a plant with LLQ of 20 m^3/s can vary its total flow (discharge + bypass + spillway) by at most 10 m^3/s within a 24h period. Across the 213 plants subject to this constraint, the median LLQ is 8.16 m^3/s (range 0.01–67.18 m^3/s),

yielding a median daily variation limit of 4.08 m^3/s. LLQ values generally increase downstream as tributaries contribute additional baseflow. There is no standardized definition of what constitutes a hydropeaking constraint; our plant-level daily variation limit represents one possible approach. For comparison, Haas *et al.* [14] use a system-wide hourly flashiness index that penalizes aggregate hour-to-hour ramps across all plants rather than imposing plant-specific daily limits. To ensure problem feasibility, approximately 5% of total facilities were exempted from these daily variation constraints based on preliminary optimization tests (see Supplementary Material Section S.3 for details).

The *Natural flow* scenarios (Table 1) represent the most stringent environmental restoration measures, serving as a test of how eliminating flow regulation capabilities would affect the electricity system. These scenarios require operations to follow natural inflow patterns within narrow bands. While it is not realistic to assume that all inflow would discharge immediately, as even natural rivers exhibit storage-discharge relationships through natural thresholds and topographic controls, we lack detailed data on these natural hydraulic characteristics. Therefore, we approximate this natural behavior by requiring discharge to remain between 90-110% of instantaneous inflow for the majority of river stretches. This is modelled via Eq.7 for total flows (Q^{tot}). The standard 90-110% constraint was applied to approximately 86% of river stretches, while the remaining 14% were assigned wider tolerance bands (ranging from 50-120% to 80-120%) to ensure problem feasibility based on preliminary optimization tests (see Supplementary Material Section S.3 for details). The *Natural flow + Connectivity* scenario combines these natural flow constraints with mandatory 5 m^3/s fish passage flows at all facilities, using Eq.7 for bypass flows (Q^b), representing an upper bound of environmental restoration.

2.3 Case study design

To compare how different environmental constraint categories affect electricity systems and market actor groups, we use Swedish hydropower as a case study. Sweden provides a timely and detailed case with comprehensive environmental permit revisions currently being implemented under the EU Water Framework Directive, with a target completion by 2040. We run the model as a dispatch model with fixed generation, storage, and transmission capacity using 2024 data. This fixed-capacity approach allows us to compare the impacts of different environmental constraint categories without confounding effects from investment responses. The longer-term implications, including how investment responses might mitigate the impacts we identify, are discussed in Section 4.

We model the Northern European electricity system with both broad geographical coverage and detailed hydropower representation where environmental constraints are imposed. This multi-region scope is essential for examining how the economic burden of environmental constraints on Swedish hydropower is distributed both across regions (through trade and price effects) and across market actor groups (consumers, producers, transmission system operators) within and beyond Sweden. The geographical scope encompasses 19 bidding zones across 11 countries (see Figure 2), interconnected through the existing transmission network. Swedish hydropower in SE1-SE3, containing approximately 98% of Sweden's hydropower capacity, is modelled at individual plant and turbine resolution, while other regions employ a simpler two-level storage approach (see Section 2.1.2). Each model run covers three full years with hourly resolution, necessary to capture hydropower's multi-timescale operations: inter-year reservoir storage, seasonal storage dynamics, and hourly flexibility provision on the day-ahead market.

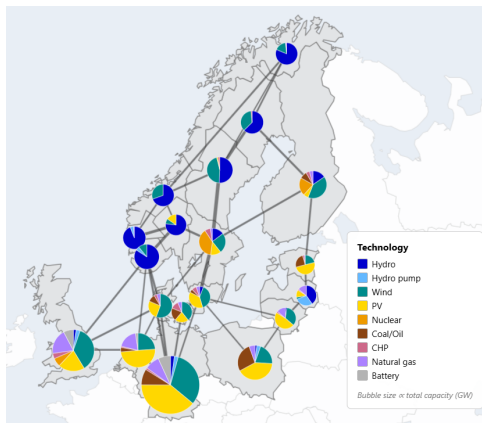

Figure 2: Map over the modelled regions. 19 bidding zones across 11 countries in Northern Europe. Pie charts show the installed generation capacity mix in each bidding zone based on 2024 data (see S.2.2), with size relative to total installed capacity.

To assess the sensitivity of our results to hydrological and meteorological conditions, we model three different weather periods spanning 2016-2024 using historical data, three years at a time (2016-2018, 2019-2021, 2022-2024). This approach captures substantial variation in hydropower inflows (from dry to wet years), wind and solar production patterns, and different electricity demand profiles across diverse climatic conditions. Each weather period is modelled as an independent three-year period with the 2024 capacity mix.

2.4 Economic analysis

To address our research objectives of quantifying the economic efficiency losses caused by environmental constraints on hydropower and assessing how these impacts are distributed across market actor groups, we derive a comprehensive set of economic metrics from the model outputs. These metrics capture changes in generation costs, electricity prices, and economic surpluses across market actor groups. Throughout this analysis, economic efficiency refers strictly to electricity market outcomes and does not account for the environmental benefits of stricter regulations. These benefits fall outside our modelling scope but are essential considerations for comprehensive policy evaluation.

System cost: The total electricity system cost is the objective function value minimized by the model, consisting of variable generation costs (fuel, variable O&M, and CO_2 emissions costs) and cycling costs for thermal units, across all modelled regions. System cost changes quantify the economic efficiency loss from environmental constraints, measured as the difference in total system cost between the reference scenario (current regulations) and each constraint scenario. We report both absolute cost increases (M€/yr) and normalized costs per unit of affected hydropower capacity (€/kW/yr or M€/GW/yr) to enable comparison across studies with different hydropower shares in the system. For the connectivity scenarios, we also calculate cost per unit production loss (€/MWh), dividing the system cost increase by the reduction in hydropower generation, which indicates the marginal system value of each lost MWh of hydropower generation. This metric is not reported for the hydropeaking scenario, where the primary cost driver is the loss of temporal flexibility rather than energy, making the small and variable production difference an inappropriate denominator.

Electricity prices: Electricity prices emerge endogenously as the dual variables (shadow prices) of the hourly energy balance constraints in each bidding zone. We report changes in electricity prices as consumption-weighted averages, representing the effective price experienced by consumers.

Market actor impacts: To understand how the economic efficiency loss of introducing environmental constraints is distributed, we calculate economic impacts for three market actor groups. For consumers, we calculate the change in electricity purchase costs due to price changes, assuming inelastic demand. For producers, we calculate the change in profit from selling electricity, given by revenues (price times generation) minus generation costs. To analyze distributional impacts, we partition producers into two groups: *Restricted hydropower producers* (plants in SE1-SE3 subject to the environmental constraint scenarios) and *Other producers* (all remaining generation technologies in all regions, including hydropower outside SE1-SE3). For transmission system operators (TSO), we calculate changes in congestion rents earned. When a transmission line reaches its capacity limit, the price difference between connected zones reflects the scarcity value of transmission capacity. The TSO captures this rent, calculated as the sum of price differences multiplied by transmitted energy across all congested interconnections and hours. We assume that congestion rents between two bidding zones are split equally between each region's TSO. We calculate net market actor impacts by summing changes across the four market actor groups (consumers, restricted hydropower producers, other producers, and TSOs) for each region, revealing which regions bear the economic burden of constraints imposed on Swedish hydropower.

3 Results

This section presents the results in three parts: the physical effects of environmental constraints on hydropower operations and in the electricity system (Section 3.1), the resulting economic consequences (Section 3.2), and a broader contextualization across the full spectrum of operational constraints (Section 3.3).

3.1 Connectivity decreases energy production – limited hydropeaking affects flexibility

The effect of environmental constraints on hydropower operations can be categorized into two fundamentally different ways: through reduced total electricity production (TWh/year) or through reduced operational flexibility. In this paper, we focused on evaluating the effect on daily flexibility from new environmental permits at hourly resolution, not subhourly balancing services such as frequency regulation. The scenarios analyzed in this study illustrate this distinction clearly. The connectivity scenarios (+ *Connectivity 1* and + *Connectivity 5*), which imposes fishway flow requirements to enable fish migration, primarily affects total annual production but has no impact on flexibility. Conversely, the reduced hydropeaking scenario (- *Hydropeaking*), which limits hourly and daily flow fluctuations to reduce hydropeaking impacts, primarily constrains operational flexibility while maintaining more of the annual energy production.

Figure 3 quantifies the reduction in optimal hydropower production in SE1-SE3 under three environmental constraint scenarios compared to current conditions. The + *Connectivity 1* and + *Connectivity 5* scenarios reduce annual hydropower generation by an average of 0.7 and 3.1 TWh respectively (corresponding to

1 and 4.5% of average production in the *Current* scenario), with losses relatively consistent across years. Production loss is proportional to bypass flow magnitude: the fivefold higher fish passage flow in + *Connectivity 5* compared to + *Connectivity 1* leads to a fivefold higher energy loss.

The - *Hydropeaking* scenario reduces production by on average 0.2 TWh (0.3% of baseline), with a larger variation than the connectivity scenarios. The production loss in this scenario occurs because the daily variation constraint requires relatively constant flows throughout the day. Without this constraint, operators could produce minimally during hours with low net load and ramp up during peak hours. However, maintaining constant flow means that producing at peak capacity during high-price hours requires maintaining that same high flow all day, which leads to spillage when net load is zero or below.

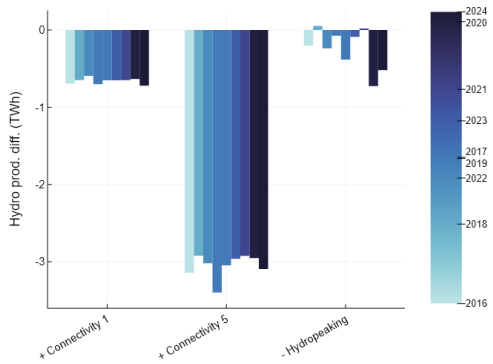

Figure 3: The reduction in hydropower production in SE1-SE3 compared to the optimal production under current environmental constraints. The different bars are for different weather years, ordered in dryest year to wettest. The colorbar to the right shows the different modelled weather years (2016-2024) on the scale from dryest to wettest. For reference, the average hydropower production for these regions in the *Current* sceario is 67.8 TWh.

While the - *Hydropeaking* causes some production loss through spillage, its primary impact is on operational flexibility rather than total energy availability. The operational differences become clear when examining production patterns over time. Figure 4 illustrates a representative week in February 2024 for SE1. Under current conditions, hydropower production exhibits pronounced daily cycles, ramping between low nighttime output and high daytime peaks. The connectivity scenarios preserve this flexibility pattern, maintaining similar daily ramping capabilities but at an overall lower absolute production level due to bypass flows. In contrast, the - *Hydropeaking* scenario fundamentally alters the production profile, with output remaining roughly constant throughout each day, as the scenario was designed to limit flow variation within days.

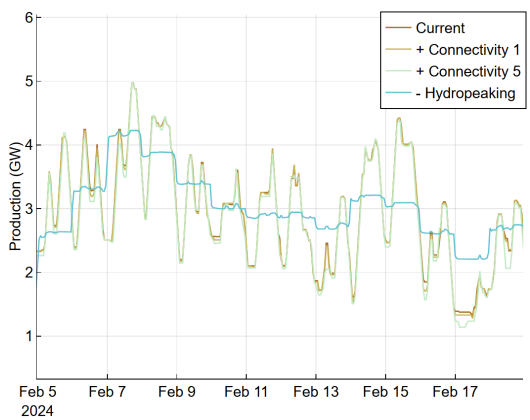

Figure 4: The hydropower production profile for SE1 a week in February 2024.

Figure 5a quantifies this flexibility loss across all nine years analyzed through boxplots showing the distribution of daily production range (maximum minus minimum production within each 24-hour period) aggregated across 2016-2024 for Swedish hydropower in SE1-SE3. Under current conditions, the median daily production range is 3.4 GW (2.5-4.5 GW interquartile range), reflecting hydropower's ability to provide daily flexibility. The connectivity scenarios maintain a nearly identical pattern, demonstrating that bypass flows do not fundamentally constrain hourly flexibility. In contrast, the - *Hydropeaking* scenario compresses the daily production range dramatically to a daily production range of 0.8 GW (0.6-1.0 GW interquartile range), representing approximately 75% reduction compared to baseline.

This pattern is confirmed through analysis of hourly ramping rates shown in Figure 5b, which displays the distribution of absolute hour-to-hour production changes. Current conditions exhibit median ramping of 0.22 GW/h with frequent ramps close to 0.6 GW/h during rapid response to price signals. The connectivity scenarios show nearly identical ramping distributions, again demonstrating that bypass flows do not fundamentally constrain hourly flexibility. In contrast, the - *Hydropeaking* scenario fundamentally alters ramping behavior. The median drops to 0.08 GW/h as production remains roughly constant within each day, while day-to-day transitions create occasional large ramps that appear as statistical outliers.

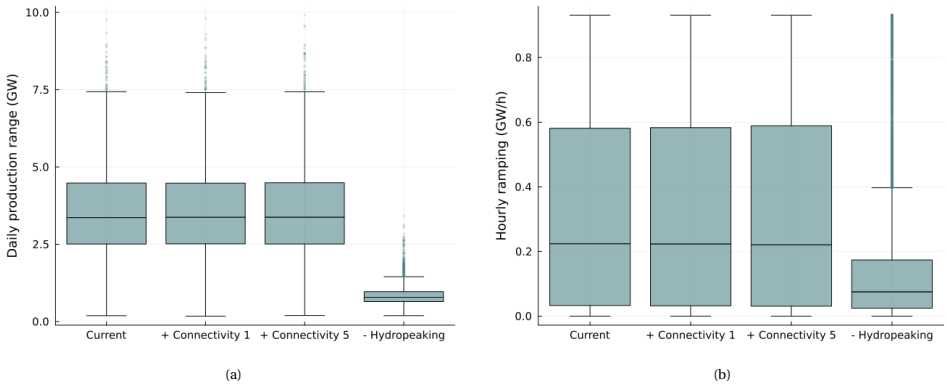

Figure 5: Distribution of hydropower flexibility metrics across all weather years (2016-2024) for the aggregated Swedish hydropower in SE1-SE3. Figure a) shows daily production range (maximum minus minimum production within each 24-hour period), where each box represents 3,285 daily observations (365 days × 9 years). Figure b) shows hourly ramp rates (absolute hour-to-hour changes), where each box represents 78,840 hourly transitions (8,760 hours × 9 years). Boxes show median (center line), interquartile range (box), whiskers extending to 1.5×IQR, and outliers beyond whiskers (points).

In summary, the results demonstrate two distinct mechanisms by which environmental constraints impact hydropower operations. The connectivity scenario imposes an energy constraint, reducing total available MWh while preserving operational flexibility. The - *Hydropeaking* scenario maintains most annual production but fundamentally limits the ability to provide daily balancing services.

3.1.1 Thermal generation and pumped hydro compensate for greater limitations on hydropower

Reductions in hydropower energy and flexibility are compensated by different technologies in the system. Figure 6 shows that gas generation provides the largest share of replacement energy in the connectivity scenarios, while pumped hydro dominates the flexibility response in the - *Hydropeaking* scenario. In the + *Connectivity* scenarios, hydropower energy is permanently removed from the system, shifting dispatch upward along the merit order. As a result, marginal generation is primarily provided by thermal plants (gas and coal, see Figure 6), which have available capacity and can increase output at the margin.

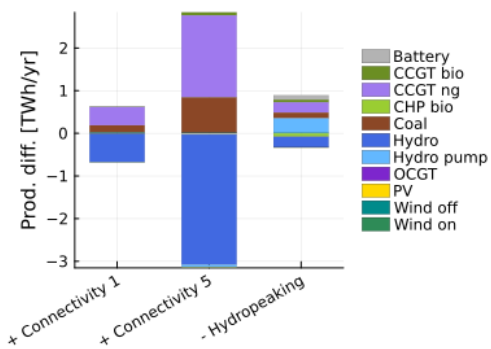

Figure 6: Average annual electricity production difference by technology compared to the reference scenario. Values represent the average across all model runs covering 2016-2024. Positive values indicate increased production relative to the reference, while negative values indicate reduced production. For results per bidding zone, see S.3.

While connectivity constraints primarily create an energy deficit that is met by thermal generation, hydropeaking constraints create a flexibility deficit that is met by storage (pumped hydro and batteries) and flexible generation (gas). This flexibility is primarily provided outside Sweden (Germany, Latvia, and Norway; see Figure S.3). In addition, hydropower in Norway is partly compensating for the lost intraday flexibility (Figure 4). Analyses of the daily production range in Sweden and Norway show that it drops by about 2.6 GW in Sweden (Figure 5a) while increasing by 0.6 GW in Norway (Figure S.1 in Supplementary material).

This highlights that while energy deficits are met by thermal generation, the loss of hydropower flexibility is primarily absorbed by storage and flexible generation. Both energy- and flexibility deficits are compensated for in other regions and mediated by cross-border trade.

These distinct substitution patterns underpin the differing system cost impacts analyzed in the following section.

3.2 Economic consequences of stricter environmental constraints

The loss in energy production and flexibility outlined in the previous section are reflected in increased system costs. The economic impact is differentiated across regions, and also across market actor groups.

3.2.1 Stricter environmental constraints increase electricity costs by 40-240 M€

Stricter environmental constraints, as defined in our scenarios (see Section 2.2), lead to higher system costs both due to lower total hydropower generation (by between 0.2 and 3.1 TWh, see Figure 3) as well as less flexibility from hydropower generators (see Figure 5). System cost increases are the sum of (i) replacement energy costs and (ii) balancing inefficiency costs. In the (+ *Connectivity* scenarios, energy withdrawal dominates, while the - *Hydropeaking*) scenario introduces intra-day constraints, thus incurring increased costs due to temporal misallocation of water resources. The economic efficiency loss, here measured as the difference in total energy system cost between the case with current environmental constraints and the scenarios with more stringent constraints, varies between on average 44–236 million €/year depending on scenario. To give a sense of the order of magnitude, this corresponds to roughly 0.5–2.7% of total consumer electricity expenditure in SE1–SE3 under current conditions; this comparison is intended only to contextualize the scale of system costs and does not describe how these costs are distributed across market actors. These system costs reflect only operational effects within the electricity system. For connectivity scenarios, additional capital expenditures would be required to construct fish passages at affected facilities, which are not included in our analyis.

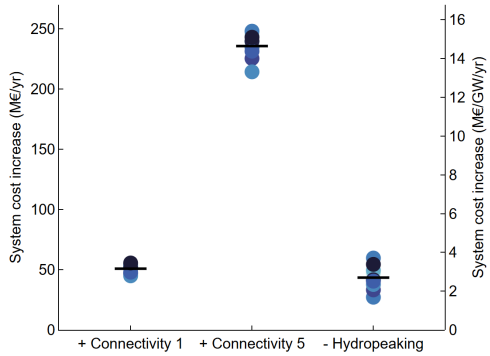

Figure 7: The implementation of environmental constraints results in increased average annual system costs. The + *Connectivity 5* scenario shows the highest increase at 236 M€/yr (15 M€/GW/yr), followed by + *Connectivity 1* at 51 M€/yr (3 M€/GW/yr), while the - *Hydropeaking* scenario results in an increase of 44 M€/yr (3 M€/GW/yr). These cost increases reflect operational effects for the electricity system only; capital expenditures for building the connectivity solutions are not included.

The connectivity scenarios average 51 M€ (+ *Connectivity 1*) and 236 M€ (+ *Connectivity 5*), differing with a factor 5 (see Figure 3). Thus, the economic efficiency loss from connectivity measures is approximately proportional to the production loss (see Table 2), which, in turn, is proportional to the sizes on bypass flows.

The system cost increase for the case when daily variation is limited (- *Hydropeaking*) is 44 M€ (averaged over the years 2016-2024), see Figure 7, which is lower than the connectivity scenarios. It is important to note that connectivity and hydropeaking restrictions address fundamentally different ecological stressors and are not interchangeable; connectivity restores migratory pathways while hydropeaking restrictions reduce downstream flow fluctuation impacts. The cost comparison therefore should not be interpreted as suggesting one measure over the other, but rather reveals that hydropeaking restrictions can be implemented at relatively modest cost in the current Northern European system (2024 capacity mix). Furthermore, the connectivity scenarios impose bypass flows of 1 and 5 m^3/s, while the hydropeaking scenario uses a daily variation limit of 50% of LLQ at each plant and reservoir, resulting in a median daily variation limit of only 4.08 m^3/s across constrained plants. There is little physical room for a more stringent daily variation limit, and bypass flows below 1 m^3/s are unlikely to provide meaningful ecological benefit. The ranking of energy versus flexibility costs is therefore not contingent on the specific parameterization of each scenario, but robust within the practically relevant range. A more important source of uncertainty is how many plants are subject to each type of constraint in a given policy implementation. More broadly, the ranking of costs depends critically on the broader system context: the relative value of energy versus power flexibility shifts as variable renewable penetration increases, transmission

Scenario	System cost increase (M€/yr)	Hydro prod. loss (TWh/yr)	Cost per lost MWh (€/MWh)
+ Connectivity 1	51 (45–56)	0.7 (0.6–0.7)	77.0 (72.0–81.0)
+ Connectivity 5	236 (214–248)	3.1 (2.9–3.4)	77.0 (71.0–82.0)
- Hydropeaking	44 (27–60)	0.2 (-0.05–0.7)	– [a]

Table 2: Summary of impacts. The first two columns summarize the energy reduction and system cost increase as presented in Figure 3 and Figure 7. The third column shows the cost per unit production loss for the connectivity scenarios, indicating the marginal system value of each lost MWh of hydropower generation. Values show averages with ranges in parentheses across nine modeled years (2016-2024). [a] Not reported: The hydropeaking scenario's system cost is driven by lost temporal flexibility, not by lost energy. The small and highly variable production loss (-0.05–0.7 TWh/yr) is a side effect of maintaining constant flows, making cost per lost MWh a misleading metric for this constraint type.

capacity expands, and alternative flexibility providers (batteries, demand response) become available. This is discussed further in Section 4.

The increase in system cost depends on the size of the power plant fleet that is affected by the stricter environmental constraints. In our case, the hydropower affected by the environmental constraints is around 16 GW, which is less than 2.5% of the total capacity of the system (Figure 1). Therefore, in order to provide generalizable results, we relate the cost increase to the size of the capacity that is affected, i.e hydropower in SE1-SE3 (Figure 7). The average cost increase ranges from 3 to 15 €/kW/yr (which could, for contextualization, be compared to O&M costs for hydropower at 45 USD/kW/yr [36]). Such numbers may be used to benchmark our results to previous and future studies.

The cost per lost MWh of hydropower production (Table 2) is 77 €/MWh for both connectivity scenarios, indicating that each MWh of bypass flow diverted from turbines imposes a consistent system cost regardless of the flow magnitude.

3.2.2 The impact on economic efficiency is mostly local

It is of general interest to understand to what extent the increase in electricity system cost, or equivalently decrease in economic efficiency [37], is borne by the regions in which the more stringent environmental constraints are implemented, and to what extent it is borne by neighboring regions. The net market actor impact per region presented in Figure 8 is the total change in consumer cost, producer profit and transmission system operator revenues (see Section 2.4).

The main efficiency loss is borne locally by the three Swedish regions where environmental constraints are implemented (SE1, SE2, SE3). Together, these regions experience net market actor losses of 47, 217, and 57 M€/yr for the + *Connectivity 1*, + *Connectivity 5*, and - *Hydropeaking* scenarios respectively (Figure 8). In the connectivity scenarios, impacts outside SE1-SE3 are minor, with neighboring regions experiencing only small changes. In the - *Hydropeaking* scenario, SE1-SE3 remain the primary losers, but impacts in other regions are more pronounced than in the connectivity scenarios. When Swedish hydropower can no longer provide daily balancing, other regions increase their cycling of storage and dispatchable generation to fill this gap (Figure 6). These generators benefit from higher revenues when providing balancing services that Swedish hydropower previously supplied, creating gains in some regions that partially offset the losses in SE1-SE3. Notably, despite the lower total system cost increase for - *Hydropeaking* compared to + *Connectivity 1* (44 vs. 51 M€/yr), Swedish regions experience higher net market actor losses under - *Hydropeaking* (57 vs. 47 M€/yr), indicating that flexibility constraints generate stronger cross-border redistribution effects than energy constraints of comparable system cost.

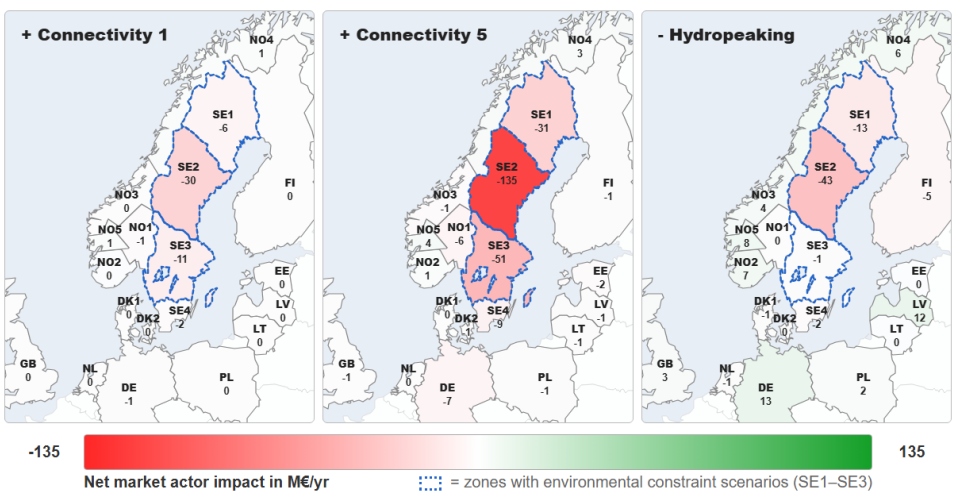

Figure 8: Annual net market actor impact (M€/yr) by region for three environmental scenarios compared to current environmental regulations, averaged across the weather years 2016-2024. Net market actor impact comprises changes in consumer costs, producer profits, and TSO income, where negative values indicate net losses. Blue borders highlight Swedish regions SE1-SE3, which are the regions where stricter environmental constraints are implemented in the scenarios. The figure shows that these regions experience substantially larger impacts than other regions. Results for individual weather years are shown in Figure S.4.

3.2.3 Hydropower producers and consumers lose

The increased system cost is unequally shared, not only between regions, but also between market actors (consumers, restricted hydro producers, other producers, and TSOs). Environmental regulation acts as constraints on the hydropower producers, thus affecting electricity prices, which, in turn, impact consumer-, producer- and TSO surplus.

The largest impact was found locally, in the regions where the stricter environmental regulations was implemented (Figure 8). Therefore, in the following, we focus on local (regions SE1, SE2 and SE3) effects, but the results in the rest of the modelled countries are qualitatively similar, and are presented in the Supplementary material (see Section S.4.3).

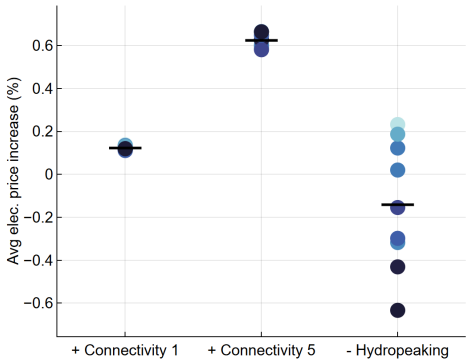

Figure 9: Average electricity price change in SE1-SE3 by scenario relative to the reference scenario. SE1-SE3 are the bidding zones containing hydropower plants subject to environmental constraint scenarios tested in this study. Each dot represents one weather year (2016-2024), colored by year. Horizontal lines show the average.

The electricity prices for the connectivity scenarios increase by 0.1% (+ *Connectivity 1*) and 0.6% (+ *Connectivity 5*). The higher electricity prices may be explained by the fact that the stricter environmental constraints impose an effective withholding of capacity and energy. Hence, the supply is limited, while the demand is the same, leading to higher equilibrium prices. Just like the system cost increase (Figure 7), the difference in average electricity price between + *Connectivity 1* and + *Connectivity 5* is proportional to the energy loss. Perhaps contrary to intuition, the price slightly *decreases* for some years (by 0.1% on average) when the hydropower plants are prevented from hour-to-hour regulation (- *Hydropeaking* scenario); see Figure 9. However, there is a greater spread between the modelled years, indicating that weather-related factors determine the sign of the effect of decreased ability for hydropeaking on the price.

Figure 10a shows the economic impact on each market actor in SE1-SE3. The change in consumer surplus reflects the changes in average (demand-weighted) electricity prices. Thus, consumers pay for part of the efficiency loss through higher electricity prices in the + *Connectivity* scenarios, and benefit from lower prices on average in the *Hydropeaking* scenario.

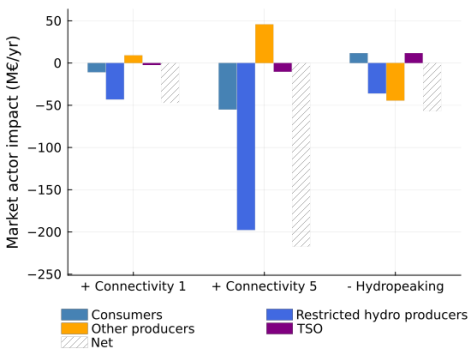

(a) Absolute impacts in M€/year.

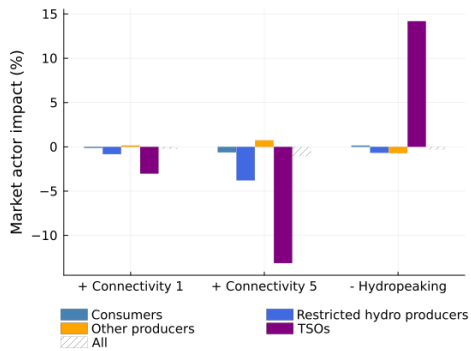

(b) Relative impacts as percentage of each market actor's total costs or revenues in the reference scenario.

Figure 10: Annual net impacts relative to the reference scenario, averaged across 2016-2024 weather years. Market actors include: consumers (affected through electricity price changes), restricted hydro producers (Plants in SE1-SE3 subject to changed environmental regulations), other producers (all remaining generation technologies), and TSOs (transmission system operators earning congestion rents). Net shows the total impact summed across all market actors.

The market actor group to suffer the greatest economic loss is the hydropower producers affected by the regulation. The loss is between 40 and 200 M€ (Figure 10a), the equivalent of a decrease in profits by 0.7% - 4% (Figure 10b). The effect of restricting hydropeaking is the least intrusive on hydropower revenues of the three scenarios.

The producers not affected by the regulation (for example wind-, nuclear power) benefit from the higher prices induced by the higher prices in the + *Connectivity* scenarios, thus increasing their surplus (Figure 10a). Conversely, the on average lower prices in the *Hydropeaking* scenario decrease their revenue too. Finally, the TSOs revenues from transmission scarcity rents are lower in the two + *Connectivity* scenarios and higher in the - *Hydropeaking* scenario, reflecting respectively lower and higher use of trade.

In summary, much in accordance with expectation, the hydropower producers subject to the environmental regulation are the market actor group most (negatively) affected by them. However, in stark contrast to previous assumptions, it is the regulations that remove energy, rather than those that limit flexibility, that are the most costly for them. Thus, at least with our experimental set-up which reflects current conditions, the flexibility of hydropower is less important for hydropower producer revenue, than is the loss of bulk energy. The relatively modest cost of hydropeaking constraints reflects current system conditions, which is discussed further in Section 4.

3.3 From unconstrained operations to run-of-river conditions, system costs span –165 to +1220 M€/yr

To contextualize the magnitude of the connectivity and limited hydropeaking environmental measures, we examine the full spectrum of operational constraints from unconstrained operations of existing plants to operations that closely track natural inflow patterns. Figure 11 presents both hydropower production loss system cost changes (bars and left axis) and corresponding system cost increases (right axis) for six scenarios relative to current regulations, spanning from completely removing existing environmental constraints (*No env. constraints*) to requiring operations to follow natural inflow patterns (*Natural flow* scenarios).

The *No env. constraints* scenario, which removes all existing environmental regulations, demonstrates that current regulations already impose a cost of 165 M€/yr (or 10 €/kW/yr when normalized by affected capacity), corresponding to a production loss of approximately 2 TWh/yr (3% of average production in the *Current* scenario). This establishes a baseline economic value that has been foregone under today's regulatory framework to achieve current environmental protection levels.

The connectivity and hydropeaking scenarios analyzed here (with bypass flows of 1 and 5 m^3/s and a daily variation limit of 50% of LLQ, see Section 3.2) impose system cost increases of 44–236 M€/yr. In stark contrast, the *Natural flow* and *Natural flow + Connectivity* scenarios, which require operations to closely track natural inflow patterns and thereby eliminate most storage and flexibility functions, result in system costs increases of on average 1024 M€/yr (*Natural flow*) and 1220 M€/yr (*Natural flow + connectivity*) and production losses of 11 and 14 TWh/yr (16-21% of baseline production, Figure 11). This dramatic cost difference reflects both a significant production loss and the fundamental transformation of hydropower's operational role: from flexible, dispatchable generation providing system balancing services to essentially run-of-river operation with minimal storage capability.

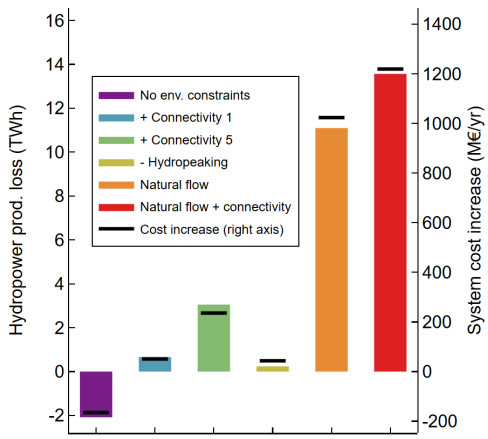

Figure 11: Average hydropower production loss (colored bars, left axis) and running cost increase (black horizontal lines, right axis) for each environmental regulation scenario, relative to the Current scenario. Bars represent the reduction in annual hydropower production in SE1–SE3 (TWh), while horizontal lines indicate the corresponding increase in total system running costs (M€/yr), including fuel, variable, CO_2, and cycling costs across all modeled regions. Values are averaged over all available simulation years (2016–2024).

4 Discussion

This study quantifies how environmental constraints on hydropower affect electricity system costs, electricity prices, and the distribution of economic impacts across market actors. By embedding detailed plant-level hydropower scheduling within a large-scale dispatch model for Northern Europe, this study is among the few to evaluate how environmental constraints impact the entire electricity system and how these impacts are distributed between regions and market actors. Furthermore, by categorizing environmental constraints by

their primary effect type rather than modeling specific policy packages, our approach enables more generalizable insights into how different constraint types affect system operations and economics.

4.1 Energy vs flexibility

Our results confirm that connectivity constraints primarily reduce annual energy production [11–13, 16, 18, 19], while hydropeaking constraints primarily limit operational flexibility [11, 14, 15, 17–19]. However, in contrast to common wisdom within the energy policy debate about the main system value of hydropower being its flexibility, we find that connectivity constraints impose larger system costs than hydropeaking constraints. The explanation for this is the features of the other generation types that substitutes for the lost energy/flexibility: Connectivity constraints divert water through fish passages that bypass turbines entirely, permanently removing zero-marginal-cost generation from the system. This lost energy must be replaced by thermal generators higher in the merit order, and no amount of temporal reallocation from other resources can compensate. Hydropeaking constraints, by contrast, do not remove water from the turbines—they only require that generation be distributed more evenly across the hours of each day. The same volume of water still produces electricity, and the modest balancing services lost can be partially substituted by other flexible resources in the Northern European system—Norwegian reservoir hydropower, gas turbines, batteries, and cross-border interconnectors—at limited incremental cost, since these resources need to adjust mainly their *timing*, not produce additional net energy. Aubin *et al.* [11] provide corroborating evidence from the Norwegian system: unconstrained hydropower plants increase their average ramping by up to 4% when other plants receive environmental constraints, but this redistribution does not fully recover the lost flexibility within the existing hydropower infrastructure. Similarly, Arvesen *et al.* [12] find that flexibility losses are to some degree offset by increased flexible operation of unaffected reservoirs and transmission interconnectors. Our results point in the same direction: while Norwegian hydropower partly compensates for the lost Swedish flexibility, as indicated by the increased daily production range in Norway (Section 3.1.1), the compensation also comes from pumped hydro and batteries in other parts of Europe, mediated through interconnectors. This is also reflected in increased TSO congestion rents under the - *Hydropeaking* scenario, indicating more intensive cross-border trade to substitute for lost Swedish hydropower flexibility, similar to the increase in transmission congestion found by Aubin *et al.* [11] for Norwegian hydropower constraints.

These system-level findings are consistent with plant-level results from Guisández *et al.* [18], who assess the revenue impact of minimum environmental flows and maximum ramping rates on twelve Spanish hydropower plants using a scheduling model with exogenous prices. They find that minimum flows reduce total energy generation much more than ramping rates, while ramping rates have a larger effect on the ability to track high-price hours—paralleling our system-level distinction between energy and flexibility impacts.

Importantly, this ranking between energy and flexibility costs is contingent on the current system configuration. If battery storage, demand-side flexibility, and sector coupling expand substantially, they would further reduce the cost of hydropeaking constraints relative to connectivity constraints. Conversely, if variable renewable penetration grows without corresponding flexibility alternatives, the scarcity value of hydropower flexibility could increase, potentially reversing the ranking observed here. In lines with this, Aubin *et al.* [11] show that system-level impacts of environmental constraints is dependent on the the system configuration.

Our analysis relies on metrics to identify which scenarios reduce flexibility. An alternative to the daily production range and hourly ramping rates used in our analysis is the Flexibility Factor (FF). The FF is defined as the ratio of the production-weighted electricity price to the average market price, where values above 1 indicate flexible operation. The FF for our scenarios actually *increases* under the - *Hydropeaking* scenario in SE2 (see Figure S.2 in the Supplementary material), contradicting the obvious flexibility reduction demonstrated by our physical metrics. This paradox arises because the FF conflates physical flexibility with market outcomes: when environmental constraints reduce hydropower flexibility, market prices adjust in response. In particular, scarcity during peak hours can raise prices and thus increase the production-weighted price even when the plant can no longer actively chase those peaks. Our finding confirms Mathisen *et al.* [15]'s caution that the FF "does not always lead to intuitive interpretations" and should be supplemented with metrics that directly assess physical flexibility. In system-wide studies with endogenous price formation, where the constraints themselves alter the price signals against which flexibility is measured, other metrics are more appropriate, as also noted by Aubin *et al.* [11].

4.2 Impact on economic efficiency

To enable comparison across studies with different hydropower shares, we normalize the system cost increase by the affected hydropower capacity in SE1-SE3 (approximately 16 GW). This yields an increase in cost of 3-

15 €/kW/yr across our scenarios (Figure 7). Out of the three studies we found that look at the effect on whole electricity systems [11, 12, 14], only one report the impact on system cost. Haas *et al.* [14] report system cost increases of up to 15% from hydropeaking constraints, but since the system sizes are different, and they do not report the absolute system cost increase or the size of the hydropower fleet it is difficult to make a direct comparison. Our connectivity scenarios impose a system cost of 77 €/MWh of lost production (Table 2).

Average electricity prices in SE1-SE3 increase by at most 0.6% for the connectivity scenarios and slightly decrease under hydropeaking constraints (Figure 9), while our most extreme scenario, *Natural flow + connectivity*, leads to a price increase of about 3%. This is substantially lower than the up to 14% price increase reported by Aubin *et al.* [11] for Norwegian hydropower, despite comparable magnitudes of affected hydropower capacity. One potential explanation is that Aubin *et al.* [11] model a future electricity system with an assumed, rather than investment-optimized, generation mix, which may introduce capacity scarcities that would not occur if investments could respond to market signals, whereas our analysis uses the existing 2024 system. The modest price impact in our results indicates that Northern European market integration in today's system effectively dampens the consumer price effect of constraints imposed on Swedish hydropower. To contextualize these price impacts, stated preference studies estimate consumer willingness to pay for environmental improvements in regulated rivers at approximately 18 €/MWh for Swedish households [38] and up to 9 €/MWh for Finnish households [39]. Our consumption-weighted price increases range from -0.1 to 2.3 €/MWh across scenarios (including the most stringent scenario tested, *Natural flow + Connectivity*), well below these WTP estimates, which could be an indication that the consumer cost of environmental constraints tested in this study remains within the range households are willing to pay for river improvements.

Regarding producer impacts, our regulated hydropower producers lose up to 4% of their revenues (Figure 10b), substantially more than in Aubin *et al.* [11], where constrained Norwegian plants slightly increase revenues in the near term (+1%) and lose only marginally in 2050 (-1%). This difference likely reflects the much larger price increase in Aubin *et al.* [11] (up to 14% versus our 0.6%), which compensates Norwegian producers for their production losses. Both studies, however, find that *unconstrained* producers benefit from the higher prices induced by constraining others. Two other studies, both harder to compare since they use models with exogenous pricing, report similar producer-side impacts: Widén *et al.* [16] found revenue decreases of 0.7-4.0% for the Umeå River under comparable connectivity scenarios, consistent with our results, and Pavičević *et al.* [13] estimated a lost economic value of approximately 60 $/MWh from bypass flow alternatives at Glen Canyon Dam which is in the same order as our revenue loss per lost production of 64-65 €/MWh for connectivity scenarios. Guisández *et al.* [18] find that plant-level revenue losses from minimum flows grow approximately linearly with flow magnitude. We find a slightly lower proportionality: lost revenues increase by a factor 4 (-50 to -200M€/yr) when increasing bypass flow size by a factor 5 (Figure 10a). A reason for the slightly smaller revenue loss per m^3/s bypass flow for the larger bypass flow scenario (+ Connectivity 5) is that the higher price increase in this scenario partially compensates for the production loss.

4.3 Implications for Swedish hydropower policy

Our results challenge the assumption, common in the Swedish policy debate, that reducing hydropeaking would impose substantial costs on the electricity system. Given that connectivity measures both induce higher electricity system costs and additional capital investments in fish passage infrastructure (as noted in Section 3.2), this cost asymmetry has implications for implementation planning. While comprehensive river restoration may require both types of measures to address their respective ecological stressors, the cost differential is informative for implementation planning: daily hydropeaking restrictions can be imposed at relatively low system cost, while connectivity improvements can carry higher costs that may warrant targeted application to priority watersheds.

The economic burden of environmental measures falls unevenly across regions and market actor groups: hydropower producers in the constrained bidding zones absorb the large majority of the costs, while consumers face only modest price increases and generators in neighboring regions can benefit from higher prices (Section **??**). This geographical and sectoral concentration of costs may be relevant for the political feasibility of implementing environmental measures and suggests that compensation mechanisms or cost-sharing arrangements may merit consideration in the policy design.

The Swedish government has established an aim that production losses from environmental permit re-evaluations should not exceed 1.5 TWh [ref]. Our results show production losses of 0.2 TWh for - *Hydropeaking* and 0.7 TWh for + *Connectivity 1*, representing only 13% and 47% of this threshold respectively. Both scenarios thus allow substantial headroom within the policy constraint, suggesting that significant environmental improvements can be achieved without approaching the production loss limit. The more stringent + *Connectivity 5* scenario results in 3.1 TWh production loss, exceeding the threshold by more than double, which suggests that achieving ambitious connectivity goals across all facilities may require either phased im-

plementation or targeting specific priority watersheds rather than universal bypass flow requirements. Given that production loss scales approximately linearly with bypass flow magnitude (as demonstrated by the near-proportional relationship between the two connectivity scenarios), interpolation suggests that approximately 2 m^3/s of bypass flow at all facilities would be within the 1.5 TWh production loss aim. However, it should be noted that effective fish passage flows vary substantially depending on site-specific conditions, target species, and migration patterns, and our uniform flow assumptions serve as benchmarks to illustrate the size of bypass flows achievable within the 1.5 TWh production loss aim and do not represent optimal site-specific design.

4.4 Limitations

Several methodological choices and scope limitations should be considered when interpreting our results.

4.4.1 Technology representations

Two interrelated modeling assumptions collectively overestimate how easily the broader electricity system can compensate for reduced Swedish hydropower, likely causing us to underestimate the true economic efficiency losses and cost increases from environmental constraints.

First, while Swedish hydropower is represented in unprecedented detail with plant-specific environmental constraints, hydropower in neighboring regions (particularly Norway, which accounts for approximately 30 GW of the modelled system capacity) uses an aggregated two-storage representation. This simplified representation overestimates the full flexibility potential of Norwegian hydropower to compensate for Swedish constraints, making it appear easier for the system to substitute for lost Swedish hydropower production and flexibility than would be possible in reality.

Second, beyond the availability of alternative flexibility, our simplified transmission representation may overestimate its accessibility. Our model uses aggregated Net Transfer Capacity (NTC) values between bidding zones without modeling internal grid constraints or DC power flow. This approach underestimates transmission bottlenecks within bidding zones and overestimates the ease with which generation in other regions can substitute for reduced Swedish hydropower energy and flexibility. More detailed transmission modeling could reveal additional costs associated with grid congestion when Swedish hydropower faces environmental constraints, further increasing the system costs beyond our estimates.

Another model assumption to have in mind when interpreting the results is that the optimization assumes perfect foresight of inflows, electricity demand, and variable renewable generation over the three-year modeling horizon. While this assumption is standard in energy system optimization studies and enables identification of theoretical cost minima, real-world operations face uncertainty that would likely increase actual system costs. The perfect foresight assumption is particularly consequential for reservoir operations, where optimal water values depends on future inflow and price realizations. Moreover, the bias introduced by perfect foresight is likely asymmetric across our scenarios: hydropeaking constraints, which restrict temporal allocation within each day, are more sensitive to inflow and price forecast errors than connectivity constraints, which impose a fixed water diversion regardless of system conditions, potentially narrowing the cost gap between hydropeaking and connectivity constraints observed here.

4.4.2 Day-ahead market scope

Our analysis focuses exclusively on day-ahead market operations at hourly resolution, without modeling intraday markets, balancing markets, or ancillary services such as frequency regulation and reserves. Consequently, our estimates of hydropower producer revenues and total system costs capture operational effects in the day-ahead market but not the full spectrum of revenue streams and system value that hydropower provides. The total economic impact on hydropower producers could differ from our estimates if environmental constraints affect participation in faster timescale markets. However, Juutinen *et al.* [17] found that balancing market revenue for a Finnish hydropower plant on the Kemijoki River accounted for less than 0.4% of total revenue, and that when hydropeaking was restricted by 50%, only 20% of the total revenue loss came from the balancing market while 80% came from the day-ahead market. This suggests that todays day-ahead market captures the dominant revenue stream and that omitting balancing markets likely has a modest effect on estimated producer impacts.

5 Conclusions

This study quantifies how tighter environmental constraints on hydropower affect electricity system costs, electricity prices, and the distribution of economic impacts across market actors. By embedding detailed plant-level hydropower scheduling within a large-scale dispatch model for Northern Europe, we capture both the physical impacts of environmental constraints and their system-wide market effects through endogenous price formation.

A central contribution is the explicit distinction between environmental constraints that primarily reduce annual energy generation and those that mainly limit operational flexibility. This distinction enables more general conclusions across regulatory designs and hydropower systems. We show that these two types of constraints affect electricity systems through different mechanisms and lead to markedly different economic outcomes.

Across the tested scenarios, stricter environmental constraints increase total system costs by 50–250 M€ per year, corresponding to 0.5–2.7% of consumer electricity expenditure in the regulated regions. Contrary to the common assumption that hydropower's main system value lies in its intra-day flexibility, restricting daily hydropeaking results in the smallest increase in system costs. Instead, the dominant driver of economic efficiency loss is the reduction in annual hydropower generation associated with increased connectivity requirements. In the current electricity system, replacing lost energy is more costly than replacing lost daily flexibility. These findings suggest that the common emphasis on hydropower's flexibility value may overstate its relative importance in current systems, where the loss of dispatchable energy remains the primary driver of system costs.

The economic burden of environmental constraints is unevenly distributed. Regulated hydropower producers bear the largest share of the cost, with revenue reductions of 40–200 M€ per year, corresponding to up to 4% of annual revenues. Consumers in affected regions experience small electricity price increases (up to 0.15%). Other producers, including nuclear and wind generators, benefit from higher revenues due to these price increases.

Overall, our results indicate that environmental regulations on hydropower can be implemented with relatively modest system-level cost increases but substantial distributional effects. From a policy perspective, hydropeaking restrictions appear less costly than connectivity measures that reduce total energy availability, particularly in systems with sufficient alternative flexibility. However, while aggregate system costs remain small, these costs are borne almost entirely by hydropower producers in the constrained regions, an asymmetry that may raise questions about cost-sharing or compensation mechanisms in the implementation of such regulations. Future work should assess how these trade-offs evolve under higher renewable shares, investment responses, and participation in balancing and ancillary service markets.

References

1. Hirth, L. The benefits of flexibility: The value of wind energy with hydropower. en. *Applied Energy* **181,** 210–223. ISSN: 03062619. https://linkinghub.elsevier.com/retrieve/pii/S0306261916309801 (2025) (Nov. 2016).
2. Dimanchev, E. G., Hodge, J. L. & Parsons, J. E. The role of hydropower reservoirs in deep decarbonization policy. en. *Energy Policy* **155,** 112369. ISSN: 03014215. https://linkinghub.elsevier.com/retrieve/pii/S0301421521002391 (2025) (Aug. 2021).
3. Graabak, I., Korpås, M., Jaehnert, S. & Belsnes, M. Balancing future variable wind and solar power production in Central-West Europe with Norwegian hydropower. en. *Energy* **168,** 870–882. ISSN: 03605442. https://linkinghub.elsevier.com/retrieve/pii/S0360544218322801 (2025) (Feb. 2019).
4. BUNN, S. E. & ARTHINGTON, A. H. Basic Principles and Ecological Consequences of Altered Flow Regimes for Aquatic Biodiversity. en. *Environmental Management* **30,** 492–507. ISSN: 1432-1009. https://doi.org/10.1007/s00267-002-2737-0 (2025) (Oct. 2002).
5. Palmer, M. & Ruhi, A. Linkages between flow regime, biota, and ecosystem processes: Implications for river restoration. *Science* **365,** eaaw2087. https://www.science.org/doi/full/10.1126/science.aaw2087 (2025) (Sept. 2019).
6. European Council. *European Green Deal* English. https://www.consilium.europa.eu/en/policies/european-green-deal/ (2025).
7. Commission, E. *Water Framework Directive* en. Nov. 2025. https://environment.ec.europa.eu/topics/water/water-framework-directive_en (2025).
8. NVE. *Vannkraftkonsesjoner som kan revideres innen 2022: nasjonal gjennomgang og forslag til prioritering [Hydropower licenses subject to revision by 2022: National review and prioritization proposal]* Norwegian. Tech. rep. 49/2013 (Norges vassdrags- og energidirektorat, 2013). https://publikasjoner.nve.no/rapport/2013/rapport2013_49.pdf (2025).
9. Miljödepartementet. *Nationell plan för moderna miljövillkor* Swedish. 2020.
10. Riekkola, S., Hassan, A. & Pettersson, M. Disproportionate Costs Under EU Water Law: The Swedish Approach to Hydropower. en. *Water* **18,** 794. ISSN: 2073-4441. https://www.mdpi.com/2073-4441/18/7/794 (2026) (Jan. 2026).
11. Aubin, V., Helseth, A. & Korpås, M. Do we have to choose between the ecosystems and the energy transition? Environmental trade-offs with operation of Norwegian hydropower. en. *Renewable Energy* **244,** 122595. ISSN: 09601481. https://linkinghub.elsevier.com/retrieve/pii/S0960148125002575 (2025) (May 2025).
12. Arvesen, A. *et al.* Power system impacts of potential environmental constraints for hydropower in Norway. en. *Environmental Research Letters* **20,** 084004. ISSN: 1748-9326. https://doi.org/10.1088/1748-9326/ade4e1 (2025) (July 2025).
13. Pavičević, M. *et al.* Hydropower and environmental flow management: System-level trade-offs at Glen Canyon Dam. en. *Journal of Hydrology: Regional Studies* **61,** 102624. ISSN: 22145818. https://linkinghub.elsevier.com/retrieve/pii/S2214581825004495 (2025) (Oct. 2025).
14. Haas, J., Hagen, D. & Nowak, W. Energy storage and transmission systems to save the fish? Minimizing hydropeaking for little extra cost. en. *Sustainable Energy Technologies and Assessments* **35,** 41–47. ISSN: 22131388. https://linkinghub.elsevier.com/retrieve/pii/S2213138818305447 (2025) (Oct. 2019).
15. Mathisen, S., Mo, B., Helseth, A., Bladh, J. & Funkquist, J. *Measuring the Impact of Environmental Constraints on Hydropower Flexibility* in *2022 18th International Conference on the European Energy Market (EEM)* (Sept. 2022), 1–6. https://ieeexplore.ieee.org/document/9921047 (2025).
16. Widén, Å., Malm Renöfält, B., Degerman, E., Wisaeus, D. & Jansson, R. Environmental Flow Scenarios for a Regulated River System: Projecting Catchment-Wide Ecosystem Benefits and Consequences for Hydroelectric Production. en. *Water Resources Research* **58,** e2021WR030297. ISSN: 1944-7973. https://onlinelibrary.wiley.com/doi/abs/10.1029/2021WR030297 (2025) (2022).
17. Juutinen, A. *et al.* Impact of environmental flow policy on power system balancing costs and river ecosystem service benefits. *Water Resources and Economics* **52,** 100269. ISSN: 2212-4284. https://www.sciencedirect.com/science/article/pii/S2212428425000143 (2026) (Oct. 2025).
18. Guisández, I., Pérez-Díaz, J. I. & Wilhelmi, J. R. Approximate formulae for the assessment of the long-term economic impact of environmental constraints on hydropeaking. *Energy* **112,** 629–641. ISSN: 0360-5442. https://www.sciencedirect.com/science/article/pii/S0360544216308507 (2026) (Oct. 2016).
19. Schäfer, L. E., Korpås, M. & Bakken, T. H. Implications of environmental constraints in hydropower scheduling for a power system with limited grid and reserve capacity. *Energy Systems.* https://doi.org/10.1007/s12667-023-00594-z (2023).
20. Jafari Aminabadi, M., Séguin, S., Fofana, I., Fleten, S.-E. & Aasgård, E. K. Short-term hydropower optimization in the day-ahead market using a nonlinear stochastic programming model. en. *Energy Systems.* ISSN: 1868-3975. https://doi.org/10.1007/s12667-023-00618-8 (2026) (Sept. 2023).

21. Helseth, A., Mo, B., Lote Henden, A. & Warland, G. Detailed long-term hydro-thermal scheduling for expansion planning in the Nordic power system. en. *IET Generation, Transmission & Distribution* **12,** 441–447. ISSN: 1751-8695. https://onlinelibrary.wiley.com/doi/abs/10.1049/iet-gtd.2017.0903 (2026) (2018).

22. Wolfgang, O. *et al.* Hydro reservoir handling in Norway before and after deregulation. *Energy. 11th Conference on Process Integration, Modelling and Optimisation for Energy Saving and Pollution Reduction* **34,** 1642–1651. ISSN: 0360-5442. https://www.sciencedirect.com/science/article/pii/S0360544209003119 (2026) (Oct. 2009).

23. Ek Fälth, H., Mattsson, N., Reichenberg, L. & Hedenus, F. Trade-offs between aggregated and turbine-level representations of hydropower in optimization models. en. *Renewable and Sustainable Energy Reviews* **183,** 113406. ISSN: 13640321. https://linkinghub.elsevier.com/retrieve/pii/S1364032123002630 (2025) (Sept. 2023).

24. Göransson, L. The impact of wind power variability on the least-cost dispatch of units in the electricity generation system. en.

25. Weber, C. *Uncertainty in the Electric Power Industry: Methods and Models for Decision Support* en (ed Hillier, F. S.) ISBN: 978-0-387-23047-4 978-0-387-23048-1. http://link.springer.com/10.1007/b100484 (2026) (Springer, New York, NY, 2005).

26. Mattsson, N., Verendel, V., Hedenus, F. & Reichenberg, L. An autopilot for energy models – Automatic generation of renewable supply curves, hourly capacity factors and hourly synthetic electricity demand for arbitrary world regions. *Energy Strategy Reviews* **33,** 100606. ISSN: 2211-467X. https://www.sciencedirect.com/science/article/pii/S2211467X20301590 (2026) (Jan. 2021).

27. niclasmattsson. *niclasmattsson/GlobalEnergyGIS* original-date: 2019-05-21T08:27:31Z. Dec. 2025. https://github.com/niclasmattsson/GlobalEnergyGIS (2026).

28. *Transparency Platform* https://transparency.entsoe.eu/ (2026).

29. *Digest of UK Energy Statistics (DUKES)* en. July 2025. https://www.gov.uk/government/collections/digest-of-uk-energy-statistics-dukes (2026).

30. *Kraftbalansen på den svenska elmarknaden, rapport 2025* tech. rep. 2025/2726 (Svenska Kraftnät, Stockholm, May 2025). https://www.svk.se/49bb53/siteassets/om-oss/rapporter/2025/kraftbalansen-pa-den-svenska-elmarknaden-rapport-2025.pdf.

31. IAEA PRIS. *Nuclear statistics - energy availability factor* https://pris.iaea.org/PRIS/CountryStatistics/ReactorDetails.aspx?current=532.

32. ENTSO-E. *Monthly hourly load values* https://www.entsoe.eu/data/power-stats/.

33. EURACOAL. *EURACOAL Market Report 2024 no.2* tech. rep. (). https://public.euracoal.eu/download/Public-Archive/Library/Market-Reports/EURACOAL-Market-Report-2024-2_v04-hes.pdf.

34. Baltpool. *Trade statistics - biomass exchange* https://www.baltpool.eu/en/home-page/.

35. Danish Energy Agency. *Technology Data for Generation of Electricity and District Heating* https://ens.dk/en/analyses-and-statistics/technology-data-generation-electricity-and-district-heating.

36. Hydropower Technology Brief. en.

37. Harberger, A. C. Three Basic Postulates for Applied Welfare Economics: An Interpretive Essay. *Journal of Economic Literature* **9,** 785–797. ISSN: 0022-0515. (2026) (1971).

38. Kataria, M. Willingness to pay for environmental improvements in hydropower regulated rivers. *Energy Economics* **31,** 69–76. ISSN: 0140-9883. https://www.sciencedirect.com/science/article/pii/S0140988308001011 (2026) (Jan. 2009).

39. Ruokamo, E. *et al.* Estimating the economic value of hydropeaking externalities in regulated rivers. *Applied Energy* **353,** 122055. ISSN: 0306-2619. https://www.sciencedirect.com/science/article/pii/S0306261923014198 (2026) (Jan. 2024).

40. Andersson, A. & Johansson, H. Hydropower optimization with detailed reservoir representation. eng. https://hdl.handle.net/20.500.12380/309382 (2026) (2025).

S Supplementary material

This supplementary material is organized into three sections. Section S.1 provides the detailed description of the RAPID model, including the complete mathematical formulation of the optimization problem, all input data tables for technology and regional assumptions, and the hydropower cascade topology. Section S.3 documents the implementation of the environmental constraint scenarios. Section S.4 presents additional results that complement the main text.

S.1 Detailed description of the RAPID model

This section provides the complete mathematical formulation and input data for the RAPID model. The model minimizes total system operating cost across 19 interconnected bidding zones in Northern Europe, subject to energy balance, generation, storage, and transmission constraints. It is implemented in Julia using the JuMP optimization framework and solved with the Gurobi LP solver. For Swedish bidding zones SE1–SE3, hydropower production is modeled at the individual plant level using the FORSA cascade framework, while all other regions use an aggregated two-reservoir representation.

The mathematical framework is presented in Sections S.1.1–S.1.11, starting with the definition of sets, indices, and decision variables, followed by the full set of constraint equations. The technology-specific cost and operational parameters that enter these equations are documented in Section S.2.1, and the region-specific capacity and energy data are provided in Section S.2.2. Section S.2.3 details the hydropower cascade topology.

S.1.1 Sets, indices, variables and paramters

Table S.1 defines the index sets that structure the optimization problem (left panel) and the decision variables determined by the solver (right panel). The general sets define the spatial, temporal, and technological dimensions of the model, while the hydropower topology sets capture the river cascade structure used in the detailed FORSA representation of Swedish rivers.

Table S.2 lists all exogenous input parameters. Energy system parameters (left panel) include cost coefficients, demand profiles, and technology characteristics, while the detailed hydropower parameters (right panel) define the physical properties of each facility in the FORSA cascade model.

Table S.1: Sets and indices (left) and variables (right) of the optimization model.

Symbol	Idx	Description
General		
$\mathscr{R}$	r	Regions (bidding zones)
$\mathscr{T}$	t	Hours (time steps)
$\mathscr{P}$	p	Generation technologies
$\mathscr{S}$	s	Eff. curve PWL segments
$\mathscr{L}$	l	Tailrace regr. lags (0–2 h)
Subsets		
$\mathscr{P}^{\text{th}}$	$\subset \mathscr{P}$	Thermal technologies
$\mathscr{P}^{\text{VRE}}$	$\subset \mathscr{P}$	Variable RE technologies
$\mathscr{R}^{\text{agg}}$	$\subset \mathscr{R}$	Aggr. hydro regions
$\mathscr{R}^{\text{FORSA}}$	$\subset \mathscr{R}$	Detailed hydropower representation
$\mathscr{R}^{\text{pump}}$	$\subset \mathscr{R}$	Pumped hydro regions
Hydropower topology		
$\mathscr{V}$	ri	Rivers (FORSA)
$\mathscr{H}_{ri}$	pl	Hydropower facilities in ri
$\mathscr{H}^{P}_{ri}$	$\subset \mathscr{H}_{ri}$	Power plants
$\mathscr{J}_{ri,pl}$	j	Turbines at plant pl
$\mathscr{B}_r$	(ri, pl)	River–plant pairs in zone r
$\mathscr{U}(pl)$	pl'	Upstream neighbours of pl
$\mathscr{U}^{\text{d/b/sp}}(pl)$	$\subset \mathscr{U}(pl)$	by flow type
$\mathscr{D}(pl)$	pl'	Downstream neighbours of pl
$\mathscr{D}^{\text{b/sp}}(pl)$	$\subset \mathscr{D}(pl)$	by flow type

Symbol	Unit	Description
Energy system		
$E_{r,p,t}$	MWh/h	Generation by tech. p
$T_{r,r',t}$	MWh/h	Power flow $r \rightarrow r'$
$B^{\text{ch}}_{r,t}$	MWh/h	Battery charging
$B^{\text{st}}_{r,t}$	MWh	Battery state of charge
$Z^{\text{ch}}_{r,t}$	MWh/h	Pumped hydro pumping
$Z^{\text{st}}_{r,t}$	MWh	Pumped hydro SoC
$X_{r,p,t}$	MWh/h	VRE curtailment
Γ_r	tCO_2	Total CO_2 emissions
Thermal unit commitment		
$K_{r,p,t}$	MW	Committed capacity
$\Delta K_{r,p,t}$	MW	Capacity increase (start-up)
$C^{\text{cyc}}_{r,p,t}$	€	Cycling cost
Aggregated hydropower		
$S^{\text{sh}}_{r,t}$	MWh	Short-term reservoir
$S^{\text{lo}}_{r,t}$	MWh	Long-term reservoir
$\Phi_{r,t}$	MWh/h	Long→short transfer
Detailed hydropower (FORSA)		
$Q^{\text{d}}_{ri,t,pl,j}$	m^3/s	Turbine discharge
$D_{ri,t,pl,j}$	m^3/s	Effective discharge
$Q^{\text{tot}}_{ri,t,pl,pl'}$	m^3/s	Total flow $pl \rightarrow pl'$
$Q^{\text{b}}_{ri,t,pl,pl'}$	m^3/s	Bypass (fish passage) flow
$Q^{\text{sp}}_{ri,t,pl,pl'}$	m^3/s	Spillway flow
$V_{ri,t,pl}$	$m^3/s{\cdot}h$	Reservoir content
$W^{\text{f}}_{ri,t,pl}$	m	Forebay water level
$W^{\text{t}}_{ri,t,pl}$	m	Tailrace water level
$H_{ri,t,pl}$	m	Hydraulic head
$P_{ri,t,pl,j}$	MWh/h	Turbine production
$\overline{W}^{\text{f}}_{ri,per,pl}$	m	Max forebay level ∀ t ∈ per
$\underline{W}^{\text{f}}_{ri,per,pl}$	m	Min forebay level ∀ t ∈ per
$\overline{Q}^{\text{fp}}_{ri,per,pl,pl'}$	m	Max flow level ∀ t ∈ per
$\underline{Q}^{\text{fp}}_{ri,per,pl,pl'}$	m	Min flow level ∀ t ∈ per

Superscripts: th = thermal; VRE = variable renewable energy (wind onshore, wind offshore, solar PV); agg = aggregated hydropower representation; FORSA = detailed hydropower representation; pump = pumped hydro; days/weeks = day/week index sets; cyc = cycling cost; ch = charging; st = state (of charge); sh = short-term; lo = long-term; d = discharge; b = bypass (fish passage); sp = spillway; tot = total (all flow paths); fp = flow pathway (can be d,b,sp or tot); f = forebay; t = tailrace.

Table S.2: Parameters of the optimization model. Left: energy system parameters. Right: detailed hydropower parameters (FORSA).

Symbol	Unit	Description
Cost parameters		
c_p^{fuel}	€/MWh$_{\text{fuel}}$	Fuel cost
c_p^{var}	€/MWh	Variable O&M cost
c^{CO_2}	€/tCO$_2$	Carbon price
$c_p^{\text{start,fixed}}$	€/MW	Fixed start-up cost
f_p^{start}	MWh/MW	Start-up fuel use
c_p^{start}	€/MW	Total start-up cost (Eq. S.32)
$c_{p,r}^{\text{partload}}$	€/MW/h	Part-load cost (Eq. S.33)
Demand and transmission		
$\ell_{r,t}$	MWh/h	Electricity demand
$\gamma_{r,r'}$	–	Transmission loss factor
$\overline{v}_{r,r',t}$	MW	Net transfer capacity
Thermal generation		
η_p	–	Fuel-to-elec. efficiency
$\kappa_{p,r}$	MW	Installed capacity
μ_p	–	Min. load fraction
μ_p^{η}	–	Min-load relative efficiency
τ_p^{start}	h	Start-up time
α_r	–	Nuclear availability factor
$\alpha_{r,t}^{\text{uo}}$	–	Nuclear unplanned outages
$\overline{\omega}_r$	–	Available waste
Variable renewables		
$\kappa_{p,r}$	MW	Installed capacity
$sc_{r,p,t}$	–	Scale factor
$cf_{p,r,t}$	–	Capacity factor
Storage		
η^{batt}	–	Battery one-way eff.
$\overline{b}_r^{\text{st}}$	MWh	Battery storage capacity
$\overline{b}_r^{\text{ch}}$	MW	Battery power capacity
η^{pump}	–	Pump efficiency
$\overline{z}_r^{st}$	MWh	Pumped hydro storage capacity
$\overline{z}_r^{ch}$	MW	Pumped hydro capacity
Aggregated hydropower		
$i_{r,t}^{\text{sh}}$	MWh/h	Short-term res. inflow
$i_{r,t}^{\text{lo}}$	MWh/h	Long-term res. inflow
$\overline{\phi}_r^{lo}$	MWh	Long term storage capacity
$\overline{\phi}_r^{sh}$	MWh	Short term storage capacity
$\overline{\phi}_r$	MW	Installed hydro capacity
Physical constants		
ϵ_p	tCO$_2$/MWh$_{\text{fuel}}$	CO$_2$ emission factor
g	m/s^2	Grav. accel. (= 9.81)
ρ	kg/m^3	Water density (= 1000)

Symbol	Unit	Description
Inflows and time delays		
$i_{ri,t,pl}$	m^3/s	Local inflow at facility pl
τ^d	h	Discharge time delay
τ^b	h	Bypass flow time delay
τ^{sp}	h	Spillway flow time delay
Forebay and tailrace		
$f_{ri,pl}^{\text{lin}}(\cdot)$	m	Linear forebay–vol. fn
$f_{ri,pl}^{\text{pwl},k}(\cdot)$	m	PWL forebay–vol. fn
$m_{ri,pl}^0$	m	Tailrace regression const.
$k_{l,ri,pl}$	m/(m^3/s)	Tailrace flow–level coeff.
$k_{ri,pl,pl'}^{\text{f}}$	m/m	Tailrace forebay coeff.
Hydropower production & turbine efficiency		
$\overline{h}_{pl}$	m	Mean hydraulic head
$d_{pl,j}^*$	m^3/s	Best-eff. discharge
$\eta_{pl,j}^*$	–	Best-eff. value
$k_{ri,pl,j}^s$	–	Efficiency segment slope
$m_{ri,pl,j}^s$	m^3/s	Efficiency segment intercept
$\sigma_{ri,t,pl,j}$	{0,1}	Turbine availability
Operational and Environmental constraints		
$\overline{q}_{ri,t,pl,pl'}^{\text{fp}}$	m^3/s	Upper bound on flow pathway
$\underline{q}_{ri,t,pl,pl'}^{\text{fp}}$	m^3/s	Lower bound on flow pathway
$\overline{w}_{ri,t,pl}^{\text{f}}$	m	Upper bound on forebay level
$\underline{w}_{ri,t,pl}^{\text{f}}$	m	Lower bound on forebay level
$\delta_{ri,t,pl,pl'}^{\uparrow,\text{fp}}$	m or m^3/s	Flow/Level ramp-up limit
$\delta_{ri,t,pl,pl'}^{\downarrow,\text{fp}}$	m or m^3/s	Flow/Level ramp-down limit
$\overline{\delta}_{ri,per,pl}^{\text{per,fp}}$	m or m^3/s	Max variation per period

Superscripts: d = discharge (turbine flow); b = bypass flow; sp = spillway flow; tot = total (all flow paths); fp = flow pathway (can be d,b,sp or tot); uo = unplanned outage; batt = battery; sh = short-term; lo = long-term; st = state (of charge); ch = charging; lin = linear; pwl = piecewise-linear; f = forebay; t = tailrace; $*$ = best-efficiency point; per = period (day, week or month); $\uparrow/\downarrow$ = ramp-up/ramp-down.

S.1.2 Objective function

The model minimizes total system operating cost:

$$\min \sum_{r \in \mathscr{R}} \left[\sum_{p \in \mathscr{P}^{\text{th}},\, t \in \mathscr{T}} \frac{E_{r,p,t}}{\eta_p} \cdot c_p^{\text{fuel}} + \sum_{p \in \mathscr{P},\, t \in \mathscr{T}} E_{r,p,t} \cdot c_p^{\text{var}} + \sum_{p \in \mathscr{P}^{\text{th}},\, t \in \mathscr{T}} C_{r,p,t}^{\text{cyc}} + \Gamma_r \cdot c^{\text{CO}_2} \right] \tag{S.1}$$

with η_p the fuel-to-electricity efficiency, c_p^{fuel} the fuel cost (€/MWh$_{\text{fuel}}$), c_p^{var} the variable O&M cost (€/MWh), and c^{CO_2} the carbon price (€/tCO$_2$).

S.1.3 Energy balance

Supply must equal demand in each region and hour. Under the NTC transmission mode used in this study:

$$\sum_{p \in \mathscr{P}} E_{r,p,t} - B_{r,t}^{\text{ch}} - \frac{Z_{r,t}^{\text{ch}}}{\eta^{\text{pump}}} + \sum_{r' \in \mathscr{R}} \left[T_{r',r,t} - (1 + \gamma_{r,r'}) \cdot T_{r,r',t} \right] = \ell_{r,t} \quad \forall\, r \in \mathscr{R},\, t \in \mathscr{T} \tag{S.2}$$

where $\gamma_{r,r'}$ is the transmission loss factor (5% per 1000 km of distance between r and r'). The dual variable $\lambda_{r,t}$ of this constraint is the endogenous electricity price.

Transmission flows are bounded by net transfer capacities:

$$0 \le T_{r,r',t} \le \overline{v}_{r,r',t} \quad \forall\, r, r' \in \mathscr{R},\, t \in \mathscr{T} \tag{S.3}$$

S.1.4 Detailed hydropower representation (FORSA)

This section describes the hydropower cascade model applied to Swedish rivers in SE1–SE3. Each river $ri \in \mathscr{V}$ consists of a set of hydropower facilities $\mathscr{H}_{ri}$, of which a subset $\mathscr{H}_{ri}^{P}$ are power plants equipped with turbines. The remaining facilities are reservoir-only nodes that route water but do not generate electricity.

Water balance: For each facility $pl \in \mathscr{H}_{ri}$ and hour t:

$$\begin{aligned} V_{ri,t,pl} = V_{ri,t-1,pl} + i_{ri,t,pl} \quad &- \sum_{j \in \mathscr{J}_{ri,pl}} Q_{ri,t,pl,j}^{\text{d}} - \sum_{pl' \in \mathscr{D}^{\text{b}}(pl)} Q_{ri,t,pl,pl'}^{\text{b}} - \sum_{pl' \in \mathscr{D}^{\text{sp}}(pl)} Q_{ri,t,pl,pl'}^{\text{sp}} \\ &+ \sum_{pl' \in \mathscr{U}^{\text{d}}(pl)} \sum_{j \in \mathscr{J}_{ri,pl'}} Q_{ri,t-\tau^d,pl',j}^{\text{d}} + \sum_{pl' \in \mathscr{U}^{\text{b}}(pl)} Q_{ri,t-\tau^b,pl',pl}^{\text{b}} + \sum_{pl' \in \mathscr{U}^{\text{sp}}(pl)} Q_{ri,t-\tau^{sp},pl',pl}^{\text{sp}} \end{aligned} \tag{S.4}$$

where τ^d, τ^b, and τ^{sp} are the plant-specific time delays (in hours) for discharge, bypass, and spillway flows from upstream plant pl'.

Total flow decomposition: The total flow from plant pl to downstream plant pl' is the sum of all flow pathways:

$$Q_{ri,t,pl,pl'}^{\text{tot}} = \sum_{j \in \mathscr{J}_{ri,pl}} Q_{ri,t,pl,j}^{\text{d}} + Q_{ri,t,pl,pl'}^{\text{b}} + Q_{ri,t,pl,pl'}^{\text{sp}} \quad \forall\, pl' \in \mathscr{D}^{\text{d/b/sp}}(pl) \tag{S.5}$$

Not all downstream nodes receive all flow types; a plant may have separate downstream destinations for discharge, bypass flow, and spillway flow.

Forebay level: The forebay level (upstream water surface elevation) is related to reservoir content through piecewise-linear functions fitted to site-specific data. A lower bound:

$$W_{ri,t,pl}^{\text{f}} \ge f_{ri,pl}^{\text{lin}}(V_{ri,t,pl}) \tag{S.6}$$

and additional piecewise-linear upper bounds refine the approximation:

$$W_{ri,t,pl}^{\text{f}} \le f_{ri,pl}^{\text{pwl},k}(V_{ri,t,pl}) \quad \forall\, k \in \text{segments} \tag{S.7}$$

The upper and lower bound approximation, rather then an equality constraint, is chosen to preserve convexity of the problem. Inspection of model results shows that the upper bound segments are most often the active constraint (alining with real reservoir curves), due to the benefit of maximizing water levels and therebye head. Andersson & Johansson [40] describe this implementation and its benefits and limitations.

Water level ramp limits constrain drawdown and filling rates:

$$-\delta^{\downarrow,\mathrm{f}}_{ri,t,pl} \le W^{\mathrm{f}}_{ri,t,pl} - W^{\mathrm{f}}_{ri,t-1,pl} \le \delta^{\uparrow,\mathrm{f}}_{ri,t,pl} \tag{S.8}$$

Tailrace level: The tailrace (downstream) water level is a linear function of recent total flow and the forebay level of the downstream plant:

$$W^{\mathrm{t}}_{ri,t,pl} = m^{0}_{ri,pl} + \sum_{l \in \mathscr{L}} k_{l,ri,pl} \cdot Q^{\mathrm{tot}}_{ri,t-l,pl,pl'} + k^{\mathrm{f}}_{ri,pl,pl'} \cdot W^{\mathrm{f}}_{ri,t,pl'} \tag{S.9}$$

where $\mathscr{L}$ is the set of lags (0–2 hours is used in this paper), $m^{0}_{ri,pl}$, $k_{l,ri,pl}$ and $k^{\mathrm{f}}_{ri,pl,pl'}$ are coefficients fitted to historical data on flow–level observations using linear regression.

Head: The hydraulic head is the difference between forebay and tailrace levels:

$$H_{ri,t,pl} = W^{\mathrm{f}}_{ri,t,pl} - W^{\mathrm{t}}_{ri,t,pl} \quad \forall\, pl \in \mathscr{H}^{P}_{ri} \tag{S.10}$$

Turbine flow and efficiency: maximum flow is specified for each turbine:

$$Q^{\mathrm{d}}_{ri,t,pl,j} \le \overline{q}^{\mathrm{d}}_{ri,t,pl,j} \quad \forall\, ri,t,pl,j \tag{S.11}$$

The effective discharge $D_{ri,t,pl,j}$ represents the efficiency-weighted flow through turbine j. It is bounded by piecewise-linear segments fitted to each turbine's individually calibrated efficiency–discharge curve:

$$D_{ri,t,pl,j} \le \left(k^{s}_{ri,pl,j} \cdot Q^{\mathrm{d}}_{ri,t,pl,j} + m^{s}_{ri,pl,j}\right) \cdot \sigma_{ri,t,pl,j} \quad \forall\, s \in \mathscr{S} \tag{S.12}$$

where $k^{s}_{ri,pl,j}$ and $m^{s}_{ri,pl,j}$ are the slope and intercept of efficiency segment s, and $\sigma_{ri,t,pl,j} \in \{0,1\}$ indicates whether the turbine is available (accounting for maintenance stop periods). The piecewise-linear upper bound ensures that at any discharge level, the effective discharge equals the minimum across all segments, correctly approximating the concave efficiency curve.

Power production: Power output at each turbine is computed via a Taylor expansion (first-order linearization) around the mean head $\overline{h}_{pl}$ and best-efficiency operating point:

$$P_{ri,t,pl,j} \le \left[\overline{h}_{pl} \cdot D_{ri,t,pl,j} + H_{ri,t,pl} \cdot d^{*}_{pl,j} \cdot \eta^{*}_{pl,j} - \overline{h}_{pl} \cdot \eta^{*}_{pl,j} \cdot d^{*}_{pl,j}\right] \cdot g \cdot \rho \cdot 10^{-6} \tag{S.13}$$

where $d^{*}_{pl,j}$ and $\eta^{*}_{pl,j}$ are the best-efficiency discharge and corresponding efficiency, $g = 9.81\,\mathrm{m/s^2}$, $\rho = 1000\,\mathrm{kg/m^3}$, and 10^{-6} converts W to MW. This linearization captures the first-order effect of head variation on production while maintaining LP tractability.

Total hydropower production in each FORSA region aggregates across all plants and turbines:

$$E_{r,\mathrm{Hydro},t} \le \sum_{(ri,pl) \in \mathscr{B}_r} \sum_{j \in \mathscr{J}_{ri,pl}} P_{ri,t,pl,j} \quad \forall\, r \in \mathscr{R}^{\mathrm{FORSA}},\, t \in \mathscr{T} \tag{S.14}$$

where $\mathscr{B}_r$ is the set of (river, plant) pairs belonging to bidding zone r.

S.1.5 Environmental constraints

Environmental constraints act on flow variables, reservoir levels, and forebay levels. The framework supports several constraint types that can be activated per plant and per scenario.

Bounds on flows and levels: Each flow pathway is bounded:

$$\underline{q}^{\mathrm{tot}}_{ri,t,pl,pl'} \le Q^{\mathrm{tot}}_{ri,t,pl,pl'} \le \overline{q}^{\mathrm{tot}}_{ri,t,pl,pl'} \quad \forall\, ri,t,pl,pl' \tag{S.15}$$

with analogous bounds on Q^{b} and Q^{sp}.

Forebay levels are bounded analogously:

$$\underline{w}^{\mathrm{f}}_{ri,t,pl} \le W^{\mathrm{f}}_{ri,t,pl} \le \overline{w}^{\mathrm{f}}_{ri,t,pl} \quad \forall\, ri,t,pl \tag{S.16}$$

Ramp constraints on flows and levels: Hourly ramp limits constrain the rate of change in flows:

$$\delta^{\downarrow,\text{tot}}_{ri,t,pl,pl'} \le Q^{\text{tot}}_{ri,t,pl,pl'} - Q^{\text{tot}}_{ri,t-1,pl,pl'} \le \delta^{\uparrow,\text{tot}}_{ri,t,pl,pl'} \tag{S.17}$$

with analogous constraints on Q^{b} and Q^{sp}.

The same constraint type applies to forebay levels:

$$-\delta^{\downarrow,\text{f}}_{ri,t,pl} \le W^{\text{f}}_{ri,t,pl} - W^{\text{f}}_{ri,t-1,pl} \le \delta^{\uparrow,\text{f}}_{ri,t,pl} \tag{S.18}$$

Variation limits on flows and levels: Variation within a time period (e.g. each day, week, or month) is constrained for both flows and forebay levels using auxiliary variables that track the period maximum and minimum.

For flows:

$$\overline{Q}^{\text{tot}}_{ri,per,pl} - \underline{Q}^{\text{tot}}_{ri,per,pl} \le \overline{\delta}^{\text{per,tot}}_{ri,per,pl} \tag{S.19}$$

$$\overline{Q}^{\text{tot}}_{ri,per,pl} \ge Q^{\text{tot}}_{ri,t,pl,pl'} \quad \forall\, t \in per \tag{S.20}$$

$$\underline{Q}^{\text{tot}}_{ri,per,pl} \le Q^{\text{tot}}_{ri,t,pl,pl'} \quad \forall\, t \in per \tag{S.21}$$

with analogous constraints on Q^{b} and Q^{sp}.

For forebay levels:

$$\overline{W}^{\text{f}}_{ri,per,pl} - \underline{W}^{\text{f}}_{ri,per,pl} \le \overline{\delta}^{\text{per,f}}_{ri,per,pl} \tag{S.22}$$

$$\overline{W}^{\text{f}}_{ri,per,pl} \ge W^{\text{f}}_{ri,t,pl} \quad \forall\, t \in per \tag{S.23}$$

$$\underline{W}^{\text{f}}_{ri,per,pl} \le W^{\text{f}}_{ri,t,pl} \quad \forall\, t \in per \tag{S.24}$$

S.1.6 Aggregated hydropower model

For regions $r \in \mathscr{R}^{\text{agg}}$ outside the detailed FORSA scope, hydropower is represented by a two-storage model.

Short-term reservoir balance:

$$S^{\text{sh}}_{r,t} \le \overline{\phi}^{sh}_{r} \tag{S.25}$$

$$S^{\text{sh}}_{r,t} \le S^{\text{sh}}_{r,t-1} + i^{\text{sh}}_{r,t} + \Phi_{r,t} - E_{r,\text{Hydro},t} \tag{S.26}$$

Long-term reservoir balance:

$$S^{\text{lo}}_{r,t} \le \overline{\phi}^{lo}_{r} \tag{S.27}$$

$$S^{\text{lo}}_{r,t} \le S^{\text{lo}}_{r,t-1} + i^{\text{lo}}_{r,t} - \Phi_{r,t} \tag{S.28}$$

The transfer is bounded by the installed hydropower capacity: $\Phi_{r,t} \le \overline{\phi}_r$.

S.1.7 Thermal generation constraints

Unit commitment: Thermal plants use a two-variable approach to approximate unit commitment without binary variables:

$$E_{r,p,t} \le K_{r,p,t} \quad \forall\, p \in \mathscr{P}^{\text{th}} \tag{S.29}$$

$$E_{r,p,t} \ge \mu_p \cdot K_{r,p,t} \tag{S.30}$$

Cycling cost:

$$C^{\text{cyc}}_{r,p,t} \geq \Delta K_{r,p,t} \cdot c^{\text{start}}_{p} + \left(K_{r,p,t} - E_{r,p,t}\right) \cdot c^{\text{partload}}_{p,r} \tag{S.31}$$

The total start-up cost c^{start}_{p} combines a fixed cost with the cost of fuel consumed during start-up (Table S.5):

$$c^{\text{start}}_{p} = c^{\text{start,fixed}}_{p} + f^{\text{start}}_{p} \cdot c^{\text{fuel}}_{\text{fuel}(p)} \tag{S.32}$$

where $c^{\text{start,fixed}}_{p}$ (€/MW) is the fixed start-up cost, f^{start}_{p} (MWh/MW) is the start-up fuel use, and $c^{\text{fuel}}_{\text{fuel}(p)}$ is the price of the start-up fuel (Table S.4).

The part-load cost $c^{\text{partload}}_{p,r}$ captures the efficiency penalty of operating below full load. It is derived from the minimum-load relative efficiency μ^{eff}_{p} (Table S.5):

$$c^{\text{partload}}_{p,r} = \frac{c^{\text{run}}_{p}}{\kappa_{p,r}(1-\mu_p)} \left(\frac{1}{\mu^{\eta}_{p} \cdot \eta_p} - \frac{1}{\eta_p} \right) \tag{S.33}$$

where $c^{\text{run}}_{p} = c^{\text{fuel}}_{\text{fuel}(p)}/\eta_p + c^{\text{var}}_{p}$ is the full-load running cost, and $\kappa_{p,r}(1-\mu_p)$ is the range of output between minimum load ($\mu_p \cdot \kappa_{p,r}$) and full capacity ($\kappa_{p,r}$), used to normalize the per-unit efficiency penalty. This cost applies per MW of committed but unused capacity ($K_{r,p,t} - E_{r,p,t}$).

Start-up dynamics: The increase in committed capacity is tracked and limited by start-up time:

$$\Delta K_{r,p,t} \geq K_{r,p,t} - K_{r,p,t-1} \tag{S.34}$$

$$\Delta K_{r,p,t} \leq \kappa_{p,r} - K_{r,p,t-\tau^{\text{start}}_{p}} \tag{S.35}$$

where $\kappa_{p,r}$ is installed capacity and τ^{start}_{p} is the technology-specific start-up time (hours).

Nuclear availability: Nuclear plants are subject to both unplanned and planned outages. Unplanned outages limit nuclear production in specific hours based on historical patterns:

$$E_{r,\text{Nuclear},t} \leq \kappa_{\text{nuc},r} \cdot \alpha^{\text{uo}}_{r,t} \tag{S.36}$$

where $\alpha^{\text{uo}}_{r,t}$ is set to zero for specific regions and hours based on historical unplanned outage patterns.

Total annual generation is bounded by historical unplanned and planned outages:

$$\sum_{t \in \mathcal{T}} E_{r,\text{Nuclear},t} \leq \kappa_{\text{nuc},r} \cdot \alpha_r \cdot |\mathcal{T}|/8760 \tag{S.37}$$

where α is the availability factor, i.e the maximum full load hours obtainable based on historical unplanned and planned outages.

CHP seasonal constraints: CHP generation is limited seasonally to reflect heat demand: 10% of capacity in summer (June–August), 50% in spring and autumn (April, May, September, October), and unconstrained in winter. For all technologies $p \in \mathcal{P}^{\text{CHP}}$:

$$E_{r,p,t} \leq \beta^{\text{s}} \cdot \kappa_{p,r} \quad \forall\, t \in \mathcal{T}^{\text{s}} \tag{S.38}$$

$$E_{r,p,t} \leq \beta^{\text{sa}} \cdot \kappa_{p,r} \quad \forall\, t \in \mathcal{T}^{\text{sa}} \tag{S.39}$$

where $\beta^{\text{s}} = 0.1$ and $\beta^{\text{sh}} = 0.5$ are the seasonal capacity factors, $\mathcal{T}^{\text{s}}$ covers June–August, and $\mathcal{T}^{\text{sa}}$ covers April, May, September, October.

Waste availability constraint: Annual waste incineration is bounded by the available waste supply $\overline{\omega}_r$ (Table S.9):

$$\sum_{t \in \mathcal{T}} \sum_{p \in \mathcal{P}^{waste}} E_{r,p,t} \leq \overline{\omega}_r \cdot \frac{|\mathcal{T}|}{8760} \tag{S.40}$$

S.1.8 Variable renewables and curtailment

Wind and solar power production is modelled using hourly capacity factors, $cf_{r,p,t}$, derived from the Global Energy GIS package [26, 27]. Capacity factors are multiplied by installed capacity to determine hourly generation potential. Technology-specific and region-specific scaling factors (0.7-0.9), $sc_{r,p}$, adjust the capacity factors for modelled production to match actual reported generation in 2024, accounting for non-ideal siting, old fleets etc. The model can curtail VRE production if system balancing requires it:

$$E_{r,p,t} + X_{r,p,t} = \kappa_{r,p} \cdot cf_{r,p,t} \cdot sc_{r,p} \quad \forall r \in \mathscr{R}, t \in \mathscr{T}, p \in \mathscr{P} \tag{S.41}$$

S.1.9 Battery storage

$$B^{\text{st}}_{r,t} \leq B^{\text{st}}_{r,t-1} + B^{\text{ch}}_{r,t} - \frac{E_{r,\text{batt},t}}{\eta^{\text{batt}}} \tag{S.42}$$

$$0 \leq B^{\text{st}}_{r,t} \leq \overline{b}^{\text{st}}_{r} \tag{S.43}$$

$$0 \leq B^{\text{ch}}_{r,t} \leq \overline{b}^{\text{ch}}_{r} \tag{S.44}$$

$$0 \leq E_{r,batt,t} \leq \kappa_{r,batt} \tag{S.45}$$

S.1.10 Pumped hydro storage

$$Z^{\text{st}}_{r,t} \leq Z^{\text{st}}_{r,t-1} + Z^{\text{ch}}_{r,t} - \frac{E_{r,\text{pump},t}}{\eta^{\text{pump}}} \tag{S.46}$$

$$0 \leq Z^{\text{st}}_{r,t} \leq \overline{z}^{\text{st}}_{r} \tag{S.47}$$

$$0 \leq Z^{\text{ch}}_{r,t} \leq \overline{z}^{\text{ch}}_{r} \tag{S.48}$$

$$0 \leq E_{r,pump,t} \leq \kappa_{r,pump} \tag{S.49}$$

S.1.11 CO_2 emissions

$$\Gamma_r \geq \sum_{p \in \mathscr{P}, t \in \mathscr{T}} \frac{E_{r,p,t}}{\eta_p} \cdot \epsilon_p \tag{S.50}$$

where ϵ_p is the technology-specific CO_2 emission factor (tCO_2/MWh_{fuel}).

S.2 Data

S.2.1 Technology assumptions

This section documents the cost and operational assumptions for all generation and storage technologies represented in the model. These values directly parameterize the cost coefficients and technical constraints defined in Table S.2.

Table S.3 summarizes the key technical and economic characteristics for each technology. Investment costs are annualized using technology-specific capital recovery factors. Thermal plants are represented with two vintages (old and new), where old plants have 20% lower conversion efficiency, reflecting the age distribution of the existing fleet. Table S.4 lists the fuel price assumptions, and Table S.5 specifies the operational constraints governing thermal plant dispatch, including minimum stable load levels, start-up costs and durations, and fuel consumed during start-up.

Table S.3: Technology characteristics and cost assumptions retained from the Danish Energy Agency [35]. Investment costs are annualized using technology-specific capital recovery factors based on lifetime and discount rate. Old plants have an assumed 20% lower efficiency than new plants.

Technology	**Lifetime (years)**	**Investment (€/kW)**	**Variable (€/MWh)**	**Fixed (€/kW/yr)**	**Efficiency (-)**	**Emission factor (tCO_2/MWh_{fuel})**
Hydro	100	3000	0.1	45	–	0.000
Hydro pumped	60	3600	0.1	50	0.85	0.000
Lignite (old/new)	25	3750	2.1	35.1	0.40/0.32	0.364
Hard coal (old/new)	25	3750	2.1	35.1	0.40/0.32	0.338
Oil (old/new)	25	1800	2.1	20.0	0.40/0.32	0.279
CHP biomass (old/new)	25	3655	2.1	102	0.45/0.36	0.000
CHP waste (old/new)	25	8874	2.1	211	0.30/0.24	0.132
CCGT natural gas (old/new)	25	909	0.8	29.6	0.58/0.46	0.207
CCGT biomethane (old/new)	25	909	1.6	29.6	0.58/0.46	0.000
OCGT (old/new)	25	615	0.4	19.8	0.41/0.33	0.207
Nuclear	60	6181	7.1	123	0.33	0.000
Wind onshore	30	1185	0.0	16.7	–	0.000
Wind offshore	30	2780	0.0	34.0	–	0.000
Solar PV	40	470	0.0	9.5	–	0.000
Battery	25	535	1.9	0.1	0.90	0.000
Backstop	1000	0	1000	0.0	1.00	0.500

Table S.4: Fuel price assumptions (2024 values).

Fuel	**Cost ($€/MWh_{fuel}$)**
Lignite	5.81
Coal	11.62
Natural gas	35.00
Biomass	20.00
Biomethane	49.00
Waste	1.00
Uranium	1.65
Oil	48.00
Carbon dioxide price: 65 $€/tCO_2$	

Table S.5: Thermal generation technology operational constraints. Old plants have 20% higher start-up costs and 20% longer start-up times than new plants. Parameters are used in Equations (S.30)–(S.35).

Technology	**Min. load μ_p (% cap.)**	**Fixed start-up cost $c_p^{\text{start,fixed}}$ (€/MW)**	**Min-load rel. eff. μ_p^{eff} (%)**	**Start-up time τ_p^{start} (h)**	**Start-up f_p^{start} (MWh/MW)**	**Start-up fuel type**
Lignite (old/new)	30	56.9/68.3	90	12/14	2.93	Oil
Hard coal (old/new)	30	56.9/68.3	90	12/14	2.93	Oil
Oil (old/new)	30	56.9/68.3	90	12/14	1.00	Oil
CHP biomass (old/new)	30	50.6/60.7	90	12/14	2.05	Biomass
CHP waste (old/new)	30	56.9/68.3	90	12/14	2.93	Biomass
CCGT nat. gas (old/new)	30	42.9/51.5	80	6/7	0.05	Gas
CCGT biomethane (old/new)	30	42.9/51.5	80	6/7	0.05	Gas
OCGT (old/new)	30	20.2/24.2	60	0/0	0.45	Gas
Nuclear	70	400	70	24	1.00	Uranium

S.2.2 Regional capacity and energy parameters

This section presents the region-specific input data for the 19 bidding zones modeled by RAPID. Installed generation capacities is found in Table S.6. Storage system specifications are given in Table S.7. VRE production reference data for capacity factor calibration are provided in Table S.8. Nuclear reactor data are listed in Table S.10. Waste availability limits presented in Table S.9. Hydropower reservoir parameters for the aggregated representation are found in Table S.11.

Table S.6: Installed generation capacity by technology and region (MW). Storage technologies (batteries and pumped hydro) are reported separately in Table S.7.

Technology	EE	LV	LT	DE	DK1	DK2	FI	NL	NO1	NO2	NO3	NO4	NO5	PL	SE1	SE2	SE3	SE4	UK
Hydro	10	1590	130	5140	10	0	3180	40	3960	11230	4820	5600	7940	870	5332[†]	8739[†]	2391[†]	347	1900
Lignite_old	0	0	0	9180	0	0	520	0	0	0	0	0	0	3780	0	0	0	0	0
Lignite_new	0	0	0	9180	0	0	520	0	0	0	0	0	0	3780	0	0	0	0	0
Hard_coal_old	0	0	0	9200	970	540	700	2000	0	0	0	0	0	9420	0	0	0	0	10
Hard_coal_new	0	0	0	9200	970	540	700	2000	0	0	0	0	0	9420	0	0	0	0	10
Oil_old	660	0	0	2060	100	380	520	0	0	0	0	0	0	200	0	0	0	300	620
Oil_new	660	0	0	2060	100	380	520	0	0	0	0	0	0	200	0	0	0	300	620
CHP_bio_old	70	70	90	1510	320	490	830	190	0	0	0	0	0	270	70	110	970	230	2060
CHP_bio_new	70	70	90	1510	320	490	830	190	0	0	0	0	0	270	70	110	970	230	2060
CHP_waste_old	10	0	30	910	100	80	40	390	10	10	0	0	10	0	60	270	260	200	1650
CHP_waste_new	10	0	30	910	100	80	40	390	10	10	0	0	10	0	60	270	260	200	1650
CCGT_ng_old	40	500	670	16910	440	260	780	8260	0	10	0	110	80	2440	0	0	440	310	16500
CCGT_ng_new	40	500	670	16910	440	260	780	8260	0	10	0	110	80	2440	0	0	440	310	16500
CCGT_bio_old	10	10	10	2810	30	40	10	20	0	0	0	0	0	60	0	0	0	0	410
CCGT_bio_new	10	10	10	2810	30	40	10	20	0	0	0	0	0	60	0	0	0	0	410
OCGT_old	0	50	70	1880	50	30	80	920	0	0	0	10	10	270	0	0	0	0	870
OCGT_new	0	50	70	1880	50	30	80	920	0	0	0	10	10	270	0	0	0	0	870
Nuclear	0	0	0	0	0	0	4394	482	0	0	0	0	0	0	0	0	6937	0	5683
Wind_on	570	130	1830	63610	4110	750	8330	6930	410	1450	2120	1160	0	10060	2980	7220	4430	2220	16170
Wind_off	0	0	0	9220	1800	1050	0	4750	0	0	0	0	0	0	0	0	10	160	15840
PV	1330	470	2570	89940	2740	990	1200	24050	780	0	0	0	0	20200	40	240	2270	2250	18280

[†] For SE1–SE3, Hydro capacity is not an input parameter but is calculated from turbine-level flow limits, head, and efficiencies in the detailed hydropower model. The values shown here are the resulting theoretical aggregate maximum capacity, assuming e.g. maximum head at all plants simultaneously.

Table S.7: Storage parameters by region.

Parameter	EE	LV	LT	DE	DK1	DK2	FI	NL	NO1	NO2	NO3	NO4	NO5	PL	SE1	SE2	SE3	SE4	UK
Battery storage																			
Power capacity (MW)	0	0	0	15800	0	0	0	1120	0	0	0	0	0	0	0	0	680	340	6840
Energy capacity (MWh)	0	0	0	23500	0	0	0	758	0	0	0	0	0	0	0	0	680	340	7500
Pumped hydro storage																			
Generation capacity (MW)	0	1130	0	4970	0	0	0	0	0	660	70	0	400	1760	0	0	0	0	2830
Pumping capacity (MW)	0	1110	0	4680	0	0	0	0	0	330	70	0	400	1470	0	0	0	0	2830
Reservoir capacity (MWh)	0	18700	0	54200	0	0	0	0	0	500000	71200	0	693000	27000	0	0	0	0	51000

Note: Generation capacity refers to turbine capacity when generating electricity. Pumping capacity refers to pump capacity when pumping water uphill. Battery power capacity applies to both charging and discharging.

Table S.8: 2024 VRE production reference data (GWh) used for capacity factor calibration.

Technology	EE	LV	LT	DE	DK1	DK2	FI	NL	NO1	NO2	NO3	NO4	NO5	PL	SE1	SE2	SE3	SE4	UK
Wind_on	1164	275	3448	113030	9168	1532	19461	18500	952	4516	5678	3385	0	24763	7464	16891	10116	5863	34744
Wind_off	0	0	0	25664	6134	3606	0	15000	0	0	0	0	0	0	0	0	0	0	48539
PV	1004	398	1397	74297	2622	1077	1206	21266	533	0	0	0	0	17345	54	313	2962	2936	14789

Note: PV production for Swedish regions is distributed proportionally to installed capacity since we could not find this reported by bidding zone.

Table S.9: Annual waste availability limits by region (MWh).

Fuel	**EE**	**LV**	**LT**	**DE**	**DK1**	**DK2**	**FI**	**NL**	**NO1**	**NO2**	**NO3**	**NO4**	**NO5**	**PL**	**SE1-4**	**UK**
Waste (GWh)	116	0	682	6573	497	344	277	2797	139	40	15	0	111	0	4335[*]	10673

[*] Swedish total distributed among SE1-SE4 proportionally to installed CHP capacity

Table S.10: Nuclear reactor specifications by region. Each reactor is characterized by its capacity (MW) and average annual outage hours based on 2016-2024 historical data from IAEA PRIS database. † data for only 2023 due to newly started reactor.

Region	Reactor ID	Capacity (MW)	Avg. unplanned outage (h/yr)	Avg. planned outage (h/yr)	Availability factor (%)
Finland	1	507	188	706	89.8
	2	507	96	671	91.2
	3	890	127	443	93.5
	4	890	315	442	91.4
	5	1600	2144†	0†	75.5†
	Total	4394	–	–	**85.8**
Netherlands	1	482	271	808	87.7
	Total	482	–	–	**87.7**
SE3	1	1040	181	700	89.9
	2	1121	263	687	89.2
	3	1172	231	686	89.5
	4	1400	569	734	85.1
	5	1074	406	936	84.7
	6	1130	369	1041	83.9
	Total	6937	–	–	**87.0**
UK	1	590	1383	1593	66.0
	2	595	1190	1500	69.3
	3	485	1273	1536	67.9
	4	575	1449	1485	66.5
	5	620	409	930	84.7
	6	620	566	956	82.6
	7	1198	516	706	86.1
	8	595	311	918	86.0
	9	605	453	855	85.1
	Total	5883	–	–	**78.3**

The capacity-weighted total availability factor (last column) for each bidding zone is used as α_r in Equation (S.37) and is computed as:

$$\alpha_r = \frac{\sum_i C_i \, (8760 - u_i^{\mathrm{o}} - p_i^{\mathrm{o}})}{\sum_i C_i \times 8760} \tag{S.51}$$

where i indexes reactors in region r, C_i is reactor capacity (MW), u_i^{o} is average unplanned outage (h/yr), and p_i^{o} is average planned outage (h/yr).

Table S.11: Hydropower reservoir parameters for regions with aggregated (non-FORSA) reservoir modeling, used in Equations (S.26)–(S.28). Long-term storage captures seasonal variations; short-term storage captures weekly variations. Capacities are based on the 95th/5th percentile of historical reservoir levels where available, otherwise estimated from production data. Short-term capacity is set to one week of mean annual production. Inflow shares determine the fraction of total inflow directed to each reservoir.

Region	Long-term capacity $\overline{\phi}_r^{lo}$ (GWh)	Short-term capacity $\overline{\phi}_r^{sh}$ (GWh)	Long-term inflow share $i_{r,t}^{lo}$ (-)	Short-term inflow share $i_{r,t}^{sh}$ (-)
DE	15529	299	0.2	0.8
FI	2340	259	0.2	0.8
NO1	4856	342	0.4	0.6
NO2	18036	896	0.6	0.4
NO3	6404	362	0.7	0.3
NO4	11640	443	0.7	0.3
NO5	12577	566	0.5	0.5
PL	1744	34	0.3	0.7
SE1†	10303	36	0.7	0.3
SE2†	11381	233	0.6	0.4
SE3†	1339	67	0.5	0.5
UK	2368	46	0.2	0.8

†SE1–SE3 use detailed hydropower modeling; shown here for comparison only.

S.2.3 Hydropower plants and turbines by river system

The detailed hydropower cascade model represents 219 individual power plants with 421 turbines across nine major Swedish river systems. Table S.12 shows the distribution of plants and turbines by river.

Table S.12: Number of power plants and turbines by river system.

River System	Total Entries	Power Plants	Turbines	Reservoir-Only
Ångermanälven	48	39	69	9
Dalälven	41	36	70	5
Götaälv	25	23	52	2
Indalsälven	39	35	70	4
Ljungan	18	15	25	3
Ljusnan	23	22	41	1
Luleälven	19	15	34	4
Skellefteälven	18	15	24	3
Umeälven	21	19	36	2
Total	**252**	**219**	**421**	**33**

Note: Power plants are defined as facilities with at least one turbine. Reservoir-only facilities (33 entries) have no turbines and do not generate electricity, but are included in the cascade hydraulics model to accurately represent water storage and flow routing between generating plants.

S.3 Scenario specifications

This section provides the detailed implementation of the seven environmental constraint scenarios summarized in the main text (Table 1). Each scenario is defined by a specific parameterization of the flow and level constraint equations introduced in Sections S.1.4–S.1.5. The constraints are specified per river stretch (i.e., per plant–plant pair (pl, pl')) and may vary by season and time of day on an hourly basis. Full plant-by-plant specifications are available upon request.

S.3.1 Constraint implementation

The environmental constraint framework operates on four flow pathways and two water-surface types, as summarized in Table S.13. The flow pathways represent distinct physical routes through or around each hydropower facility, while the level constraints act on reservoir forebay and tailrace water levels. Each constraint type maps directly to the mathematical formulation in Sections S.1.4–S.1.5.

Table S.13: Environmental constraint types and their mapping to model equations.

Category	Constraint type	Model equation	Unit
Flow constraints (per pathway: total, bypass, passage, spillway)			
	Minimum flow	Eq. S.15	m^3/s
	Maximum flow	Eq. S.15	m^3/s
	Ramp-up limit	Eq. S.17	m^3/s
	Ramp-down limit	Eq. S.17	m^3/s
	Period variation limit	Eq. S.19–S.21	m^3/s
Level constraints (forebay and tailrace)			
	Minimum level	Eq. S.16	m
	Maximum level	Eq. S.16	m
	Ramp-up limit	Eq. S.18	m/s
	Ramp-down limit	Eq. S.18	m/s
	Period variation limit	Eq. S.22–S.24	m/s

Constraint values can be specified as absolute values (e.g., 10.0 m^3/s) or as percentages of accumulated upstream inflow (e.g., 90% or 110% of natural inflow). The latter is used in the natural flow scenarios to define flow bands relative to instantaneous hydrological conditions.

S.3.2 Scenario definitions

Table S.14 summarizes the constraint parameters that define each scenario. The scenarios are ordered by increasing stringency, from the unconstrained reference through connectivity and hydropeaking measures to full natural flow regimes.

Table S.14: Summary of environmental constraint parameters by scenario. Constraints are applied to all 252 facilities in SE1–SE3 unless otherwise noted. "Current permits" refers to the plant-specific constraints from existing environmental court rulings that vary by plant, season, and time of day.

Scenario	Constraint specification
No env. constraints	All flow bounds ($\underline{q}^{\text{tot}}$, $\overline{q}^{\text{tot}}$), ramp limits ($\delta^{\uparrow/\downarrow}$), level variation limits ($\overline{\delta}^{\text{day}}$, $\overline{\delta}^{\text{week}}$), and minimum flow requirements from current permits are removed. Only physical equipment limits apply.
Current	Plant-specific constraints from existing environmental court rulings, including: seasonal minimum flows (bypass and total), hourly ramp limits, daily and weekly forebay variation limits, minimum reservoir levels, rolling-average flow requirements, and spillway variation limits. Constraints vary by plant, season, and time of day.
+ Connectivity 1	Current permits plus mandatory fish passage flow $Q^{\text{b}}_{ri,t,pl,pl'} \geq 1$ m^3/s at all facilities, year-round.
+ Connectivity 5	Current permits plus mandatory fish passage flow $Q^{\text{b}}_{ri,t,pl,pl'} \geq 5$ m^3/s at all facilities, year-round.
– Hydropeaking	Current permits plus daily total flow variation limited to 50% of LLQ: $\max_{t\in d} Q^{\text{tot}} - \min_{t\in d} Q^{\text{tot}} \leq 0.5 \cdot \text{LLQ}_{pl}$ for each facility. Exemptions apply to 13 stretches (Table S.15).
Natural flow	Total flow constrained to 90–110% of instantaneous accumulated upstream inflow: $0.9 \cdot i^{\text{acc}}_{ri,t,pl} \leq Q^{\text{tot}}_{ri,t,pl,pl'} \leq 1.1 \cdot i^{\text{acc}}_{ri,t,pl}$. Current permits are removed. Wider bands at 25 stretches (Table S.16).
Natural flow + Connectivity	Natural flow constraints (as above) combined with $Q^{\text{b}}_{ri,t,pl,pl'} \geq 5$ m^3/s fish passage flow at all facilities.

S.3.3 Scenario exemptions for computational feasibility

Two scenarios required site-specific relaxations to maintain a feasible optimization problem: the *– Hydropeaking* scenario (Table S.15) and the *Natural flow* scenarios (Table S.16). These exemptions were determined through iterative preliminary optimization tests.

Table S.15: River stretches exempted from daily flow variation constraints in the *– Hydropeaking* scenario. These 13 stretches (5% of 252 total facilities) were exempted because physical constraints made it infeasible to simultaneously satisfy all environmental and operational requirements.

River system	Stretch (upstream → downstream)	Count
Ljungan	Järnvägsforsen → Parteboda, Parteboda → Hermansboda, Hermansboda → Ljungaverk, Ljungaverk → Nederede, Torpshammar → Nederede, Nederede → Skallböle, Skallböle → Matfors, Matfors → Viforsen, Viforsen → Hav	9
Dalälven	Eldforsen → Mockfjärd, Hansjö → Gråda, Näs → Söderfors, Unnån → Hansjö	4
Total exempted		**13**

Table S.16: River stretches with wider tolerance bands in the *Natural flow* scenarios. The standard 90–110% inflow band was applied to approximately 86% of stretches; the remaining 14% required wider bands due to limited reservoir storage, high inflow variability, or hydraulic interactions between plants.

River system	Stretch	Band (% of inflow)
Umeälven	Umluspen → Stensele	80–120
	Stensele → Grundfors	80–120
	Grundfors → Rusfors	80–120
Luleälven	Seitevare → Parki	70–120
	Parki → Randi	70–120
	Randi → Akkats	50–120 (min. only)
Indalsälven	Lillå → Strömbacka	70–140
Dalälven	Gråda → Forshuvud	90–110 winter, 90–180 spring/summer
	Avestaforsen → Avesta Lillfors	90–110 winter, 90–180 spring/summer
	Johannisholm → Gävunda	90–130
	Runn → Långhag	≥50 (no max.)
	Ljugaren → Borgärdet	≥50 (no max.)
	Snesen → Mockfjärd	≤110 (no min.)

S.4 Additional results

This section presents supplementary results that complement the analysis in the main text.

S.4.1 Flexibility analysis

Figure S.2 shows the daily production range in Norway under the different scenarios. It is provided here to show to what extent Norwegian hydropower compensate for the lost ability for Swedish hydropower to vary production within days in the - *Hydropeaking scenario*.

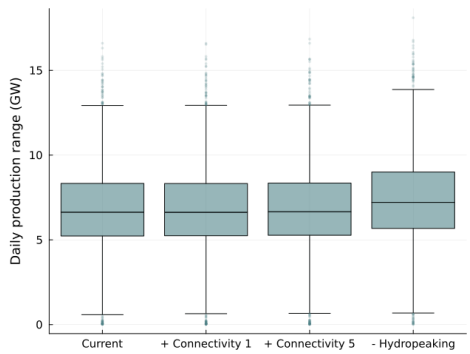

Figure S.1: The figure shows daily production range (maximum minus minimum production within each 24-hour period), across all weather years (2016-2024) for Norwegian hydropower in NO1-NO5 combined, where each box represents 3,285 daily observations (365 days × 9 years) Boxes show median (center line), interquartile range (box), whiskers extending to 1.5×IQR, and outliers beyond whiskers (points).

Figure S.2 shows the Flexibility Factor for Swedish hydropower under different environmental constraints, calculated following [15]. As discussed in the main text, the FF increases in SE2 when operational constraints are tightened, contradicting the physical flexibility reduction demonstrated by the daily production range and hourly ramping metrics. This paradox arises because the FF conflates physical flexibility with endogenous market price responses.

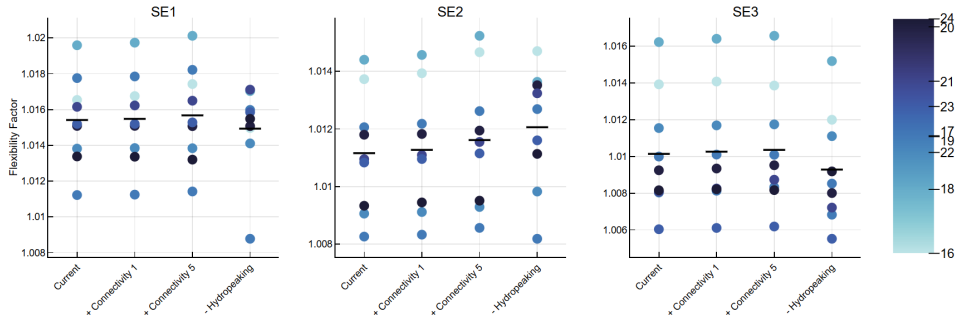

Figure S.2: Flexibility Factor (FF = achieved price / average price) for hydropower in Swedish bidding zones SE1-SE3. Points show individual weather years (colored from driest to wettest), horizontal lines show scenario averages. FF increases under the - *Hydropeaking* constraint in SE2 despite reduced physical flexibility, due to endogenous price increases.

S.4.2 Change in generation by technology

Figure S.3 shows how the generation mix adjusts across the entire modeled system in response to each environmental constraint scenario. As discussed in the main text, the energy lost from constrained Swedish hydropower is primarily compensated by increased gas and coal generation in neighboring regions, illustrating the cross-border redistribution of balancing services.

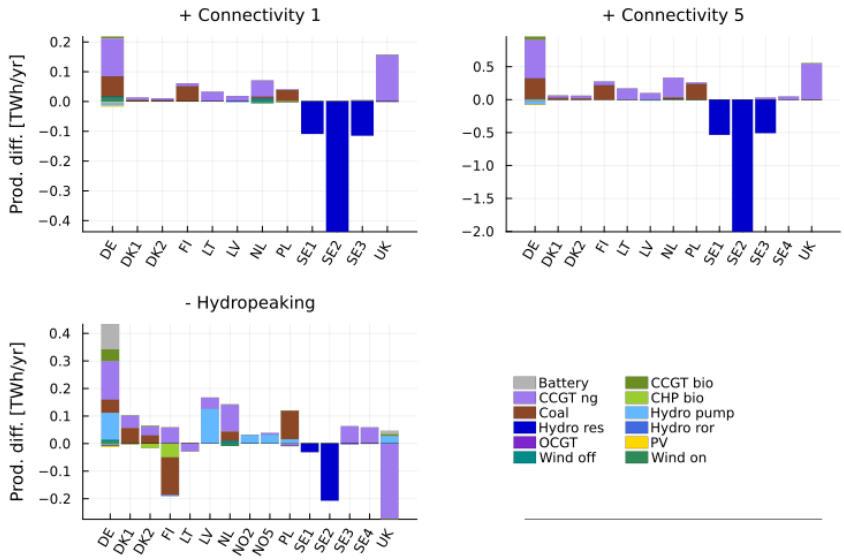

Figure S.3: Average annual electricity production difference by technology compared to the reference scenario. Stacked bars show the contribution of each technology group to the total production change in each scenario. Values represent the average across all model runs covering 2016-2024 (9 years total). Positive values indicate increased production relative to the reference, while negative values indicate reduced production.

S.4.3 Market actor impacts across all regions

Figure S.4 extends the regional market actor analysis from the main text (Figure 8) by showing individual weather years rather than averages.

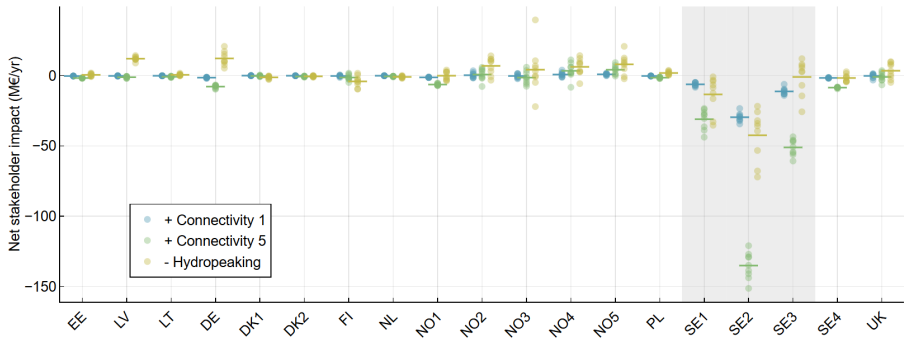

Figure S.4: Annual net stakeholder impact (M€/yr) by region for three environmental scenarios compared to current environmental regulations, shown for individual weather years 2016-2022. Net stakeholder impact comprises changes in consumer costs, producer profits, and TSO income, where negative values indicate net losses. Gray shading highlights Swedish regions SE1-SE3, which are the regions where stricter environmental constraints are implemented in the scenarios.